UNIVERSITÉ DE MONTRÉAL

# TEMPERATURE-COMPENSATED MICROSTRIP ANTENNA FOR ICE MEASUREMENT AND WIRELESS SENSOR NETWORK

MARKO ZIVANOVIC

DÉPARTEMENT DE GÉNIE ÉLECTRIQUE

ÉCOLE POLYTECHNIQUE DE MONTRÉAL

MÉMOIRE PRÉSENTÉ EN VUE DE L'OBTENTION

DU DIPLÔME DE MAÎTRISE ÈS SCIENCES APPLIQUÉES

(GÉNIE ÉLECTRIQUE)

AVRIL 2018

UNIVERSITÉ DE MONTRÉAL

ÉCOLE POLYTECHNIQUE DE MONTRÉAL

Ce mémoire intitulé :

TEMPERATURE-COMPENSATED MICROSTRIP ANTENNA FOR ICE MEASUREMENT AND WIRELESS SENSOR NETWORK

présenté par : ZIVANOVIC Marko

en vue de l'obtention du diplôme de : Maîtrise ès sciences appliquées

a été dûment accepté par le jury d'examen constitué de :

M. FRIGON Jean-François, Ph. D., président

M. WU Ke, Ph. D., membre et directeur de recherche

M. TATU Serioja, Ph. D., membre

# DEDICATION

*To my grandfather*

*and*

*my mother, grandmother, uncle and his family*

# ACKNOWLEDGEMENTS

I would like to thank my professor Ke Wu for believing and giving me the opportunity to pursue Master studies. I want to express my deepest gratitude for your patience, support, encouragement through your enthusiasm and positive attitude in bringing me into this exciting and challenging field. Thank you very much for your valuable advice and understanding me.

I also want to thank Tarek Djerafi for his friendship, guidance, suggestions, valuable discussions and efficient time spent on business trips and meetings during my work on thesis's project. Thank you Tarek!

Without any exception, I want to express my gratitude to my friend Srinaga Nikhil Nallandhigal.

I am also grateful to my friends Xiaoqiang Gu, Desong Wang, Intikhab Hussain, Chunmei Liu, Lamine Bamogho, Bilel Mnasri, Marzieh Mehri Dehnavi and Parikshat Sirpal for their endless support during my research.

I would especially thank Traian Antonescu for fabricating the designed antennas.

Last but not least, I want to express gratitude to my mother, grandmother, uncle and his family for endless support.

# RÉSUMÉ

L'objectif principal de cette thèse est de concevoir et de développer une technique de compensation de température liée à la fréquence de résonance d'une antenne microruban. Une telle antenne microruban compensée en température, capable de résister à une variation importante de température, est utilisée comme une partie d'un capteur pour mesurer l'épaisseur de la charge de la glace. Les antennes microruban conçues de cette manière sont utilisées dans un réseau de capteurs de température sans fil en relation avec ses applications critiques d'un système de dégivrage d'hélicoptère. Un prototype de réseau de capteurs de température sans fil qui contrôle à distance la mise en marche ou l'arrêt des appareils de chauffage destinés au dégivrage est développé. Parmi toutes les autres antennes, l'antenne microruban est sélectionnée en raison de sa polyvalence. Aussi, sa fréquence de résonance souffre d'un problème de stabilité due à sa susceptibilité à des facteurs externes tels que les fluctuations de température. En plus, sa résonance provoquant une largeur de bande de fréquence étroite ne conduit pas à une solution directement préférée. Pour minimiser l'instabilité de fréquence induite par la température et aussi pour éviter de perdre le signal ou les interférences des canaux adjacents, on a besoin de développer une technique de compensation de température très efficace et pratique.

Dans ce travail, une technique de compensation de la température efficace et pratique est conçue pour les antennes microruban. La technique de compensation imagée est supérieure à la technique existante, tant dans sa simplicité que dans sa stabilité en fréquence. A notre, connaissance, rien de semblable n'a été fait auparavant.

Pour la première fois, la dépendance de la fréquence de résonance de l'antenne microruban en fonction de la température est étudiée à l'aide d'une formulation mathématique de la déviation de fréquence pour les géométries rectangulaires, circulaires et triangulaires. Le modèle de circuit est adopté pour l'analyse de l'impact de la température sur la fréquence de résonance de l'antenne microruban appropriée pour les procédures de CAO (conception assistée par ordinateur). Les simulations électromagnétiques sur les résultats de la théorie de déviation du modèle de circuit adopté. Les résultats de l'impact de la température sur la dérive de fréquence des antennes microruban résonnant à 2,4 GHz modélisées sur différents substrats sont présentés et comparés. La concordance entre les résultats théoriques et ceux obtenus par les simulations numériques et les

mesures expérimentales, montrent que les antennes modélisées sur des substrats plus épais présentent un meilleur comportement en température de la fréquence de résonance.

A partir d'une dérive de fréquence formulée, une condition de compensation de température pour la géométrie rectangulaire de l'antenne microruban est développée. Les contraintes imposées dans la dérivation rendent la condition de compensation valide pour le mode fondamental et ses harmoniques. Grâce à une transformation structurelle, la condition de compensation dérivée pour l'antenne microruban rectangulaire est également appliquée sur des géométries circulaires et triangulaires. Cette condition de compensation est validée par un modèle de circuit numérique et une analyse de simulateur électromagnétique. Aucun des substrats disponibles dans le commerce n'est capable de satisfaire parfaitement la condition de compensation. Parmi tous les substrats d'intérêt, les substrats RO3035 de Rogers et TMM10 sont choisis pour la vérification expérimentale car ils satisfont à la meilleure condition possible de compensation de température. Le substrat RO3035 est en polytétrafluoroéthylène (PTFE) chargé de céramique et le TMM10 est en céramique thermodurcissable chargée de particules de plastique. Onze antennes sont fabriquées et ont subi des tests approfondis. Les résultats de mesure sont en accord avec les simulations et la théorie dérivée pour les deux substrats. Les résultats de l'antenne microruban rectangulaire montrent le meilleur comportement pour TMM10 comme prévu de l'analyse. Par conséquent, de telles antennes compensées en température sont des candidats appropriés pour un nouveau concept d'utilisation d'une antenne microruban dans la détection de glace.

Une autre contribution importante de ce travail se reflète dans la détection de glace. Pour la première fois, un capteur d'épaisseur de glace basé sur une antenne microruban compensée en température est proposé. Une modélisation précise de l'effet de la charge de glace sur la fréquence de résonance de l'antenne microruban est effectuée à l'aide de mesures des propriétés électriques de cinq échantillons de glace et d'une analyse numérique. La neige recueillie dans la région de Montréal est fondue et refroidie pour former de la glace. Un soin particulier est pris lors de la collecte de la neige. Les mesures de la permittivité des glaces et de la tangente de perte sont effectuées à l'aide d'une technique de sonde coaxiale à extrémité ouverte. Les résultats obtenus pour la constante diélectrique de glace sont en accord avec les autres résultats rapportés, mais ce n'est pas le cas pour la tangente de perte. Les pertes mesurées sont beaucoup plus grandes que celles rapportées dans la littérature. La raison du désaccord est probablement causée par des incertitudes de mesure dominées par de très faibles pertes.

Dans la dernière étape du projet, le réseau de capteurs sans fil destiné au développement d'un système de dégivrage d'hélicoptères est conçu. Outre la détection de la température, le réseau sans fil dépendant de la température de chauffage et de l'épaisseur de la glace peut envoyer un signal d'activation pour les réchauffeurs de dégivrage, dans lesquels les antennes microruban compensées en température sont déployées.

# ABSTRACT

The primary goal of this thesis is to devise and develop a technique of temperature compensation related to the resonant frequency of a microstrip patch antenna (MPA). Such a temperature-compensated microstrip patch antenna capable of standing against a substantial variation of temperature is exploited as part of an ice-sensor for measuring ice loading thickness. Microstrip antennas designed in this way are used in a wireless temperature sensor network in connection with its critical applications of a helicopter de-icing system. A prototype of wireless temperature sensor network which remotely controls turning-on or turning-off heaters intended for de-icing is developed. Among all other antennas, the microstrip antenna is selected due to its versatility. Thanks to the susceptibility of the microstrip patch antenna to external factors, such as temperature fluctuations, its resonant frequency suffers from a stability issue. In addition to that, its resonance causing a narrow frequency bandwidth does not lead to a straightforwardly preferred solution. To minimize the temperature-induced frequency instability and also to prevent losing signal or interferences from adjacent channels, one needs to develop a very efficient and practical temperature compensation technique.

In this work, an efficient and practical technique through a resonant frequency temperature compensation for microstrip patch antennas is devised, which is superior to existing counterparts both in its simplicity and frequency stability. To the best of the author`s knowledge, nothing similar was done before.

For the first time, a temperature dependence of microstrip antenna resonant frequency is investigated through a mathematical formulation of frequency drift for rectangular, circular, and triangular patch geometries. The circuit model for analyzing temperature impact on microstrip antenna resonant frequency suitable for computer-aided design (CAD) procedures is adopted. Electromagnetic simulations along with results of the adopted circuit model support the derived theory. Results of temperature impact on the frequency drift of microstrip antennas resonant at 2.4 GHz modelled on different substrates are shown and compared. Analysis, simulation, and experimental results show that antennas built on thicker substrates exhibit a better temperature behaviour of the resonant frequency.

Based on a theoretically formulated frequency drift, a temperature compensation condition for the rectangular patch geometry of MPA is derived. Constraints imposed in the derivation make the

compensation condition valid for the fundamental mode and its harmonics. Through a structural transformation, the derived compensation condition for rectangular patch geometry is applied on circular and triangular patch geometries. The compensation condition is validated through numerical, circuit model- and electromagnetic simulator-based analyses. None of the commercially available substrates can perfectly satisfy the compensation condition. Among all the substrates of interest, two substrates closely satisfying a temperature compensation condition are chosen for experimental verification, which are Rogers substrates, namely RO3035 and TMM10. Substrate RO3035 is ceramic-filled polytetrafluoroethylene (PTFE), and TMM10 is thermoset ceramic loaded with plastic particles. Eleven microstrip antennas were fabricated and went through extensive testing. Measurement results show a tendency in connection with the simulations and derived theory for both substrates. The results of the rectangular microstrip patch antenna show the best behaviour for TMM10 as expected from the analysis. Therefore, such temperature-compensated antennas are suitable candidates for a new concept of using microstrip patch antenna – ice-sensing.

Another contribution of this work is reflected in ice-sensing. For the first time, an ice thickness sensor based on temperature-compensated microstrip patch antenna is proposed. Accurate modelling of the ice loading effect on the resonant frequency of microstrip antenna is conducted through measurements of electrical properties of the five ice samples and numerical analysis. Snow collected in the Montreal area is melted and cooled to form ice. Particular care is taken during the snow collection. Ice permittivity and loss tangent measurements are carried out through the use of an open-ended coaxial probe technique. Results obtained for ice dielectric constant are in agreement with other reported results, but this is not the case for loss tangent. Measured losses are much larger than those reported in the literature. Reason for the disagreement is possibly caused by dominated measurement uncertainties over very small losses.

In the final stage of the project, a wireless temperature sensor network intended for the development of a helicopter de-icing system is designed, prototyped and tested. Beside the temperature sensing, the wireless network depending on heating temperature and ice thickness can send activation signal for de-icing heaters, in which the temperature-compensated microstrip patch antennas are deployed.

# TABLE OF CONTENTS

# LIST OF TABLES

# LIST OF FIGURES

# LIST OF SYMBOLS AND ABBREVIATIONS

| | |
|---|---|
| ASK | Amplitude shift keying |
| ADS | Advanced Design System |
| CAD | Computer-aided design |
| CST | Computer Simulation Technology |
| CMPA | Circular microstrip patch antenna |
| CEPT | European Conference of Postal and Telecommunications Administrations |
| CTE | Coefficient of thermal expansion |
| EU | European Union |
| ETSI | European Telecommunication Standards Institute |
| FEM | Finite element method |
| FDTD | Finite difference time domain |
| FCC | Federal Communication Commission |
| FSK | Frequency shift keying |
| GPIO | General purpose input output microcontroller pin |
| GFSK | Gaussian frequency shift keying |
| ITU | International Telecommunication Union |
| ISM | Industrial, scientific, and medical |
| ICAO | International Civil Aviation Organisation |
| $I_h$ | Ice phase one |
| L | Resonant length of rectangular microstrip patch |
| LED | Light emitting diode |
| MoM | Method of moments |

| | |
|---|---|
| MPA | Microstrip patch antenna |
| MMIC | Monolithic microwave integrated circuit |
| m | Integer number |
| n | Integer number |
| PTFE | Polytetrafluoroethylene |
| PC | Personal computer |
| PPS | Polyphenyle-Nesulfide |
| QPSK | Quadrature phase shift keying |
| RMPA | Rectangular microstrip patch antenna |
| RFID | Radio frequency identification |
| SDA | Spectral domain approach |
| SIW | Substrate integrated waveguide |
| SRD | Short range device |
| T | Temperature |
| TC | Temperature coefficient |
| TMPA | Triangular microstrip patch antenna |
| UN | United Nations |
| WRC | World Radio Conference |
| W | Rectangular patch width |
| $\varepsilon_r$ | Substrate permittivity |
| $\varepsilon_e$ | Effective dielectric constant |
| $\delta_r$ | Temperature coefficient of the permittivity |
| $\delta_\varepsilon$ | Temperature coefficient of effective permittivity |
| $\delta_c$ | Coefficient of temperature expansion of the copper |

| | |
|---|---|
| $\delta_x$ | Coefficient of temperature expansion of the substrate in the x-plane |
| $\delta_y$ | Coefficient of temperature expansion of the substrate in the y-plane |
| $\delta_z$ | Coefficient of temperature expansion of the substrate in the z-plane |
| $\Delta T$ | Incremental change in environment temperature |
| $f_r^T$ | Resonant frequency at referent temperature |
| $f_r^{T1}$ | Resonant frequency at some temperature point |
| c | Speed of light in free space |

# CHAPTER 1 INTRODUCTION

## 1.1 Introduction

Icing presents a significant weather phenomenon causing one of the major operational troubles for airplanes and helicopters, thus affecting the ability for a stable flight [1] [2] [3]. Icing leads to increased aerodynamic drag and weight along with a reduction in lift and trust, with a direct impact on flight safety and economy [1] [2]. De-icing procedures prior to takeoff are often time-consuming and cause frequent delays at major airports [2]. Known examples are airports in Ottawa and Montreal region where icing conditions often force them to be partially or entirely closed [4]. Icing effect is often defined as the formation of ice when cold water droplets come in touch with the surface of object [5]. In the worst case, icing causes hazard to aircraft [6]. According to *Federal Aviation Administration* (FAA) [7], *NTSB Accident Database and Synopses* [8], *NASA Aviation Safety Reporting System* [9] and other conducted statistical investigations [2] [10], accidents due to icing occur very frequently. Similar and the only statistical study for Canada as the case of interest can be found in [11]. Given study represents the first analysis of icing accidents using Canadian database – *Transport Canada Civil Aviation Daily Occurrence Reporting System* (CADORS) database [12]. According to [11], the highest frequency of accidents is in Quebec and British Columbia with the most critical period of one month from *December 10$^{th}$* to *January 10$^{th}$*. Until present, methods for avoiding, preventing and decreasing accidents related to icing phenomenon rely on weather reports, forecast, pilot's reports, observations, awareness and training to react in such situation [2]. Beside continuous improvement in forecast accuracy techniques for early warning in icing conditions, better icing analysis and detection are necessary [2]. Motivated by industry, this thesis research, as a part of the project - helicopter de-icing system, has the primary objective to design resonant frequency temperature-compensated microstrip patch antennas (MPA). Such temperature-compensated MPA will be exploited in the wireless temperature sensor network intended for the development of a helicopter de-icing system. Secondary product is related to the application of a temperature-compensated MPA for ice thickness sensing. This will be the first de-icing system deployed for helicopters.

## 1.2 Why Temperature Compensated MPA

MPA due to its compactness and versatility in electrical characteristics have found applications in a large number of commercial needs and sectors [13]. Today, MPAs can be found in airplanes, missiles, satellite links, mobile communications, local area networks and they represent an extension of microstrip circuits [14]. As an important part of transmitters and receivers, MPA characteristics affect the overall system performance. Due to their inherent resonance, they are characterized by a very narrow frequency bandwidth, typically a few percent [15]. In addition, the resonant frequency is strongly affected by dimensions of patch and substrate permittivity as well as working conditions [16]. It makes them susceptible to the fabrication process, design parameters tolerance and environmental conditions. Environmental conditions have a significant impact on MPA designed for outdoor applications. For the purpose of protection from water, humidity, dust and other outside factors, the MPAs are covered with superstrate layer called radome. It does not make them resistant to temperature variations and ice or snow loading effect. Temperature stability of resonant frequency is an important criterion, especially in military and airborne applications. Change in temperature causes drift in resonant frequency of MPA subsequently causing a band rejection or interference with adjacent bands. All the stated aspects point to accurate design techniques, as well as methods for decreasing MPA sensitivity on design parameters.

## 1.3 Research Objectives

Research objectives comprise of three parts:

- The first part focuses on a mathematical formulation of temperature variation effect on the resonant frequency of rectangular, circular and triangular patch geometries of MPA, leading to a temperature compensation technique. Tolerance analysis is addressed for the purpose of determining the resonant frequency drift sensitivity of a particular patch geometry on parameters, which are important for frequency stability. Creating a circuit model for analyzing temperature impact on the patch resonance will finalize the temperature impact analysis.

- The second part aims at investigating electrical properties of ice through measurements for the purpose of better characterization ice loading effect on MPA resonant frequency. Temperature-compensated antennas or antennas with reduced resonant frequency temperature sensitivity are employed as ice sensors for ice thickness determination.
- The third part deals with the design, prototyping, and testing of a wireless temperature sensor network intended for the development of a helicopter de-icing system. Specificity of application requires wireless temperature network elements assessment through a power budget analysis to ensure a reliable communication link.

## 1.4 Thesis Organization

The thesis is organized in six chapters. Introductory Chapter 1 offers the readers a broader view of project and guidelines for solving the problem. Contemporary literature review with all relevant information is briefly outlined in Chapter 2. The chapter summarizes temperature compensation techniques along their efficiency, advantages and disadvantages, addressing the system's operating frequency band selection. The main contribution of the thesis is given in Chapter 3. This chapter is dedicated to a mathematical formulation of temperature impact on rectangular, circular and triangular microstrip patch antenna. Circuit model for analyzing temperature effect on antenna resonance is given. Tolerance analysis of the key parameters which affect antenna's resonant frequency temperature dependence is carried out, showing the impact on resonant frequency temperature behaviour. Experimental and simulation results, along with theoretical results and those obtained by the circuit model, are presented. Resonant frequency temperature compensation condition is developed in Chapter 3. Chapter 4 deals with electrical properties of ice and MPA exploited as ice sensor. The design of a wireless temperature sensor network employing the temperature compensated MPAs is given in Chapter 5. Finally, Chapter 6 gives the summary of this research and proposes future work and possible improvements.

# CHAPTER 2 BACKGROUND

This chapter presents a critical literature review on key research that describes the impact of temperature on resonant frequency of MPA. Furthermore, the developed techniques for resonant frequency temperature stabilization for MPA are described. Subsequently, this chapter guides us through frequency band selection for a wireless temperature sensor network intended for use on helicopters in North America and Europe.

## 2.1 Literature Review

To the best of the author's knowledge, not much research has been done regarding the development of temperature compensation techniques for microstrip antennas, nor do the textbooks dealing with microstrip antennas discuss this topic. Additionally, majority of textbooks dealing with microstrip antennas do not discuss temperature impact on resonant frequency of MPA. As a rule, microstrip antennas are narrowly banded. In practice, it is very important to have a stable resonant frequency under a substantial temperature variation. Notably, only a few researchers have dealt with this problem and relevant details of research collection shall be presented below.

The primary research on this topic was initiated in 1981 by Bell Aerospace System Division [17]. This work experimentally investigated temperature impact on the resonant frequency of a rectangular MPA, and proposed a temperature compensation technique of the resonant frequency. The proposed technique resulted in a reduced sensitivity of antennas' resonant frequency over temperature. According to this research, two factors mainly affected the resonant frequency. First was a copper expansion or contraction of a patch element. The second was a change in the effective dielectric constant of a substrate material. The resonant dimension of a patch element determines the operating frequency of a microstrip antenna. Due to the increase of temperature, the copper expansion of patch element results in a larger resonant dimension, thus decreasing the resonant frequency of MPA. Similarly, the opposite behaviour observed for temperature reduction. Another factor affecting the resonant dimension of patch element is the effective dielectric constant of a substrate material. Antennas designed on a Teflon-fiberglass dielectric substrate were used for experimental investigation. The Teflon-fiberglass substrate exhibited a decrease in dielectric constant, following an increase in temperature. This resulted in an increased resonant frequency with an increased temperature, i.e. making the effective dielectric constant smaller. Several

measurements were performed to confirm that the effective dielectric constant played a dominant role in the change of resonant frequency. By assuming that resonant length of a patch and effective dielectric constant of a substrate material varied linearly with temperature, a temperature-compensated MPA could be accomplished. By reducing the amount of dielectric material to a point where a change in the effective dielectric constant compensated a change in patch length, a resonant frequency would be less sensitive to temperature variations. However, this technique had no practical significance, as the frequency drift of $0.1\ MHz$ and $0.6\ MHz$ required the removal of $84\%$ to $97\%$ of dielectric material under a patch element. Such amounts of the removed dielectric material greatly reduced the robustness of a microstrip antenna.

Two decades after this research, the impact of temperature on the resonant frequency of MPA has once again received attention.

Another experimentally based research study [18] provided an extensive review of the factors that affected a resonant frequency of MPA in terms of temperature. Two major problems encountered with the modern microstrip antenna design were identified and studied in detail. The first major problem was unknown temperature dependence on the substrate electrical parameters. The second major problem was discrepancy between actual substrate parameter's value and those specified in manufacturers' datasheets. These factors were reflected in common design practices of microstrip antennas, preventing design engineers from precisely predicting the behaviour or design of MPA for non-friendly or harsh conditions. In datasheets, the relative dielectric constant is specified within a certain tolerance range at room temperature and one frequency point while the dissipation factor is specified as its maximum value at one frequency point and room temperature. A major drawback of the datasheets is the fact that they neglected the drift of electrical parameters under temperature changes. Generally speaking, datasheets provide information, such as thermal coefficient of the dielectric constant, within $0℃$ to $+100℃$ temperature range as an average value. Notably, this temperature dependence is neither linear nor symmetric. This is the main reason for discrepancies between the actual behaviour of the microstrip antenna and those predicted by computer-aided design (CAD) tools. The discrepancies can be larger if actual electrical substrate parameters are frequency dependent. One of the main reasons for incompleteness and incorrectness of manufacturers' data is the lack of accurate measurements of material's electrical parameters on manufacturing line [18]. For the purpose of determining actual electrical parameters of substrates and their impact on design, behaviour and temperature stabilization of microstrip antenna, the

following substrates are investigated: Teflon-based, ceramic-based and quartz-fibre substrates. The investigated substrate parameters are relative dielectric constant and loss tangent. Substrates have been exposed to temperature variations ranging from $-60℃$ to $+80℃$. Additionally, their behaviour has been observed at four frequencies between 800 $KHz$ and 10 $GHz$. Measurements of these parameters were performed precisely and under controlled conditions with high quality manufactured substrate samples. The accuracy of measurements was around 1.5% for the dielectric constant and 3% for loss tangent, regardless of temperature. Based on the measured results under temperature impact on measured parameters, substrates were divided into four categories: A, B, C, D. Such substrate categorization was not possible in datasheets due to the lack of information. Each category was characterized by specific behaviour of certain electrical parameters. The results of Category A and B, along with their discrepancies from manufacturers' specified values, are shown in Figure 2.1.

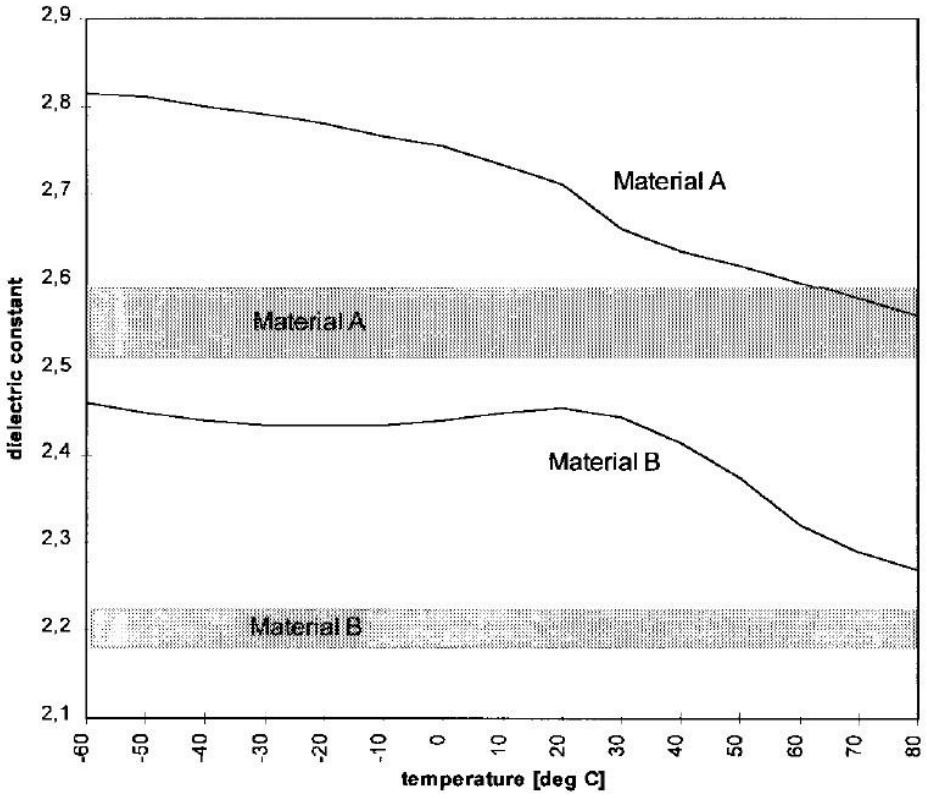


Figure 2.1 - Category A and B substrate dielectric constant temperature dependence. The shaded area is the dielectric constant range specified by the manufacturer [18], © [1999] IEEE

Category A included Teflon-glass substrates, and its typical representatives were Ultralam 2000 and CuClad 250 LX. This category has shown an almost constant negative temperature coefficient

of the dielectric constant over the entire temperature range except the temperature range where the phase transition of glass occurred. Substrates in category B were also Teflon-glass based but they had a dielectric constant gradient which differs in at least two temperature subranges.

Category B of substrate materials was characterized by an almost temperature independent dielectric constant in the lower temperature range, while showing a strong dependence in higher temperature ranges. Representatives of this category were RT/Duroid 5880 and TLX-8 substrates. The changes in dielectric were 9.7% for category A, and 8% for category B over the entire temperature range. Comparison of the measured values of the dielectric constants with those specified by the manufacturers revealed big differences. Measurements also disclosed a phase transition that has not been specified by the manufacturer. The measurements of these two categories showed no frequency dependence of electrical parameters within the considered temperature range. Measurement results for substrate categories C and D are shown in Figure 2.2 and Figure 2.3. Substrate categories C and D included ceramics substrates.

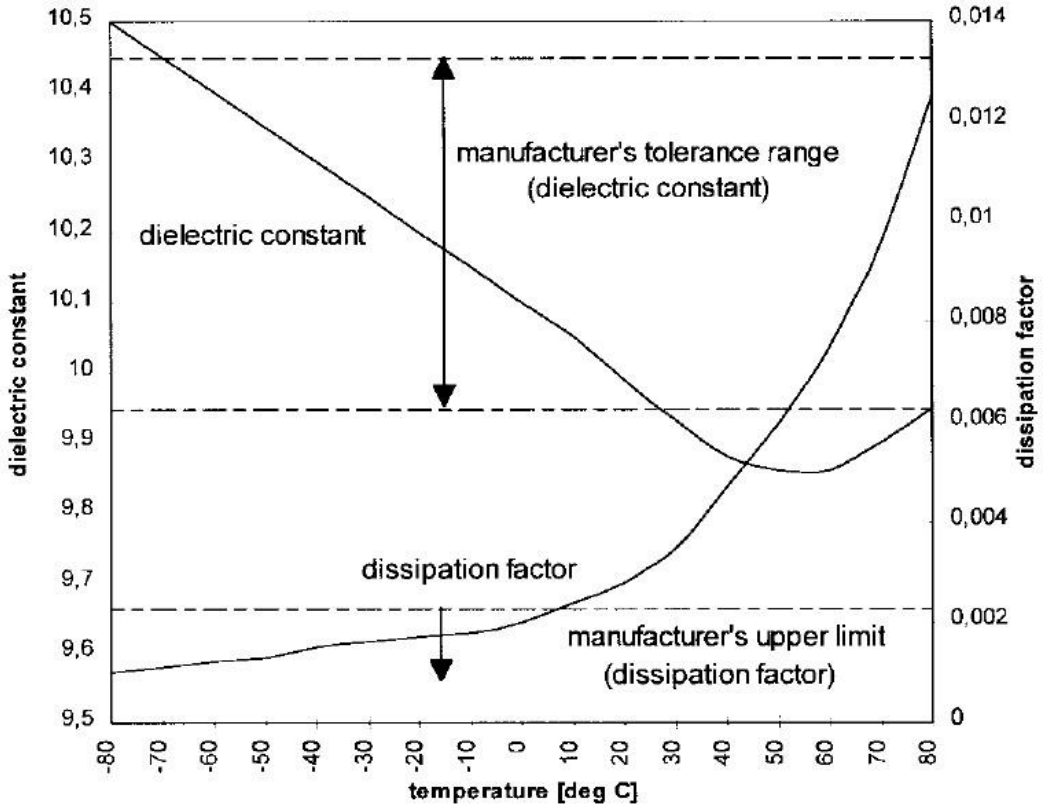


Figure 2.2 - Category C substrate dielectric constant and loss temperature dependence along manufacturer's value specifications [18], © [1999] IEEE

Substrates of Category C were characterized by uniformly dispersed ceramic filler in Teflon matrix. Representatives were RT/Duroid 6010 and AR1000. Measurement results for this category of substrate materials showed changes of 6.9% in the dielectric constant over all temperature ranges and negligible frequency dependence up to temperatures of 25℃. Slight variations of about 0.8% in measured parameters with frequency occurred in higher temperature ranges. Values of the dissipation factor complied with the manufacturer's specifications only for temperatures below 10℃. For temperatures over 10℃, there was a significant divergence from the specified datasheet value. It was found to be 5.2 times larger when compared to the maximum value specified by the manufacturer.

The dielectric constant of Category D substrate materials, Figure 2.3, compared to the Category A, B, and C was characterized by the smallest variation in the dielectric constant and ultralow dissipation factor. The observed dielectric constant variation was less than 4.3%.

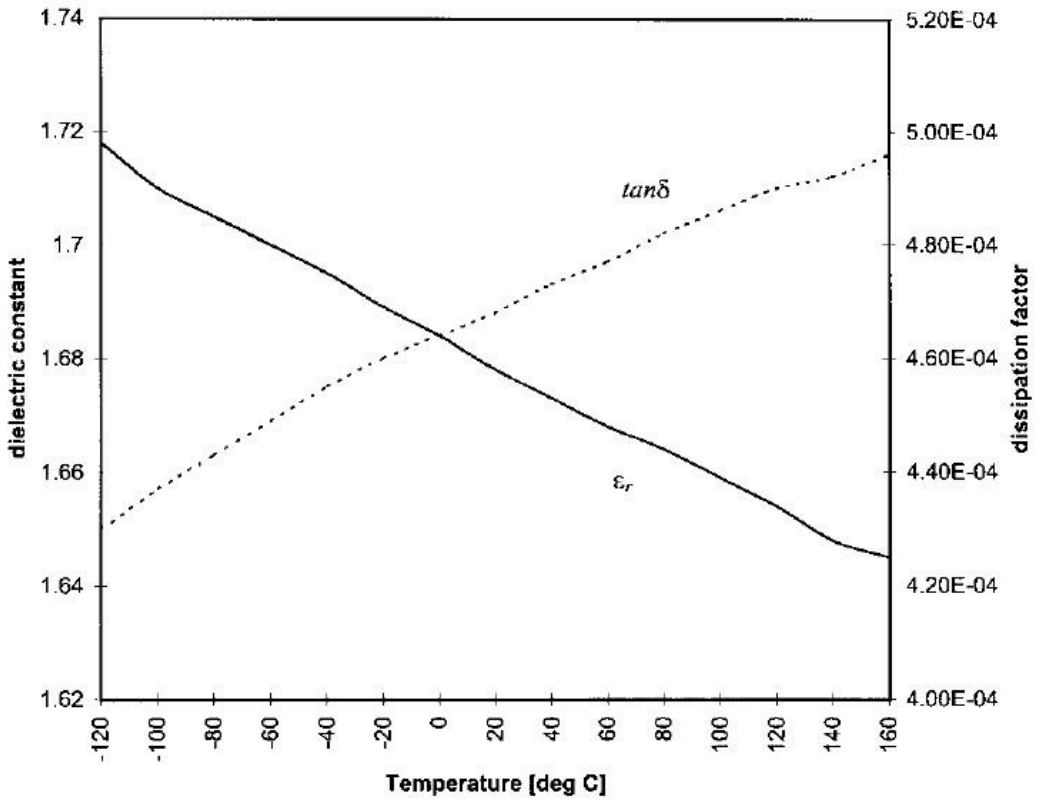


Figure 2.3 - Category D substrate dielectric constant and loss temperature dependence [18], © [1999] IEEE

A comprehensive analysis of various microstrip antennas exposed to large temperature variations was possible based on accurate data and temperature behavior of particular electrical parameters. Dual-feed aperture coupled microstrip antennas were fabricated, combining four substrate categories A, B, C, and D in different ways to create a temperature-compensated antenna. Combinations of B-D or C-D categories were observed to have the best temperature behaviour. The achieved relative frequency drift for these combinations was between 0.9% and 1%. It was observed that the combination of Teflon-glass substrate materials was unacceptable for microstrip antennas used in large temperature variation applications.

In addition to experimental investigations of temperature impact on microstrip antenna's resonant frequency, theoretical analyses employing an accurate transmission line model [19], as well as rigorous numerical techniques, such as Spectral Domain Approach [20] are employed.

In the paper [19], the improved linear transmission line model was used to analyze rectangular, circular, and triangular microstrip patch geometries for the first time. The improved linear transmission line model represents an appropriate mean for the visualization temperature effects on a resonant frequency of MPA. The simulated effects due to variation in parameters such as length, width, thickness and dielectric constant caused by temperature only confirmed the previously conducted experimental analysis. A temperature sensitivity analysis has been completed for antennas designed on three different commercially available substrates: RT/Duroid 5500, RT/Duroid 6006 and Epsilam 10 in $-40℃$ to $+60℃$ temperature range. The analysis of these substrates showed that microstrip antennas designed on substrates with a lower dielectric constant and lower thermal coefficient of dielectric constant were less sensitive to temperature variations. It was also observed that the effect of variations in substrate thickness on resonant frequency was negligible.

In research [20] that analyzed temperature variations on a resonant frequency of MPA, a more rigorous method was employed – spectral domain approach (SDA). Frequency drift results obtained by the spectral domain approach coincided with the analysis results obtained by the transmission line method [19] which required less mathematical complexity and computation time.

An entirely different approach to temperature compensation for the frequency drift of microstrip antenna material was proposed in [21]. In that research, temperature-compensated thermoplastic high dielectric constant microwave laminate was synthesized. A high dielectric constant was

desirable for miniaturization of the antenna element. Proposed new compositions were made by mixing suitable ceramics and polymers. Polyphenylene-Sulfide (PPS) was selected as a polymer matrix because of low losses and low moisture absorption. The first composite was created by adding Strontium-Titanate ceramic into PPS matrix providing a high dielectric constant and low loss tangent at a relatively low composition volume. The Strontium-Titanate/PPS composition could not satisfy the desired temperature compensation. Measurement results of frequency drift made on manufactured microstrip patch antennas on this composition showed a 4% frequency drift at the temperature of $100℃$. Hence, despite a good electrical characteristic, this composition was not satisfactory. This dissatisfaction was attributed to a large negative temperature coefficient of the Strontium-Titanate composition. To compensate for this effect in the PPS-Strontium-Titanate composition, new ceramic was added. Mica and Alumina, which both possess a positive temperature coefficient of dielectric constant were used. By fine-tuning of the new composition: Strontium Titanate/Mica/PPS, it was possible to accomplish $\pm$ 0.8 % variation in dielectric constant over $-50℃$ to $+100℃$ temperature range. Loss tangent of this new composition was not influenced by temperature variations. By adding more Mica into the composition, a better temperature compensation could be achieved. Mica had an advantage over Alumina due to its lower coefficient of thermal expansion for an equal volume of alumina, which helped Mica filled substrates to better match their temperature expansion coefficient with copper. For the experimental validation, 50 rectangular microstrip patch antennas were fabricated and measured. Measurement results showed the resonant frequency variation ofaround $1\%$ in $-40℃$ to $+100℃$ temperature range.

The patent [22] proposed a passive technique for the compensation of resonant frequency of microstrip patch antennas over a range of temperatures. This passive method for compensating the resonant frequency change overcomes the shortcomings of active compensation method. The active compensation method based on connecting high-Q GaAs varactor diodes at one of the antenna radiating edges is expensive and requires a thick substrate for the accommodating diode. This also requires an additional power supply to bias the diode and to vary its capacitance for the purpose of the resonant frequency compensation. The passive compensation method emphasizes microstrip antennas made on Teflon-based substrates. In these structures, resonant frequency tends to be increased along with an increase in temperature due to the dominance of the negative coefficient of substrate permittivity over copper thermal expansion. The proposed passive

compensation scheme is relatively inexpensive and based on the use of temperature dependent capacitors. The bi-metallic plate capacitors are adjusted on the radiating edges of the microstrip antenna. A change in capacitive loading due to temperature results in a variation of the effective electrical size of patch element, resulting in frequency compensation.

None of these researches quantify or provide equations for the temperature-compensated MPA. In this thesis along with the proposed design methodology for temperature-compensated MPA, the temperature impact on a resonant frequency of fundamental and high order modes is quantified and mathematically described.

Despite a lack of literature in temperature compensation techniques for resonant frequency of MPA, numerous compensation techniques are available for resonant cavities and filters [23] [24] [25]. Some of compensation techniques use different materials to preserve a cavity size with temperature variations [26], while other use field perturbation techniques [27]. These techniques can serve as a guideline for temperature compensation MPA, as microstrip antenna can be modelled as a resonant cavity [16] [14].

A reference of interest [23] is a starting point for developing theory in this thesis. This research deals with substrate integrated waveguide (SIW) cavities and filters. A new temperature compensation technique based on adequate substrate properties selection, providing self-temperature frequency drift compensation was proposed and demonstrated. In order to accomplish this, an appropriate ratio between the coefficient of thermal expansion of copper and the thermal coefficient of substrate dielectric constant was utilized. From the theoretical analysis presented in this work, it is possible to accomplish a complete temperature compensation when the thermal coefficient of dielectric constant reaches nearly two times the copper's thermal expansion coefficient, but opposite in sign. Experimental validation of that conclusion was done by manufacturing three cavities with different materials and by one microstrip and SIW fourth-order filter. The cavities were designed to operate at the frequency of $10\,GHz$. To ensure the same conditions for all cavities, they were designed to have the same coupling and the same number of via-holes. Cavities and filters were measured over the $-40℃$ to $+80℃$ temperature range. Substrates used in this experimental validation were RT/Duroid 6002, RT/Duroid 6010 and TMM10. Substrate RT/Duroid 6002 was used as a reference for assessing the compensation technique as it has the minimal temperature coefficient of permittivity among all substrates. Hence,

it should cause the minimum frequency drift. The substrate RT/Duroid 6010 has the largest variations in dielectric constant. Substrate TMM10 was used to verify the compensation technique as it nearly satisfies the compensation condition. All of these substrates have expansion coefficient that matches copper's expansion coefficient. The inconsistency between manufacturer's data and the real values of substrate electrical parameters, as well as the lack of information regarding their behaviour with temperature were stressed as one of the design and accurate analysis problems. The experiments revealed that cavities fabricated on TMM10 had the best stability in overall temperature range even better than RT/Duroid 6002 with the lowest temperature coefficient of dielectric constant and permittivity among all used substrates. The obtained frequency drift for TMM10 was $8\,ppm/℃$. Cavities manufactured on other materials exhibited frequency drift: $54\,ppm/℃$ for RT/Duroid 6002 and $273\,ppm/℃$ for RT/Duroid 6010. These experimental results were in good agreement with theoretically predicted ones: $2\,ppm/℃$ for TMM10, $22\,ppm/℃$ for RT/Duroid 6002 and $188\,ppm/℃$ for RT/Duroid 6010. The reason for the difference between the measurement and predicted results was an inconsistent and non-precise parameters value specified by the manufacturer. Experimental results carried out for the SIW, and a coupled-line microstrip filters also validated the compensation technique. Frequency variations were larger for microstrip filter due to condensation and moisture absorption that strongly affects the losses of microstrip lines. SIW structure was less sensitive on moisture absorption due to closed architecture, showing a very low temperature drift compared to its microstrip counterpart.

## 2.2 Frequency Regulations and Frequency Band Selection

Selecting appropriate operating frequency band is of crucial importance for the targeted project application. The importance of the frequency selection is presented as a brief review.

In early 1912, the need for frequency spectrum regulation raised for the first time due to congestion in the use of wireless telecommunication at sea [28]. During that time in the United States, the Secretary of Commerce was given right of administrating and licensing radio stations. However, with the emergence of broadcast radio, this framework did not work well, causing interference between radio stations in the broadcast market. Reason for that was recognized as de facto possession of frequency spectrum: the each first broadcaster in any given frequency band automatically owned a full right on that band [28]. Hence, it was necessary for more precise frequency spectrum regulations. As a final word on this problem in 1927, U.S. Congress passed the Radio Act bill under which *Federal Communications Commission* (FCC) was established. This regulatory body has the highest responsibility for the managing frequency spectrum, granting licensing, control users of radio spectrum and so on.

All other countries around the world followed this model of FCC in establishing their national regulatory agency to control and manage frequency spectrum.

For the purpose of harmonization, i.e. establishing the same frequency rules, regulations, protocols and standards all around the world, coordination between national regulatory agencies is done by the *International Telecommunication Union* (ITU). ITU is a specialized agency of *United Nations* (UN) and the member of UN *Development Group*, intended for information and communication technologies [29] [30]. ITUs main tasks are [29]:

- Coordination of global frequency spectrum usage
- Allocation of satellite orbits
- Developing and assistance in technical standards
- Striving for improvement in access to information and communication technologies

Once in every three years, ITU organizes the *World Radiocommunication Conference* (WRC) toward the world consensus on radio regulations [28]. Besides WRC, ITU also organizes

exhibitions and forums to bring together representatives of government and industry for exchanging experiences, ideas, knowledge and technology [29] [30].

From this review, we can understand the importance and intention dedicated to frequency spectrum utilization. Hence, the primary purpose is to avoid interference between devices which operate within the same or adjacent frequency bands, ensuring quality operation and service.

For this project, the frequency bands of interest are *Industrial, Scientific and Medical* (ISM) bands. These bands are unlicensed [28]. Unlicensed means that product intended for these bands do not need require a license from the telecommunication regulatory authorities. However, unlicensed does not mean unregulated, and devices need to meet strict regulations. Some of the regulations [31] imposed by regulatory agencies are presented below for the reference:

- "Operating frequency
- Bandwidth
- Radiated power (depends on the frequency range, specific application, services and systems already used or planned to be used in these bands)
- Spurious emission
- Modulation methods
- Transmission duty cycles", [31].

Regarding definition, these bands are reserved for industrial, scientific and medical purposes other than telecommunications [31]. It means that radio communication services operating within these bands must accept harmful interference from ISM devices [30]. ISM bands are defined under ITU Radio Regulations (Article 5) in footnotes *5.138, 5.150* and *5.280* of the Radio Regulations, and they are summarized in Table 2.1.

Table 2.1 - ISM frequency bands

| Frequency band [MHz] | Centre frequency $f_c$ [MHz] |
|---|---|
| 6.765-6.795 | 6.78 |
| 433.05-434.79 | 433.92 |
| 61000-61500 | 61250 |
| 122000-123000 | 122500 |
| 244000-246000 | 245000 |
| 13.553-13.567 | 13.56 |
| 26.957-27.283 | 27.12 |
| 40.66-40.7 | 40.68 |
| 902-928 | 915 |
| 2400-2500 | 2450 |
| 5725-5875 | 5800 |
| 24000-24500 | 24125 |

The frequencies in the green part of the table are intended for ISM devices under special conditions and provisions. They must not affect existing radio communication services in those bands [31].

The frequencies in the second part of table coloured orange are free for usage by radio communication services which must accept harmful interference caused by ISM appliances and they are not protected by a regulatory body [31].

In European Union (EU), the organization responsible for governing frequency spectrum is *European Telecommunication Standards Institut* (ETSI), recognized by EU as European Standardization Organization [31]. Unlike for North America's regulations, in EU there is one special category called *Short Range Devices* (SRD). SRD are low power radio communication systems with a typical range of operation up to 100 meters [31]. The well-known RFID systems belong to this SRD category. SRD has low capacity to interfere other communication equipment, which makes them licence free. It is very important to stress that under the meaning of ITU Radio Regulations (Article 1), SRD are not considered a Radio Service. Exactly, there is no definition for SRD devices under ITU Radio Regulations. However, under EU's regulations for most efficient implementation of these devices the following categories [31] are recommended:

- "Non-specific short-range devices
- Tracking, tracing and data acquisition

- Wideband data transmission systems
- Railway applications
- Alarms
- Inductive applications
- RFID
- Wireless audio applications
- Radio microphones
- Radio determination
- Road Transport and traffic telematics", [31].

Use of SRD bands is governed by *ERC Recommendation 70-03* [32]. This recommendation sets out spectrum management requirements to allocate frequency bands, maximum radiated power, modulation type, occupied bandwidth, duty cycles and important technical parameters for SRD devices.

A very important fact for this project stated in *ERC Recommendation 70-03* is cited here:

"The CEPT has considered the use of SRD devices on board aircraft and it has concluded that, from the CEPT regulatory perspective, such use is allowed under the same conditions provided in the relevant Annex of Recommendation 70-03. For aviation safety aspects, the CEPT is not the right body to address this matter which remains the responsibility of aircraft manufacturers or aircraft owners who should consult with the relevant national or regional aviation bodies before the installation and use of such devices on board aircraft [32]."

ITU Radio Regulations under Article 15, also touches issue regarding aircraft safety regarding frequencies. Footnote 15.8 states:

"Special consideration shall be given to avoiding interference on distress and safety frequencies, those related to distress and safety identified in Article 31 and those related to safety and regularity of flight identified in Appendix 27. (WRC - 07) [30]"

Onboard aircraft SRDS must obey both radio and aeronautical regulations. Radio regulations are responsible for devices to meet national or regional requirements, regarding radiated power and

potential impact on other services, while aeronautical regulations make sure that these devices will not cause a safety hazard to aircraft. As stated in *ERC Recommendation 70-03*, SRDs used inside or outside the aircraft if met the specified operational and technical conditions; there are no additional radio regulatory issues. However, radio regulations do not affect the responsibility of aviation body who issue safety flight certification. Hence, the radio regulations should not be seen as approval for operation until the safety certification is issued.

*International Civil Aviation Organization* (ICAO) has issued the following statement regarding SRD usage:

"Oppose operation of short-range devices in any bands allocated to aeronautical services. Support the inclusion in the Radio Regulations of appropriate regulatory provisions to ensure that short-range devices, operating outside of aeronautical bands, do not cause harmful interference to aeronautical systems operating in allocated aeronautical bands. [33]"

As a final word on using SRDs on-board aircraft, the following citation will be summarized:

"To use SRDs on board aircraft, regulators may allow usage under conditions; however, for aviation safety aspects, the right bodies to address this matter remains the responsibility of aircraft manufacturers or aircraft owners who should consult with ICAO, the relevant regional and national bodies, before installing SRDs on aircraft. [34]"

Taking into considerations all the above facts regarding SRD and ISM devices, comparing appropriate frequency bands in Canada, United States and European Union, it appears that the most appropriate bands for usage are in $2.4\ GHz$ frequency range.

# CHAPTER 3 TEMPERATURE COMPENSATED MICROSTRIP PATCH ANTENNA

## 3.1 Introduction

This chapter contains the main contribution to this thesis work. At the beginning of the chapter, the characteristics of MPA are reviewed, and followed by a mathematical formulation of temperature impact on fundamental and high order modes of rectangular, circular, and triangular MPA. Theoretically obtained results for resonant frequency drift are shown, compared and discussed. Drawn conclusions from the theoretically obtained results for frequency drift are verified by electromagnetic simulator-based simulations. Performed simulations support the formulated theory. In addition to electromagnetic simulations, an accurate circuit model for analysing the temperature impact on resonant frequency of MPA is proposed. According to the resonant frequency drift results the optimal substrates for an antenna design are selected. Conducted tolerance analysis emphasizes the key parameters which affect a resonant frequency temperature behavior for rectangular, circular, and triangular MPA. The resonant frequency temperature compensation condition is derived based on the mathematically formulated temperature dependence of the resonant frequency. Experiments are conducted in support of the results derived through the theoretical work and simulations.

## 3.2 Microstrip Patch Antenna Characteristics

Microstrip patch antenna is one of the simplest radiating structures [15] [35]. It is a resonant structure made of electrically thin dielectric sheet with patch metallization on one and ground on the other side [14]. The patch can take any shape but commonly used ones are rectangular, circular, and triangular. It consist of a very thin metallization $t \ll \lambda_0$ and substrate thickness - a small fraction of wavelength $0.003\lambda_0 \leq h \leq 0.05\lambda_0$, where $\lambda_0$ is free space wavelength [15]. Based on the substrate thickness, microstrip antennas can be divided into electrically thin and electrically thick antennas $h \geq 0.02\lambda_0$ [15]. For the substrate thicknesses of $h \geq 0.11\lambda_0$ coaxial-probe feed microstrip antenna ceases to resonate due to the inductive effect of the feed [36]. Dielectric substrate materials with a dielectric constant in the range $2 \leq \varepsilon_r \leq 12$ are widely used for the patch antennas. Considering the radiation efficiency, materials with lower dielectric constant are preferred over materials in the upper dielectric constant range due to lower dielectric losses and

better performances of antenna [14] [15] [16]. Materials with a higher dielectric constant are suitable for the microstrip antenna miniaturization at the cost of radiation efficiency. Since the rectangular MPA is a starting point for the theory derived in this thesis, its geometry is shown in Figure 3.1.

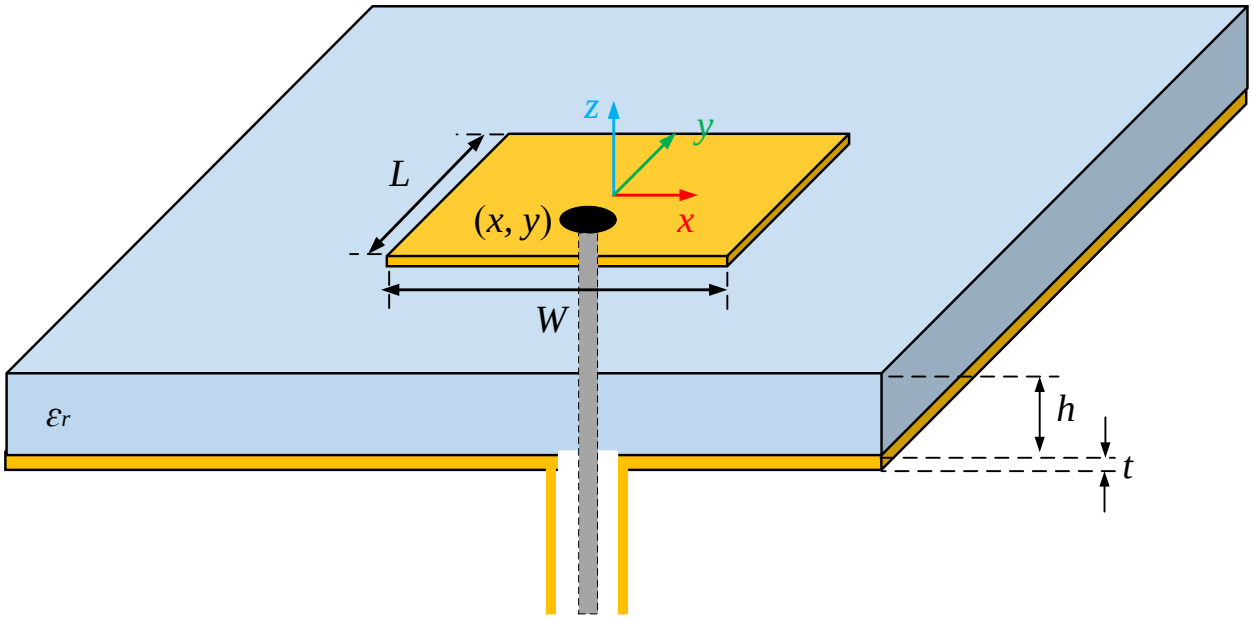


Figure 3.1 - Rectangular MPA geometry

Although MPAs are characterized by compactness and versatility, compared with other antenna structures they are not optimal in terms of electrical properties. Nevertheless, MPAs offer a lot of advantages over other radiating structures. Some of the advantages and disadvantages are listed below [13] [14] [15].

Advantages:

- low profile
- conformable to planar and non-planar surfaces
- simple and inexpensive
- mechanically robust
- compatible with MMIC design

- versatile in terms of polarization and radiation pattern
- light weight
- easy to fabricate and integrate with active devices
- reproducible and
- flexible design

Disadvantages:

- narrow frequency bandwidth
- low efficiency
- low power handling
- poor polarisation purity
- spurious feed polarization

Narrow bandwidth of such structures triggered the researchers to develop various analytical techniques and models to accurately predict antenna's resonant frequency and behaviour. The numerous proposed models can be divided into numerical (MoM, FEM, FDTD, SDA, Variational Techniques etc.) and analytical (Transmission-line model and Cavity model) models. The numerical techniques are very accurate and versatilely used to design and analyse MPA, but they involve an execution of complex codes on a computer system, demanding greater computational time and memory. Also, they do not give any physical insights unlike analytical techniques. The analytical techniques are suitable for CAD tools for a quick estimation of antenna's characteristics, behaviour and optimisation but they are less accurate and versatile compared to their numerical counterpart. Transmission-line model is the simplest one when compared to others; it is satisfyingly accurate and provides a very good physical insight [15]. Transmission-line model in its fundamental form cannot be used to analyze higher order modes (except fundamental mode harmonics) and arbitrary shaped patches (patches of a shape other than rectangular), but with minor modifications it is suitable for arbitrary shaped patches [37] [38] [39] [40] [41] as well as for multi-layered structures [42] [43].

## 3.3 Mathematical Formulation of Temperature Impact on MPA's Resonant Frequency – Frequency Drift

This section provides a mathematical expression of the temperature impact on the resonant frequency behaviour of a rectangular, circular and triangular MPA. The first three subsections describe the temperature dependence of MPA's resonant frequency for rectangular, circular, and triangular patch geometries. MPA are fabricated on different substrates and different substrate thicknesses in terms of particular parameters. The last subsection summarizes and compares results from the previous subsections for the substrates that allow antennas to exhibit the best resonant frequency behaviour.

### 3.3.1 Rectangular MPA Frequency Drift

The resonant frequency drift of the rectangular MPA on different substrates, substrate thicknesses and resonant frequencies for the fundamental mode and its harmonics is mathematically described and discussed. A derived theory is verified through simulations in CST electromagnetic simulator software.

#### 3.3.1.1 Mathematical Formulation

The resonant frequency of rectangular microstrip patch antenna (RMPA) in its fundamental $TM_{10}$ mode is given by:

$$f_r = \frac{c}{2(L + 2X)\sqrt{\varepsilon_e}} \tag{1}$$

Due to clarity in following derivation in eqn.(1) $X$ denotes the patch length extension $\Delta L$ due to fringing field effect. The term in bracket represents the resonant effective length of a patch and also due to clarity in the following derivation the notation $L_e = L + 2X$ is introduced.

Representing eqn.(1) as a function of three variables $L, \varepsilon_e$ and $X$, the change in resonant frequency due to change in some of these variables can be found by applying incremental rule:

$$\Delta f_r = \frac{\partial f_r}{\partial L}\Delta L + \frac{\partial f_r}{\partial \varepsilon_e}\Delta \varepsilon_e + \frac{\partial f_r}{\partial X}\Delta X \tag{2}$$

Derivatives in eqn.(2) are given by:

$$\begin{aligned} \frac{\partial f_r}{\partial L} &= -\frac{f_r}{L_e} \\ \frac{\partial f_r}{\partial \varepsilon_e} &= -\frac{f_r}{2\varepsilon_e} \\ \frac{\partial f_r}{\partial X} &= -\frac{2}{L_e} f_r \end{aligned} \tag{3}$$

Substituting derivatives from eqn.(3) into eqn.(2), the incremental change in resonant frequency is obtained, eqn.(4):

$$\frac{\Delta f_r}{f_r} = -\frac{1}{L_e}\Delta L - \frac{1}{2\varepsilon_e}\Delta \varepsilon_e - \frac{2}{L_e}\Delta X \tag{4}$$

Equation eqn.(4) given in this form is impractical and useless. Equation eqn.(4) has to be reduced to a suitable form in terms of design and temperature parameters.

For the effective dielectric constant $\varepsilon_e$ in eqn.(1) the frequency dependence is assumed, which is given by eqn.(5):

$$\varepsilon_e = \varepsilon_r - \frac{\varepsilon_r - \varepsilon_{e0}}{1 + P} \tag{5}$$

$\varepsilon_{e0}$ – is a quasi-static effective dielectric constant given by eqn.(6)

$P$ – is a frequency dependent term specified in [44]

Of all existing equations for a quasi-static effective dielectric constant, the simplest one is used, without affecting the final result.

$$\varepsilon_{e0} = \frac{(\varepsilon_r + 1)}{2} + \frac{(\varepsilon_r - 1)}{2} \frac{1}{\sqrt{(1 + 12\frac{h}{W})}} \tag{6}$$

Given eqn.(6) is valid for the fundamental mode and its harmonics imposing in that way a validity constrain on a final result.

Small increment $\Delta\varepsilon_e$ in effective dielectric constant $\varepsilon_e$ given by eqn.(5) under approximation $P$ term as a constant, can be found as:

$$\Delta\varepsilon_e = \frac{\partial\varepsilon_e}{\partial\varepsilon_r}\Delta\varepsilon_r + \frac{\partial\varepsilon_e}{\partial\varepsilon_{e0}}\Delta\varepsilon_{e0} \tag{7}$$

Derivatives in eqn.(7) are given by:

$$\begin{aligned} \frac{\partial\varepsilon_e}{\partial\varepsilon_r} &= 1 - \frac{1}{1+P} \\ \frac{\partial\varepsilon_e}{\partial\varepsilon_{e0}} &= \frac{1}{1+P} \end{aligned} \tag{8}$$

The incremental change in quasi-static effective dielectric constant based on eqn.(6) is:

$$\Delta\varepsilon_{e0} = \frac{\partial\varepsilon_{e0}}{\partial\varepsilon_r}\Delta\varepsilon_r + \frac{\partial\varepsilon_{e0}}{\partial W}\Delta W + \frac{\partial\varepsilon_{e0}}{\partial h}\Delta h \tag{9}$$

Derivatives in eqn.(9) are given by:

$$\frac{\partial \varepsilon_{e0}}{\partial \varepsilon_r} = \frac{1}{2}\left[1 + \frac{1}{\sqrt{\left(1 + 12\frac{h}{W}\right)}}\right]$$

$$\frac{\partial \varepsilon_{e0}}{\partial W} = 3(\varepsilon_r - 1)\frac{h}{W^2}\frac{1}{(1 + 12\frac{h}{W})\sqrt{(1 + 12\frac{h}{W})}} \tag{10}$$

$$\frac{\partial \varepsilon_{e0}}{\partial h} = -3(\varepsilon_r - 1)\frac{1}{W}\frac{1}{(1 + 12\frac{h}{W})\sqrt{(1 + 12\frac{h}{W})}}$$

Due to clarity in the following derivation and derived equations readability, the next notation is introduced:

$$A = 3(\varepsilon_r - 1)\frac{1}{(1 + 12\frac{h}{W})\sqrt{(1 + 12\frac{h}{W})}} \tag{11}$$

$$\frac{\partial \varepsilon_{e0}}{\partial \varepsilon_r} = k$$

The next term which has to be determined in eqn.(4) is the increment of the patch length extension due to fringing field effect, $\Delta X$. Equation used for the patch length extension eqn.(12) is not currently the most accurate, but it is suitable for calculations (carrying out maths).

$$\Delta L = X = 0.412h\frac{(\varepsilon_e + 0.3)(\frac{W}{h} + 0.264)}{(\varepsilon_e - 0.258)(\frac{W}{h} + 0.813)} \tag{12}$$

Representing eqn.(12) as a function of three variables $\varepsilon_e, W$ and $h$, a small increment $\Delta X$ in the patch length extension due to fringing field effect $X$ can be found as:

$$\Delta X = \frac{\partial X}{\partial \varepsilon_e}\Delta\varepsilon_e + \frac{\partial X}{\partial W}\Delta W + \frac{\partial X}{\partial h}\Delta h \tag{13}$$

Derivatives in eqn.(13) are given by:

$$\frac{\partial X}{\partial \varepsilon_e} = -\frac{C_{xe}}{2(\varepsilon_e - 0.258)^2}$$

$$\frac{\partial X}{\partial W} = C_{xw}\frac{0.6}{h(\frac{W}{h} + 0.813)^2} \tag{14}$$

$$\frac{\partial X}{\partial h} = C_{xh}\frac{0.2\left(\frac{W}{h} + 0.813\right) + \frac{W}{h}(\frac{W}{h} + 0.2)}{(\frac{W}{h} + 0.813)^2}$$

with coefficients:

$$C_{xe} = 0.412h\frac{(\frac{W}{h} + 0.264)}{(\frac{W}{h} + 0.813)}$$

$$C_{xw} = 0.412h\frac{(\varepsilon_e + 0.3)}{(\varepsilon_e - 0.258)} \tag{15}$$

$$C_{xh} = \frac{(\varepsilon_e + 0.3)}{(\varepsilon_e - 0.258)}$$

Substituting equations eqn.(7) to eqn.(14) into eqn.(4) the fractional change in the resonant frequency due to change in some of design parameters $L$, $\varepsilon_r$ and $h$ is obtained and given by eqn.(16).

$$\frac{\Delta f_r}{f_r} = -\frac{\Delta L}{L_e} + \left(\frac{C_{xe}}{L_e(\varepsilon_e - 0.258)^2} - \frac{1}{2\varepsilon_e}\right)\left\{K_p\Delta\varepsilon_r + A_p\left(\frac{h}{W^2}\Delta W - \frac{1}{W}\Delta h\right)\right\} \tag{16}$$

$$-\frac{2}{L_e}\{0.6\frac{C_{xw}}{h\left(\frac{W}{h}+0.813\right)^2}\Delta W + C_{xh}\frac{0.2\left(\frac{W}{h}+0.813\right)+\frac{W}{h}(\frac{W}{h}+0.2)}{(\frac{W}{h}+0.813)^2}\Delta h\}$$

where $K_p$ and $A_p$ coefficients are:

$$K_p = 1 - \frac{1-k}{1+P}$$

$$A_p = \frac{A}{1+P}$$

Increments $\Delta\varepsilon_r, \Delta L,\ \Delta W$ and $\Delta h$ due to temperature have a linear dependence and are given by:

$$\begin{aligned}\Delta\varepsilon_r &= \varepsilon_r(1+\delta_r\Delta T)\\ \Delta h &= h(1+\delta_z\Delta T)\\ \Delta L &= L(1+\delta_c\Delta T)\\ \Delta W &= W(1+\delta_c\Delta T)\end{aligned} \tag{17}$$

where $\delta_r -$ is a temperature coefficient (TC) of substrate permittivity, $\delta_z -$ coefficient of temperature expansion (CTE) of substrate thickness, and $\delta_c -$ CTE of copper.

Substituting eqn.(17) into eqn.(16) the resonant frequency drift over temperature is obtained and given by eqn.(18):

$$\begin{aligned}\frac{\Delta f_r}{f_r\Delta T} &= -\frac{L}{L_e}\delta_c + \left(\frac{C_{xe}}{L_e(\varepsilon_e-0.258)^2}-\frac{1}{2\varepsilon_e}\right)\{K_p\varepsilon_r\delta_r + A_p(\delta_c-\delta_z)\}\\ &-\frac{2}{L_e}\{0.6\frac{C_{xw}}{\left(\frac{W}{h}+0.813\right)^2}\frac{W}{h}\delta_c + C_{xh}\frac{0.2\left(\frac{W}{h}+0.813\right)+\frac{W}{h}(\frac{W}{h}+0.2)}{(\frac{W}{h}+0.813)^2}h\delta_z\}\end{aligned} \tag{18}$$

It should be pointed out that eqn.(18) is valid for the fundamental mode and its harmonics due to constrain imposed by eqn.(6).

### 3.3.1.2 Numerical Results

The following figures, Figure 3.2 and Figure 3.3 represent the frequency drift obtained by eqn.(18) for rectangular MPAs designed to resonate at 915 MHz and 5.8 GHz, respectively. These two frequencies are chosen so as to indicate a hidden effect of eqn.(18). The frequency of 915 MHz is selected for a quasi-static case eqn.(18) while the frequency of 5.8 GHz is chosen for being illustrative enough to reveal the concealed effect. The frequency drift is given for rectangular MPAs designed on different substrates and substrate thicknesses in terms of the patch width to substrate thickness ratio, denoted by $u = \frac{W}{h}$. Among all commercially available substrates for antenna design, Figure 3.2 and Figure 3.3 present only the results for the MPAs designed on substrates that provide the best temperature performance of the resonant frequency drift.

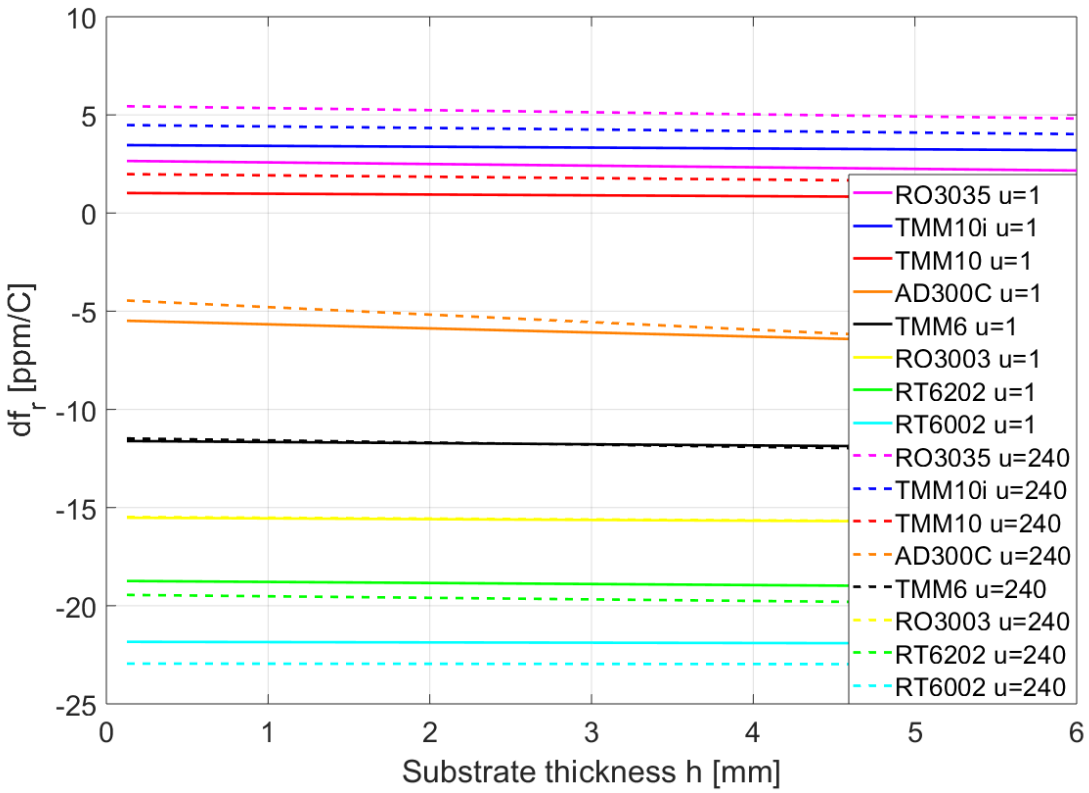


Figure 3.2 - Rectangular MPAs resonant at 915 MHz. Frequency drift for different antenna's substrate in terms of substrate thickness and patch geometry ratio - u

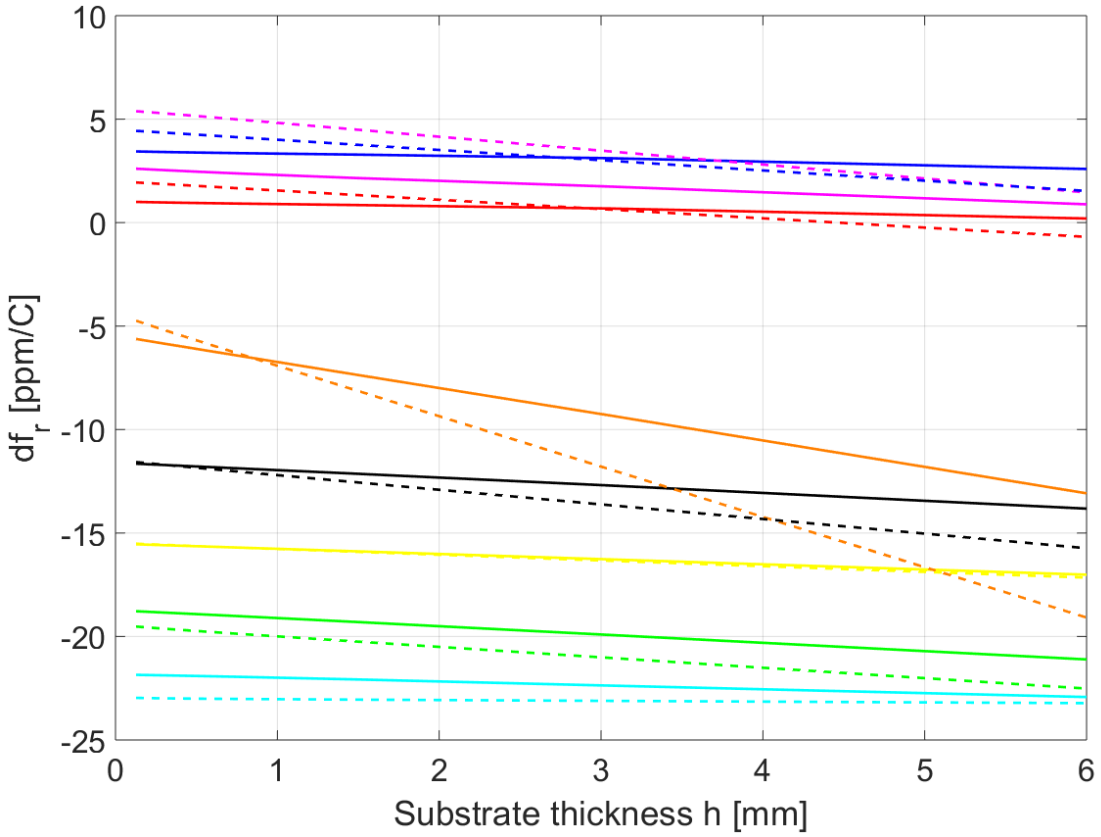


Figure 3.3 - Rectangular MPAs resonant at 5.8 GHz. Frequency drift for different antenna's substrate in terms of substrate thickness and patch geometry ratio – u

As seen in Figure 3.2 and Figure 3.3 the rectangular MPAs designed on TMM10, TMM10i, RO3035, and AD300C substrates show the best withstanding of the resonant frequency with temperature. The antennas designed on these substrates exhibit the smallest frequency drift. By carefully observing the curves in Figure 3.2 and even more so in Figure 3.3, it is noticeable that the curves' inclinations occur with an increase in the substrate thickness. All substrate curves follow the same trend. With an increasing in substrate thickness the resonant frequency drift becomes smaller only for TMM10, TMM10i, and RO3035 substrates. Also the rectangular MPAs designed with a smaller patch width to substrate thickness ratio $u = 1$ exhibit better temperature behaviour, although not much better than wider patch antennas, $u = 240$. On a closer inspection, the first two terms of eqn.(18) are substrate thickness $h$ independent, while the third term is thickness dependent, causing the inclination in the resonant frequency drift curves with increasing substrate thickness. The third term of the equation comes from the patch length extension due to the fringing field

effect. That term is identified as the only term with the substrate thickness dependence, thus causing the observed inclination in the resonant frequency drift curves. This effect is more pronounced at higher frequencies. Without accounting the fringing field effect in eqn.(1) the frequency drift would be thickness independent. Therefore, the fringing field effect has a positive impact on the resonant frequency drift for the MPA designed on TMM10, TMM10i, and RO3035 substrates.

The following figures, Figure 3.4, Figure 3.5, Figure 3.6 show the resonant frequency drift for the quasi-static case in terms of the patch width to substrate thickness ratio $u = \frac{W}{h}$, for different substrate thicknesses. The rectangular MPAs are designed to resonate at 915 MHz on the three substrates for which antennas exhibit the best temperature performance. The substrates are TMM10, RO3035, and TMM10i.

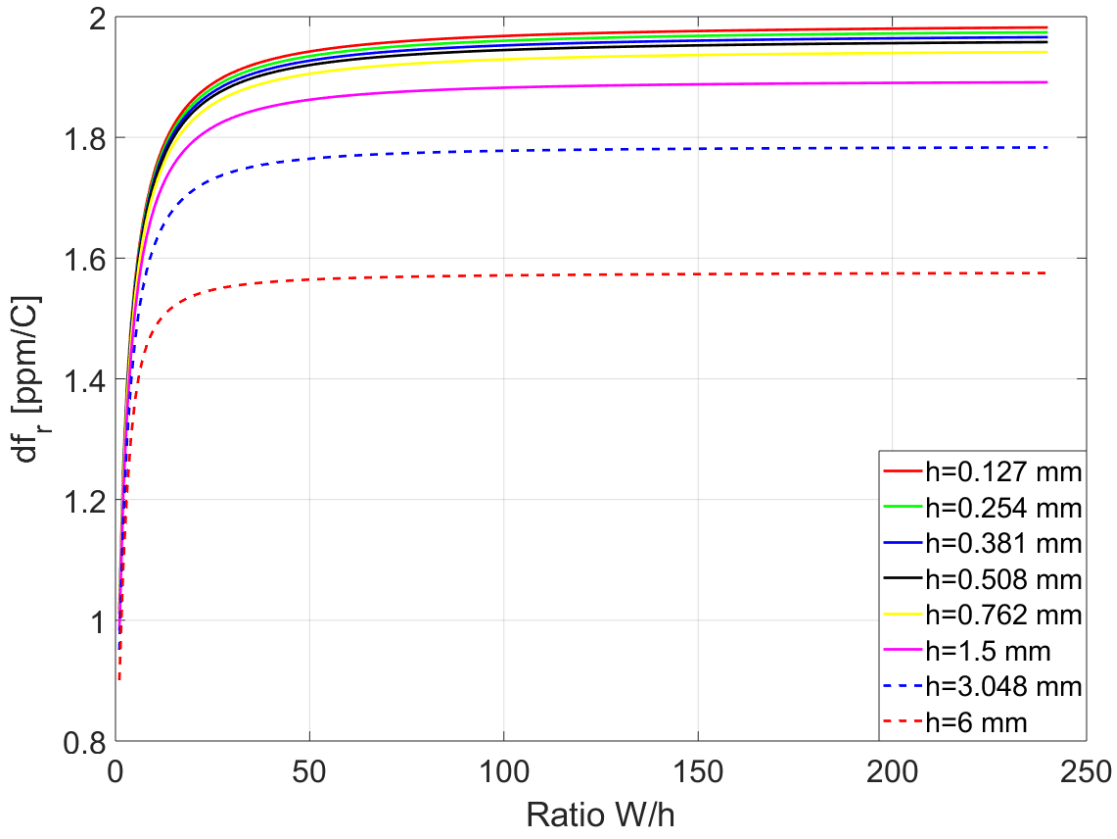


Figure 3.4 - Frequency drift for rectangular MPAs resonant at 915 MHz on TMM10 substrate

Figure 3.4 shows the resonant frequency drift for the rectangular MPAs designed on TMM10 substrate in terms of the patch width to substrate thickness ratio, for different substrate thickness values. Observing the results plotted in Figure 3.4 it can be revealed that the frequency drift for the antennas designed on substrate thicknesses of up to $h = 1.5\ mm$ is seamlessly small regardless of the patch width to substrate thickness ratio, $u$. For the rectangular MPA designed on a substrate with thickness of $h = 3\ mm$, the frequency drift curve is distinguishable from characteristics of substrates with lower thicknesses, but there is still a very small difference between them. The real difference between the resonant frequency drift curves can be observed in the curve of the MPA designed at the thickness of $h = 6\ mm$. The difference between curve with the parameter of $h = 6\ mm$ and the curve of $h = 0.127\ mm$ is approximately $0.4\ ppm/℃$.

Figure 3.5 shows the frequency drift for the rectangular MPAs designed on RO3035 substrate.

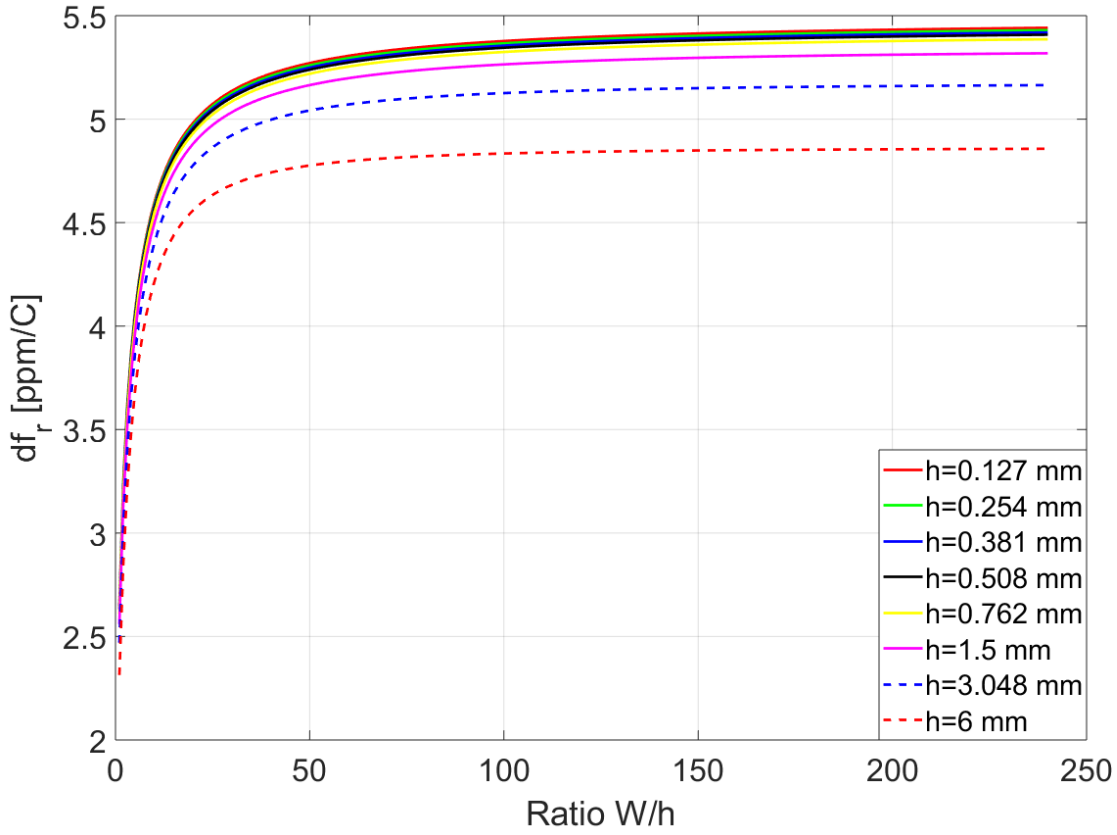


Figure 3.5 - Frequency drift for rectangular MPAs resonant at 915 MHz on RO3035 substrate

By careful observing the curves in Figure 3.5, the same conclusion for the frequency drift can be drawn for the MPA designed on TMM10 substrate. The rectangular MPAs designed on the substrate of up to $h = 1.5\ mm$ in substrate thicknesses have negligible differences in frequency drift. The only real difference in frequency drift is between the MPAs designed on $h = 0.127\ mm$ and those on $h = 6\ mm$ substrates.

Figure 3.6 shows the frequency drift for rectangular MPAs designed on TMM10i substrate.

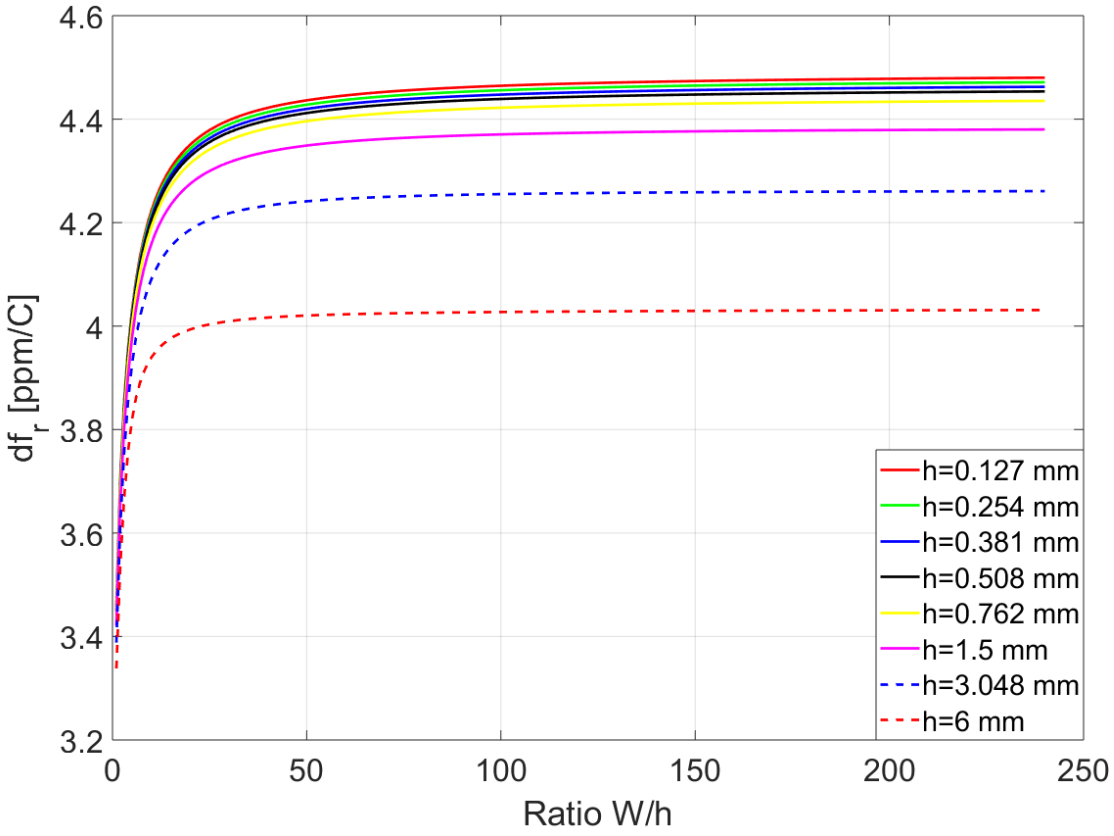


Figure 3.6 - Frequency drift for rectangular MPAs resonant at 915 MHz on TMM10i substrate

Observing curves in Figure 3.6, the same conclusion can be derived for the previous two substrates. The key characteristics of those three substrates are listed in Table 3.1. They are very similar to one other, except in dielectric permittivity.

Table 3.1 - The best substrates for rectangular MPA performance

| Coefficients | TMM10 | TMM10i | RO3035 |
|---|---|---|---|
| $\varepsilon_r$ | 9.2 | 9.9 | 3.6 |
| $\delta_r[ppm/°C]$ | -38 | -43 | -45 |
| $\delta_x\ [ppm/°C]$ | 21 | 19 | 17 |
| $\delta_y\ [ppm/°C]$ | 21 | 19 | 17 |
| $\delta_z\ [ppm/°C]$ | 20 | 20 | 24 |

## 3.3.2 Circular Disk MPA Frequency Drift

To determine a frequency drift of circular disk microstrip patch antenna (CMPA), a very accurate cavity model based on the dynamic dielectric constant is used, to study the temperature impact on higher order modes. The dynamic dielectric constant takes into account the influence of the inhomogeneous field distribution of different modes on the effective dielectric constant. Theoretically obtained results are compared and commented.

### 3.3.2.1 Mathematical Formulation

The resonant frequency of a CMPA is evaluated by using cavity model as discussed in [45] [46] and it is given here by eqn.(19).

$$f_r = \frac{\alpha_{nm} c}{2\pi r_e \sqrt{\varepsilon_d}} \tag{19}$$

where $\alpha_{nm} -$ is m$^{th}$ zero of the derivative of Bessel function of order n, $r_e -$ is an effective patch disk radius and $\varepsilon_d -$ is a dynamic dielectric constant.

Effective patch radius defined in [47] is given as follows:

$$r_e = r\sqrt{1 + \frac{2h}{\pi r \varepsilon_r}\left[\ln\left(\frac{r}{2h}\right) + (1.41\varepsilon_r + 1.77) + \frac{h}{r}(0.268\varepsilon_r + 1.65)\right]} \tag{20}$$

The resonant frequency eqn.(19) can be represented as a function of two variables: $r_e$ and $\varepsilon_d$.

Then, the incremental change in resonant frequency can be written in the form:

$$\Delta f_r = \frac{\partial f_r}{\partial r_e}\Delta r_e + \frac{\partial f_r}{\partial \varepsilon_d}\Delta \varepsilon_d \tag{21}$$

The derivatives in eqn.(21) are given by:

$$\begin{aligned} \frac{\partial f_r}{\partial r_e} &= -\frac{1}{r_e} f_r \\ \frac{\partial f_r}{\partial \varepsilon_d} &= -\frac{1}{2\varepsilon_d} f_r \end{aligned} \tag{22}$$

Substitution of eqn.(22) into eqn.(21) gives a fractional change in the resonant frequency:

$$\frac{\Delta f_r}{f_r} = -\frac{\Delta r_e}{r_e} - \frac{\Delta \varepsilon_d}{2\varepsilon_d} \tag{23}$$

An incremental change in effective disk radius can be found from eqn.(20) as following:

$$\Delta r_e = \frac{\partial r_e}{\partial \varepsilon_r}\Delta \varepsilon_r + \frac{\partial r_e}{\partial h}\Delta h + \frac{\partial r_e}{\partial r}\Delta r \tag{24}$$

The derivatives from eqn.(24) are given by:

$$\begin{aligned} \frac{\partial r_e}{\partial \varepsilon_r} &= -\frac{1}{2\sqrt{A}} \left\{ \frac{2h}{\pi \varepsilon_r^2} \left[ \ln\left(\frac{r}{2h}\right) + 1.77 + 1.65\frac{h}{r} \right] \right\} \\ \frac{\partial r_e}{\partial h} &= \frac{1}{2\sqrt{A}} \left\{ \frac{2}{\pi \varepsilon_r} \left[ \ln\left(\frac{r}{2h}\right) + (1.41\varepsilon_r + 0.77) + 2\frac{h}{r}(0.268\varepsilon_r + 1.65) \right] \right\} \end{aligned} \tag{25}$$

$$\frac{\partial r_e}{\partial r} = \sqrt{A} - \frac{1}{2\sqrt{A}} \left\{ \frac{2h}{\pi r \varepsilon_r} \left[ \ln\left(\frac{r}{2h}\right) + (1.41\varepsilon_r + 0.77) + 2\frac{h}{r}(0.268\varepsilon_r + 1.65) \right] \right\}$$

where coefficient $A$ is:

$$A = 1 + \frac{2h}{\pi r \varepsilon_r} \left[ \ln\left(\frac{r}{2h}\right) + (1.41\varepsilon_r + 1.77) + \frac{h}{r}\,(0.268\varepsilon_r + 1.65) \right]$$

Due to clarity and equation compactness the following notation is introduced:

$$\begin{aligned} R_{ER} &= \frac{\partial r_e}{\partial \varepsilon_r} \\ R_H &= \frac{\partial r_e}{\partial h} \\ R_R &= \frac{\partial r_e}{\partial r} \end{aligned} \tag{26}$$

Equations for dynamic dielectric constant are available in [45] for the first four modes.

The incremental change in the dynamic dielectric constant is defined by:

$$\Delta\varepsilon_d = \frac{\partial \varepsilon_d}{\partial \varepsilon_r}\Delta\varepsilon_r + \frac{\partial \varepsilon_d}{\partial h}\Delta h + \frac{\partial \varepsilon_d}{\partial r}\Delta r \tag{27}$$

The derivatives in eqn.(27) are given by:

$$\begin{aligned} \frac{\partial \varepsilon_d}{\partial \varepsilon_r} &= \frac{C_{DER}}{C_{D0}} \\ \frac{\partial \varepsilon_d}{\partial h} &= \frac{C_{DH}C_{D0} - C_{D0H}C_D}{C_{D0}^2} \end{aligned} \tag{28}$$

$$\frac{\partial \varepsilon_d}{\partial r} = \frac{C_{DR}C_{D0} - C_{D0R}C_D}{C_{D0}^2}$$

with coefficients:

$$\begin{gathered}
C_{D0} = r\left\{ m\varepsilon_0\pi u + \frac{2\varepsilon_0}{\delta}\left[\ln\left(\frac{u}{2}\right) + 3.11 + \frac{1.918}{u}\right]\right\} \\
C_{DER} = r[m\varepsilon_0\pi u + 1.41\varepsilon_0 + \varepsilon_0\frac{0.268}{u}] \\
C_D = r\{m\varepsilon_0\varepsilon_r\pi u + \varepsilon_0[\ln\left(\frac{u}{2}\right) + (1.41\varepsilon_r + 1.77) + \frac{0.268\varepsilon_r + 1.65}{u}]\} \\
C_{DH} = -m\varepsilon_0\varepsilon_r\pi u^2 - \varepsilon_0 u + \varepsilon_0(0.268\varepsilon_r + 1.65) \\
C_{D0H} = -m\varepsilon_0\pi u^2 - \varepsilon_0 u + 1.918\varepsilon_0 \\
C_{DR} = 2m\varepsilon_0\varepsilon_r\pi u + \varepsilon_0[\ln\left(\frac{u}{2}\right) + (1.41\varepsilon_r + 2.77)] \\
C_{D0R} = 2m\varepsilon_0\pi u + \varepsilon_0[\ln\left(\frac{u}{2}\right) + 4.11]
\end{gathered} \tag{29}$$

Substituting eqns. (24) to (29) into eqn.(23) the fractional resonant frequency change due to some of design parameters of a circular disk MPA is obtained and given by eqn.(30)

$$\begin{aligned}
\frac{\Delta f_r}{f_r} = -\left(\frac{R_{ER}}{r_e} + \frac{C_{DER}}{2\varepsilon_d C_{D0}}\right)\Delta\varepsilon_r - \left(\frac{R_H}{r_e} + \frac{C_{DH}C_{D0} - C_{D0H}C_D}{2\varepsilon_d C_{D0}^2}\right)\Delta h - (\frac{R_R}{r_e} \\
+ \frac{C_{DR}C_{D0} - C_{D0R}C_D}{2\varepsilon_d C_{D0}^2})\Delta r
\end{aligned} \tag{30}$$

Substituting $\Delta\varepsilon_r$ and $\Delta h$ from eqn.(17) into eqn.(30) along eqn.(31):

$$\Delta r = r(1 + \delta_c \Delta T) \tag{31}$$

gives the frequency drift of a circular disk MPA, eqn.(32):

$$\frac{\Delta f_r}{f_r \Delta T} = -\left(\frac{R_{ER}}{r_e} + \frac{C_{DER}}{2\varepsilon_d C_{D0}}\right)\varepsilon_r \delta_r - \left(\frac{R_H}{r_e} + \frac{C_{DH}C_{D0} - C_{D0H}C_D}{2\varepsilon_d C_{D0}^2}\right)h\delta_z - \left(\frac{R_R}{r_e} + \frac{C_{DR}C_{D0} - C_{D0R}C_D}{2\varepsilon_d C_{D0}^2}\right)r\delta_c \quad (32)$$

### 3.3.2.2 Numerical Results

The frequency drift of CMPA designed on different substrates in terms of disk radius to substrate thickness ratio for fundamental $TM_{11}$ mode is shown in Figure 3.7. As in the case of the rectangular MPA, the CMPA designed on TMM10, RO3035, and TMM10i, exhibit the best resonant frequency behaviour with temperature variations. Figure 3.7 indicates that for CMPA designed on TMM10 and RO3035 substrates the total resonant frequency compensation can be accomplished for a very small disk radius to substrate thickness ratio. However, such CMPA would not resonate. The resonant frequency determined by the radius of such antenna would be too high. At a very high frequency, the inductive effect of coaxial feed causes antenna to stop resonating.

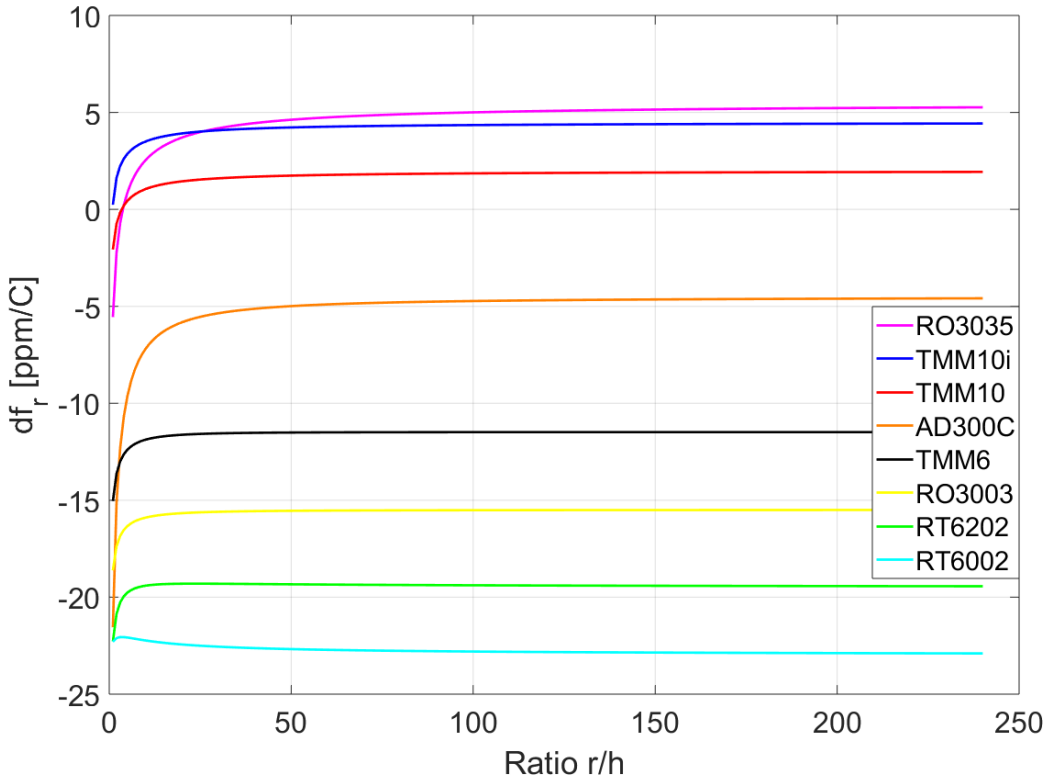


Figure 3.7 - Frequency shift for CMPAs designed on different substrates

The frequency drift values for CMAs designed on TMM10, RO3035 and TMM10i substrates are of the same order as for the rectangular MPAs. Due to fact that the ratio $u = \frac{r}{h}$ cannot be arbitrary chosen for CMAs, but it is dictated by resonant frequency, it is obvious from Figure 3.7 that frequency drift is constant in a large range of frequencies.

### 3.3.3 Equilateral Triangular MPA Frequency Drift

The frequency drift of triangular microstrip patch antenna (TMPA) is mathematically described and presented for the fundamental and higher order modes. Theoretically obtained results are compared and commented.

#### 3.3.3.1 Mathematical Formulation

The resonant frequency drift of the equilateral TMPA is derived in the same way as for the previous patch geometries and following the same. The resonant frequency of equilateral triangular MPA is quite accurately given by [48]:

$$f_r = \frac{2c}{3a_e\sqrt{\varepsilon_r}}\sqrt{m^2 + mn + n^2} \tag{33}$$

where $a_e -$ is effective side length, given by eqn.(34):

$$a_e = a + \frac{h}{\sqrt{\varepsilon_r}} \tag{34}$$

For eqn.(1) seen as function of two variables the incremental change in resonant frequency is:

$$\Delta f_r = \frac{\partial f_r}{\partial a_e}\Delta a_e + \frac{\partial f_r}{\partial \varepsilon_r}\Delta \varepsilon_r \tag{35}$$

The derivatives are:

$$\frac{\partial f_r}{\partial a_e} = -\frac{f_r}{a_e}$$
$$\frac{\partial f_r}{\partial a_e} = -\frac{f_r}{2\varepsilon_r} \tag{36}$$

Substituting the derivatives from eqn.(36) into eqn.(35) the fractional change of resonant frequency is obtained:

$$\frac{\Delta f_r}{f_r} = -\frac{\Delta a_e}{a_e} - \frac{\Delta \varepsilon_r}{2\varepsilon_r} \tag{37}$$

Regarding eqn.(34), an incremental change in side effective length can be written as:

$$\Delta a_e = \frac{\partial a_e}{\partial a}\Delta a + \frac{\partial a_e}{\partial h}\Delta h + \frac{\partial a_e}{\partial \varepsilon_r}\Delta \varepsilon_r \tag{38}$$

The derivatives are:

$$\frac{\partial a_e}{\partial a} = 1$$
$$\frac{\partial a_e}{\partial h} = \frac{1}{\sqrt{\varepsilon_r}} \tag{39}$$
$$\frac{\partial a_e}{\partial \varepsilon_r} = -\frac{h}{2\varepsilon_r\sqrt{\varepsilon_r}}$$

Substituting eqns. (36) to (39) into eqn.(35) the frequency drift of equilateral triangular MPA is obtained:

$$\frac{\Delta f_r}{f_r \Delta T} = -\frac{a}{a_e}\delta_c - \frac{h}{a_e\sqrt{\varepsilon_r}}\delta_z + \left(\frac{h}{2a_e\sqrt{\varepsilon_r}} - \frac{1}{2}\right)\delta_r \tag{40}$$

### 3.3.3.2 Numerical Results

The frequency drift for equilateral triangular MPAs designed on different substrates in term of the side length to substrate thickness ratio is shown in Figure 3.8.

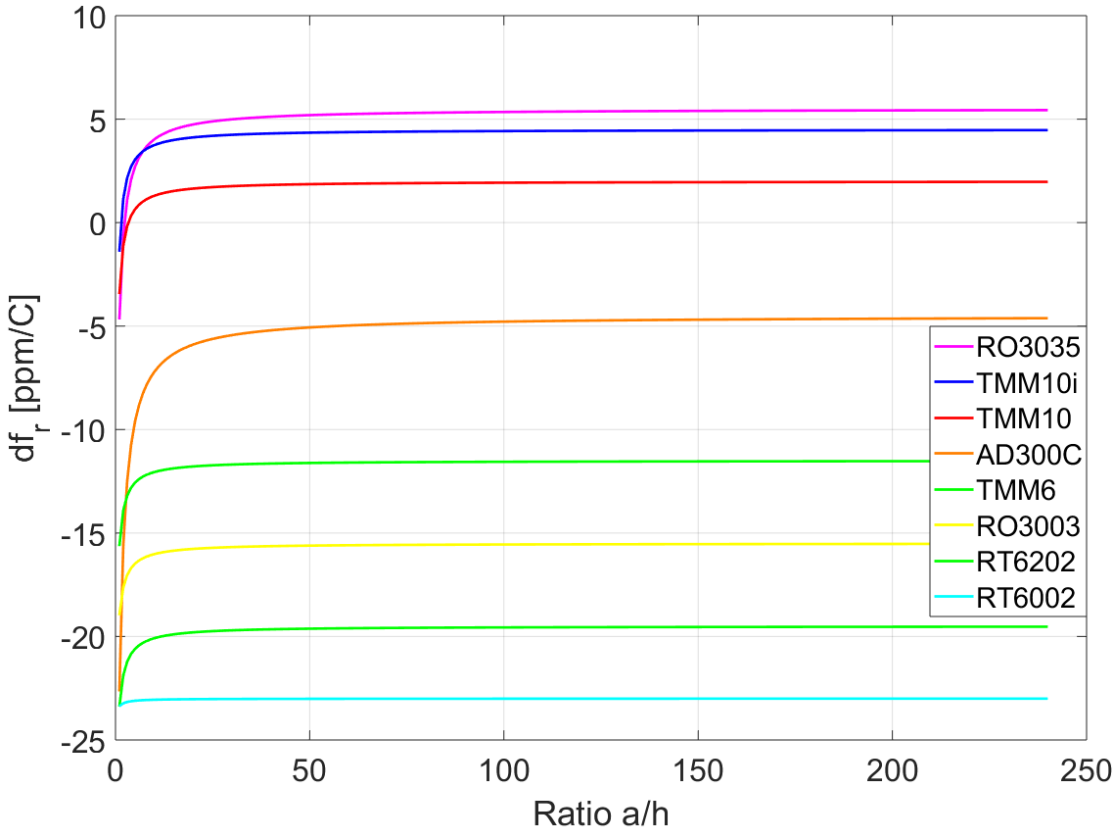


Figure 3.8 - Frequency drift of equilateral TMPAs designed on different substrate materials

As in the cases of RMPA and CMPA the equilateral TMPA designed on the TMM10, TMM10i and RO3035 substrates, show the best resonant frequency drift.

### 3.3.4 Summarizing RMPA, CMPA and TMPA Frequency Drifts

While analysing frequency drift behaviour, over 60 commercially available microwave substrates by vendors Rogers, Arlon, Taconic, DuPont, Polyflon, Aptek, Parc Electrochemical were examined. Of all substrates, the most appropriate for the antenna design in terms of antenna's resonant frequency temperature behaviour are selected and obtained results for MPA designed on them are shown in Figure 3.4, Figure 3.5, Figure 3.6. Among all microwave substrate vendors, the Rogers material specifications are presented in most details in datasheets. . In addition to providing data for the substrate thermal coefficient of the dielectric constant for most substrates, of Rogers' materials are better at performances than others and they offer a broader range of dielectric constant values. Most manufacturers do not provide information about substrate thermal coefficient of dielectric constant making it impossibly to test temperature impact and compensation technique for such substrates. In Table 3.2 there are substrate materials for which designed rectangular, circular, and triangular MPAs exhibit the best resonant frequency drift behaviour. The substrates are shown along their electrical and thermal parameters started from the best to the worst one.

Table 3.2 - Microwave substrates for analysing temperature impact on antenna resonant frequency

| | TMM 10 | TMM 10i | RO3035 | AD300C | TMM6 | RO3003 | RT/D 6202 | RT/D 6002 |
|---|---|---|---|---|---|---|---|---|
| $\varepsilon_r$ | 9.2 | 9.9 | 3.6 | 2.97 | 6.3 | 3 | 2.9 | 2.94 |
| $\delta_r$ $[ppm/°\mathrm{C}]$ | -38 | -43 | -45 | -25 | -11 | -3 | -15 | 12 |
| $\delta_x, \delta_y, \delta_z$ $[ppm/°\mathrm{C}]$ | 21/21/20 | 19/19/20 | 17/17/24 | 9/16/54 | 18/18/26 | 17/16/25 | 15/15/30 | 16/16/24 |

Comparing the frequency drift results from Figure 3.2, Figure 3.7 and Figure 3.8 for rectangular, circular, and equilateral triangular MPA, respectively, all antennas exhibit the best resonant frequency behaviour for TMM10, RO3035, TMM10i, and AD300C substrates with a very small difference between them. A reason for that will be more clearer in the following section, where a temperature compensation condition is derived. A rectangular MPA designed on TMM10 substrate exhibits somewhat better resonant behaviour compared with the other patch geometries. Figure 3.9 shows a comparison between frequency drifts of rectangular, circular, and triangular MPAs.

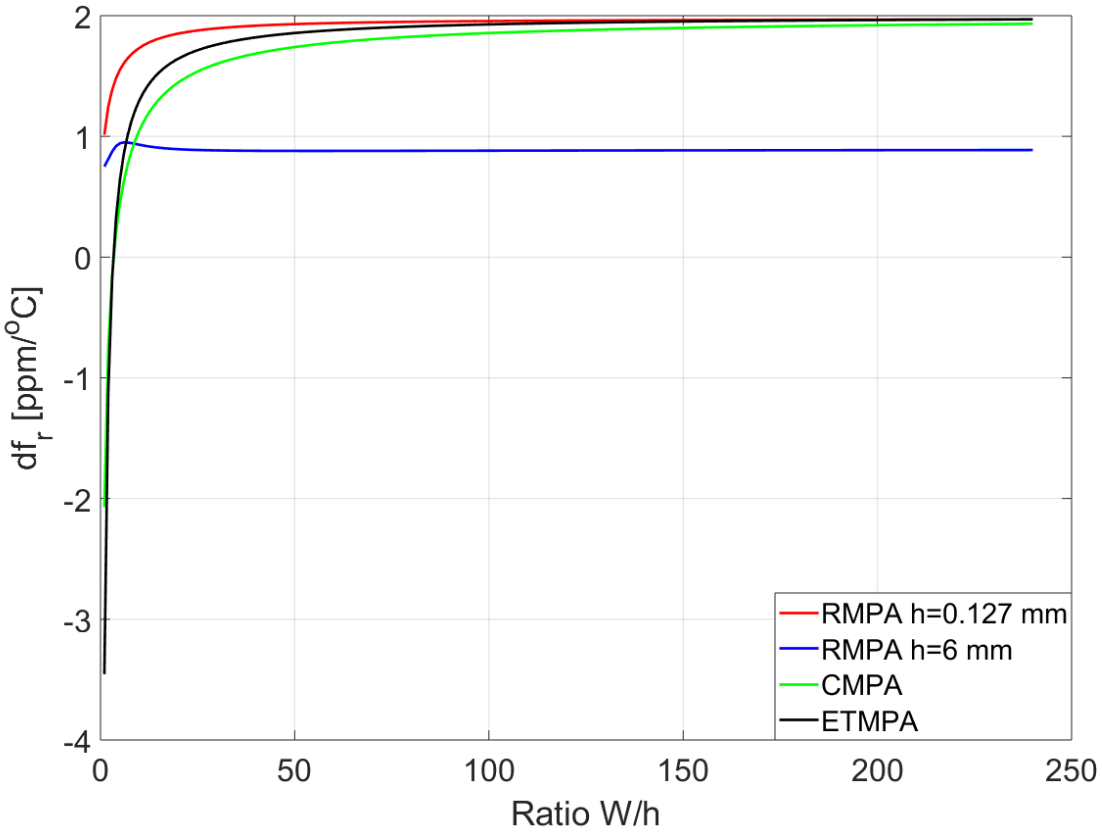


Figure 3.9 – Comparison frequency drifts for RMPA, CMPA and TMPA designed on TMM10 substrate

The frequency drift of RMPA is given for the two substrate thickness values to show a degree of freedom which has a RMPA to accomplish better resonant frequency temperature behaviour.

### 3.3.5 Circuit Model for Analysing Temperature Impact on RMPA Resonance

Not only accurate but also numerically efficient model for tracking temperature impact on rectangular patch antenna resonance is given, as shown in Figure 3.10. In addition to temperature impact investigation, the given model is suited for CAD procedures involving optimisation. Given model is based on a transmission-line concept [49]. The rectangular patch of MPA is represented with a transmission line equal in length to a resonant length of patch. The transmission line section incorporates temperature parameters.

$G$

Figure 3.10 - Circuit model for analysing temperature impact on MPA resonance

As shown in the circuit model, the transmission line consists of two sections with frequency and temperature dependent characteristic impedance $Z_c$, propagation constant $\gamma$, and effective dielectric constant $\varepsilon_e$. Transmission lines at their ends are terminated with radiation conductance $G_r$, mutuall coupling conductance $G_m$, and susceptance which takes into account fringing field effects modelled by capacitance $C_s$. Two transmission line sections are divided by coaxial probe impedance, modeled by inductance $L_F$. The expressions used for evaluation the model parameters are very accurate and given by [49]. The model and the transmission line parameters: characteristic impedance, propagation constant, and effective dielectric constant can be found in [50]. Very accurate calculation of coaxial probe-feed impedance which takes into account probe diameter and transverse waves effect is given by [51].

### 3.3.6 Comparison Simulation, Model and Theoretical Results

The frequency drift results obtained by simulations in the CST electromagnetic simulator, derived theory, and circuit model are compared and discussed for the rectangular MPA designed on TMM10 substrate, Figure 3.11.

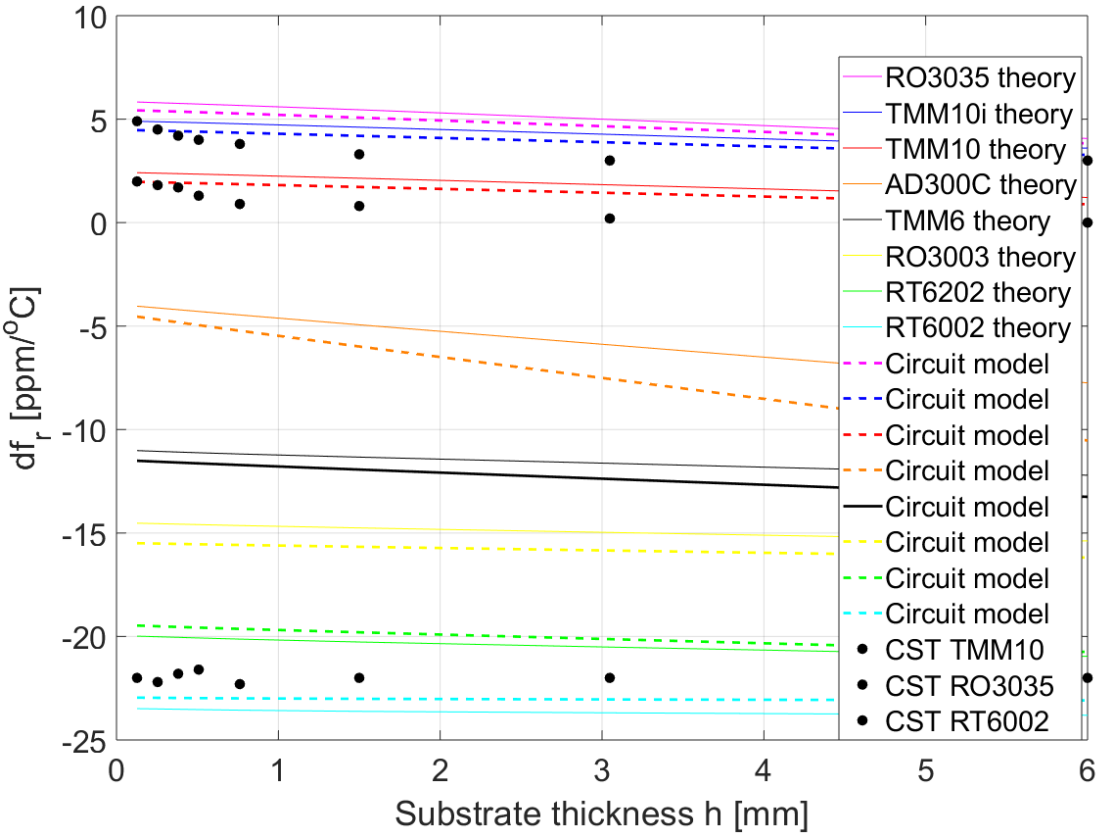


Figure 3.11 - Comparison results between simulations, theory and circuit model

The obtained results in Figure 3.11 are in a close agreement with each other. The circuit model and theoretical derived results are very close. Simulation results done for rectangular MPA designed on TMM10, RO3035 and RT/Duroid 6002 follow trends with insignificant deviations.

## 3.4 Tolerance Analysis

Due to data inaccuracies encountered in manufacturer's datasheet, the tolerance analysis arises quite naturally. Analyses were conducted regarding the tolerance impact of substrate permittivity, the TC of substrate permittivity $\delta_r$, and CTE of substrate in z-plane, $\delta_z$, on the resonant frequency drift of a rectangular, circular, and triangular MPA. In literature, there is no data on tolerances of temperature coefficients. According to the presented results in the research [18] and the way in which the temperature coefficient of substrate permittivity specified in manufacturers' datasheet is determined, it is reasonable to take variation of $\mp 10\%$ in this coefficient. For the substrate temperature expansion coefficient in the z-plane, tolerance of $\mp 5\%$ is taken. Due to negligible tolerance effects which has substrate dielectric constant and substrate temperature expansion coefficient, the frequency drift of MPAs is given only for the tolerance of the substrate permittivity temperature coefficient.

### 3.4.1 Tolerance Impact on RMPA Frequency Drift

The following figures, Figure 3.12 to Figure 3.16 present the tolerance impact of the substrate permittivity temperature coefficient for the rectangular MPA resonant at 2.4 GHz, designed on TMM10 and RT/Duroid 6002 substrates, which are taken as representatives of high and low permittivity. The tolerance analysis results for the rectangular MPAs designed on other substrates are not presented for the readability of obtained results. That will not affect generality and drawn conclusions.

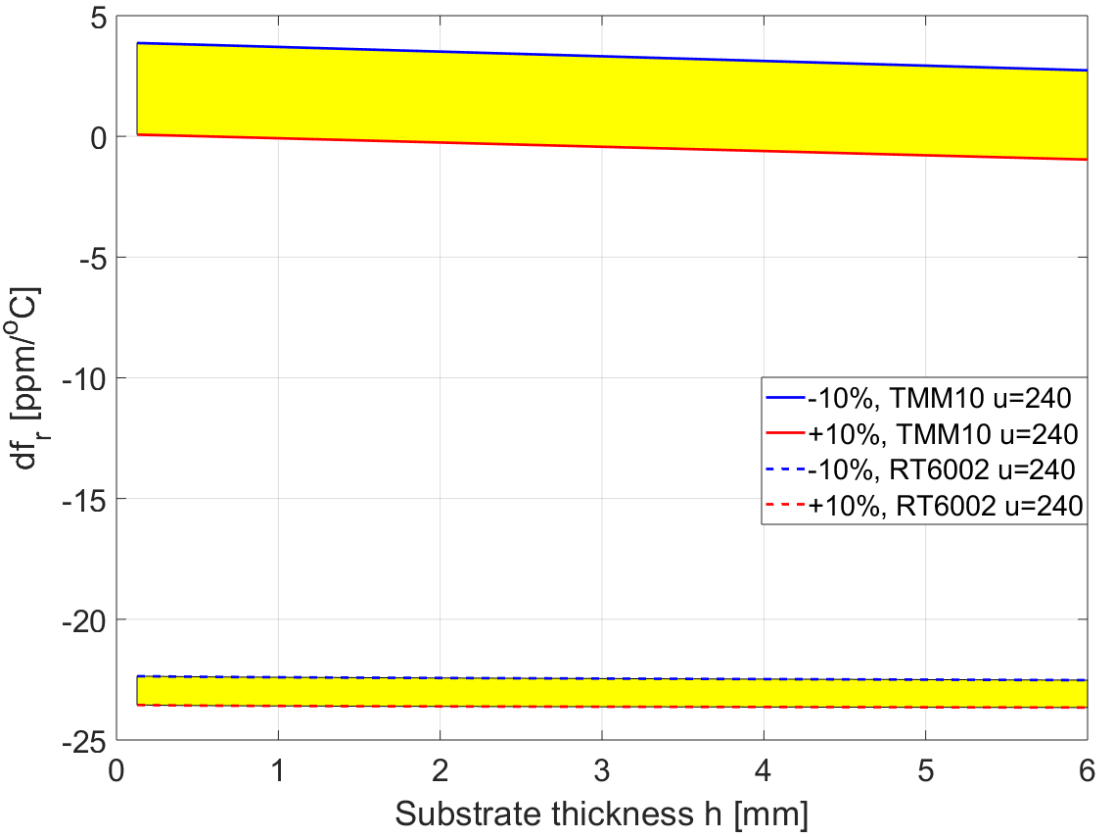


Figure 3.12 - Tolerance impact on RMPA frequency drift in terms of substrate thickness

Comparing Figure 3.12 with Figure 3.2 and Figure 3.3 it can be noticed that the frequency drift obtained by the tolerance impact for the rectangular MPA designed on TMM10 substrate overlaps with the frequency drift curves for the MPA designed on RO3035 and TMM10i substrates. The frequency drift obtained for the MPAs designed on RT/Duroid 6002 substrate has a much smaller offset compared with the antennas on TMM10 substrate. Much smaller value of substrate permittivity contributes to the smaller frequency drift offset. The results shown in Figure 3.12 represent the worst case, because MPAs designed with ratio $u = 240$ have the largest frequency drift according to the derived theory.

The tolerance impact on the frequency drift is shown in the following figures in terms of patch width to substrate thickness ratio for antennas designed on TMM10 and RT/Duroid 6002 substrates for two different substrate thickness values.

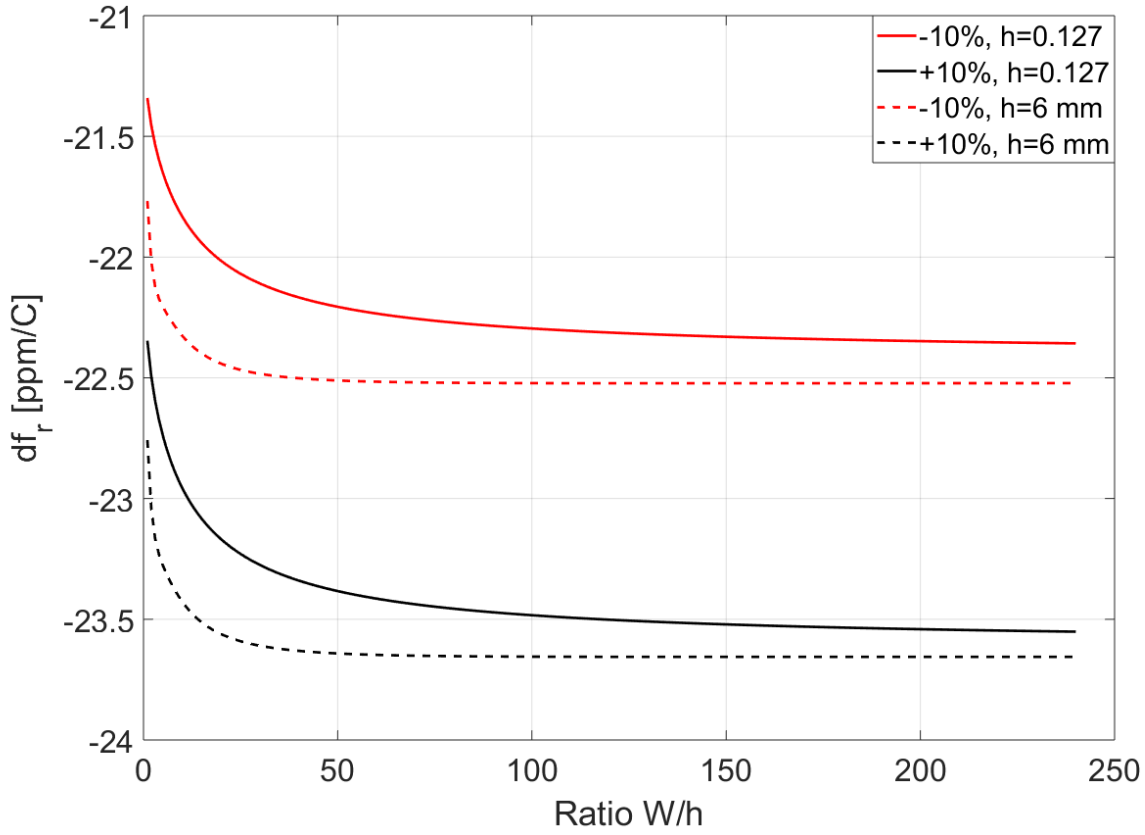


Figure 3.13 - Tolerance impact on RMPA designed on RT/duroid 6002 substrate in terms of patch width to substrate thickness ratio

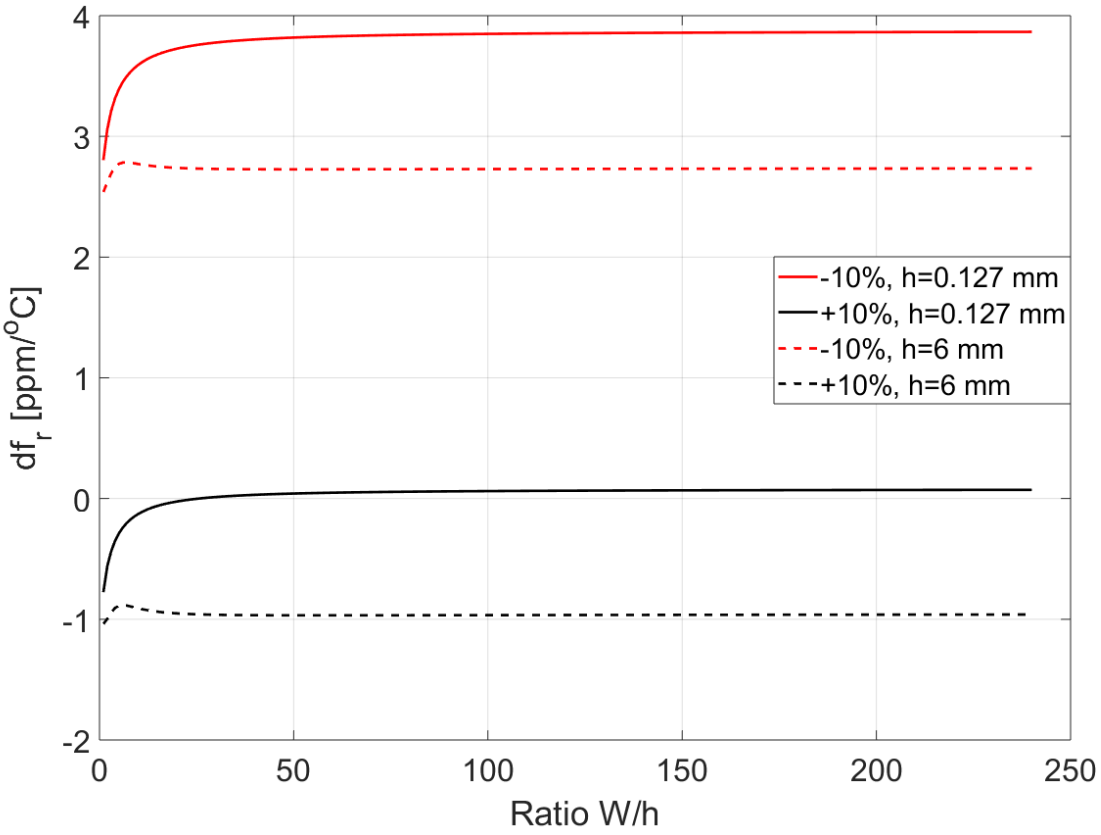


Figure 3.14 - Tolerance impact on RMPA designed on TMM10 substrate in terms of patch width to substrate thickness ratio

Based on Figure 3.13 and Figure 3.14 a conclusion can be drawn regardless of the substrate thickness and its permittivity: the tolerance effect on the frequency drift is the same.

### 3.4.2 Tolerance Impact on CMPA Frequency Drift

Tolerance analysis on the frequency drift of a circular MPA is extended to RO3035 and TMM10i substrates, Figure 3.15.

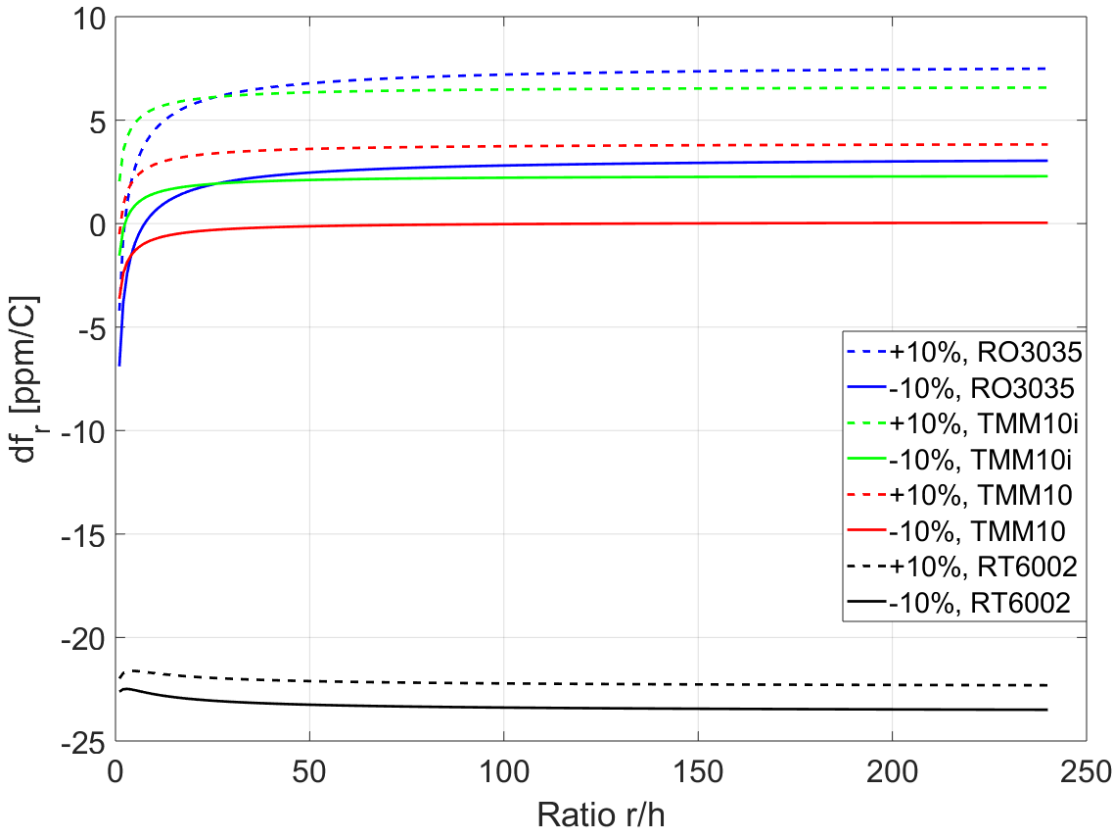


Figure 3.15 - Tolerance impact on CMPA frequency drift

By observing obtained results from Figure 3.15 it is obviously impossible to distinguish substrate materials based on the resonant frequency drift. Frequency drift zones bounded by the full and dash lines overlapping with each other make the final temperature effect on resonant frequency the same for all substrates.

Comparing with rectangular MPAs, the tolerance effect is the same. Antennas designed on RT/duroid 6002 substrate exhibit the smallest tolerance impact contributed to the low substrate permittivity.

### 3.4.3 Tolerance Impact on TMPA Frequency Drift

Tolerance impact on the resonant frequency drift of an equilateral triangular MPA is shown in Figure 3.16. Tolerance analysis is conducted for the three best performing substrates RO3035, TMM10i, TMM10 and one substrate with the lowest substrate permittivity as a referent substrate.

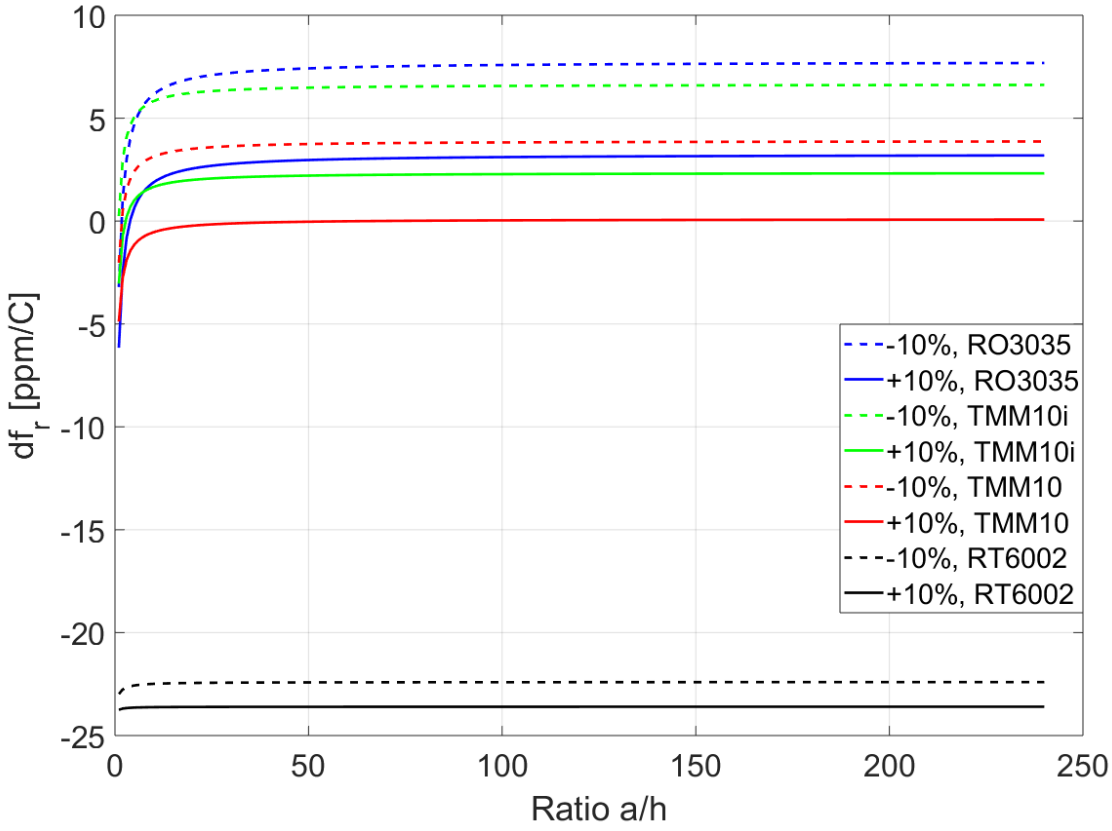


Figure 3.16 - Tolerance impact on ETMPA frequency drift

The tolerance impact effect obtained for the triangular patch geometry does not differ from the rectangular and circular geometries. Observing the obtained results presented in Figure 3.16, it is impossible to distinguish the substrate materials based on the frequency drift. The frequency drift zones bounded by full and dash lines overlap each other making the final temperature effect on the resonant frequency the same for all substrates.

## 3.5 Novel Resonant Frequency Compensation Condition for RMPA, CMPA and TMPA

### 3.5.1 Introduction

As mentioned in Chapter 2, the resonant frequency compensation condition for MPA has not been quantified until now and design methodology has not existed. In this section, the resonant frequency temperature compensation condition is derived for rectangular, circular, and triangular MPA. The design methodology of temperature-compensated MPA has been proposed along equations for the first time. It will enable design engineers to select right criteria for accomplishing temperature low sensitivity resonant frequency of MPA. A compensation condition is first derived for a rectangular MPA. Results obtained for the rectangular MPA geometry are then applied on circular and triangular patch shapes through structural transformation. A derived frequency compensation condition is based on the electrical and thermal properties of a substrate material using appropriate coefficients of thermal expansion for the patch element and substrate permittivity along with the microstrip antenna geometry i.e. patch width to substrate thickness ratio. The compensation condition determines antenna's patch geometry which has to be satisfied by a particular substrate so as to accomplish a self-compensation of the resonant frequency. Obtained results are discussed and verified by numerical simulations in CST Microwave Studio electromagnetic simulation software and transmission-line model, the results of which are in agreement with CST results.

### 3.5.2 Theoretical Analysis: Derivation Temperature Compensation Condition

The resonant frequency of a rectangular MPA is evaluated using a cavity model adopted for MPA [52]. In derivation, the fringing field effect is neglected as it does not have effect on the generality of the obtained results, section 3.3.1 of Chapter 3. The resonant frequency at the temperature of reference $T$ is given by:

$$f_r^T = \frac{c}{2\sqrt{\varepsilon_e}}\sqrt{(\frac{m}{L})^2 + (\frac{n}{W})^2} \tag{41}$$

where $L-$ and $W-$ denote patch length and width respectively, $c-$ the speed of electromagnetic waves in free space, integer numbers $m$ and $n$ are the resonant mode numbers and $\varepsilon_e-$ is an effective dielectric constant. With the temperature change the resonant frequency will change according to the copper coefficient of temperature expansion $\delta_c$ and temperature coefficient of substrate dielectric constant $\delta_r$. With the change in temperature $\Delta T$, the resonant frequency at temperature $T_1 = T + \Delta T$ will be:

$$f_r^{T_1} = \frac{c}{2\sqrt{\varepsilon_e(1+\delta_\varepsilon \Delta T)}} \sqrt{(\frac{m}{L(1+\delta_c \Delta T)})^2 + (\frac{n}{W(1+\delta_c \Delta T)})^2} \tag{42}$$

Due to the presence of effective dielectric constant which is a function of temperature in terms of the substrate permittivity temperature coefficient $\delta_r$ and patch temperature expansion coefficient $\delta_c$, the effective temperature coefficient $\delta_\varepsilon$ is introduced for convenience.

Linear frequency drift over the entire temperature range is calculated by:

$$\delta_T = \frac{\Delta f}{f_r^T \Delta T} 10^6 \ [ppm/°\text{C}] \tag{43}$$

Two conditions can be used to minimize this frequency drift yielding the same result. The first condition is based on equating the frequencies at two different temperature points:

$$f_r^T = f_r^{T_1} \tag{44}$$

while the second one is based on equating propagation constants at two different temperature points:

$$\beta^T = \beta^{T_1} \tag{45}$$

To derive the equation of the resonant frequency temperature compensation condition eqn.(44) will be used.

Substitution eqns.(41) and eqn.(42) into eqn.(44) gives equality which is mode independent:

$$(1 + \delta_\varepsilon \Delta T) = \frac{1}{(1 + \delta_c \Delta T)^2} \tag{46}$$

Expansion eqn.(46) gives:

$$2\delta_c \Delta T + {\delta_c}^2 \Delta T^2 + \delta_\varepsilon \Delta T + 2\delta_c \delta_\varepsilon \Delta T^2 + \delta_\varepsilon {\delta_c}^2 \Delta T^3 = 0 \tag{47}$$

The CTE and the temperature coefficient of substrate permittivity are in the order $10^{-6}$. Therefore, the second- and third-order terms (${\delta_c}^2 \Delta T^2, 2\delta_c \delta_\varepsilon \Delta T^2, \delta_\varepsilon {\delta_c}^2 \Delta T^3$) due to small values are negligible for the first order terms ($2\delta_c \Delta T, \delta_\varepsilon \Delta T$) and can be neglected. Neglecting these terms the relation between the temperature coefficient of effective dielectric constant and the expansion coefficient of cooper is obtained:

$$\delta_\varepsilon \approx -2\delta_c \tag{48}$$

In order to relate the temperature coefficient of effective dielectric constant $\delta_\varepsilon$ with the temperature coefficient of substrate material $\delta_r$, the temperature dependence of effective dielectric constant is needed. From eqns.(7)-(12) the change in effective dielectric constant due to temperature is:

$$\Delta\varepsilon_e = \{K_p \delta_r \varepsilon_r + A_p(\delta_c - \delta_z)\}\, \Delta T \tag{49}$$

The effective dielectric constant eqn.(5) due to changes in temperature can be written in the following form:

$$\varepsilon_e^{T_1} = \varepsilon_e^T (1 + \delta_\varepsilon \Delta T) = \varepsilon_e^T + \varepsilon_e^T \delta_\varepsilon \Delta T = \varepsilon_e^T + \Delta\varepsilon_e \tag{50}$$

giving:

$$\Delta\varepsilon_e = \varepsilon_e^T \delta_\varepsilon \Delta T \tag{51}$$

Equating $\Delta\varepsilon_e$ from eqn.(49) and eqn.(51) gives the temperature coefficient of effective dielectric constant $\delta_\varepsilon$ in terms of substrate permittivity temperature coefficient $\delta_r$.

$$\delta_\varepsilon = \frac{K_p \delta_r \varepsilon_r + A_p(\delta_c - \delta_z)}{\varepsilon_e^T} \tag{52}$$

Substitution eqn.(52) into eqn.(48) gives a resonant frequency compensation condition for the rectangular MPA valid for fundamental mode and its harmonics:

$$\delta_r = -2\delta_c \frac{\varepsilon_e^T}{\varepsilon_r K_p} - \frac{A_p}{\varepsilon_r K_p}(\delta_c - \delta_z) \tag{53}$$

For the frequency of interest 2.4 GHz the compensation condition eqn.(53) is reduced to the quasi-static case:

$$\delta_{r0} = -2\delta_c \frac{\varepsilon_{e0}^T}{\varepsilon_r k} - \frac{A}{\varepsilon_r k}(\delta_c - \delta_z) \tag{54}$$

Eqn.(54) rewritten in a much appropriate form is:

(55)

$$\delta_{r0} = -\frac{2\delta_c}{\varepsilon_r} \frac{(\varepsilon_r + 1)\sqrt{1 + 12\frac{h}{W}} + (\varepsilon_r - 1)}{1 + \sqrt{1 + 12\frac{h}{W}}} - 6 \frac{(\varepsilon_r - 1)}{\varepsilon_r (1 + 12\frac{h}{W})(1 + \sqrt{1 + 12\frac{h}{W}})}(\delta_c - \delta_z)$$

Temperature compensation condition given by eqn.(53) and eqn.(55) gives an appropriate microstrip patch width to substrate thickness ratio which has to be satisfied in terms of specified substrate parameters for accomplishing a self-temperature resonant frequency compensation.

For the case when the substrate expansion coefficient in z-plane $\delta_z$ is close to copper expansion coefficient $\delta_c$ the second term in eqn.(54) can be neglected reducing compensation condition to the form:

$$\delta_{r0} = -2\delta_c K$$

where factor $K \geq 1$, $\lim_{\frac{W}{h}\to\infty} K = 1$ is given by:

$$K = \frac{(\varepsilon_r + 1)\sqrt{1 + 12\frac{h}{W}} + (\varepsilon_r - 1)}{\varepsilon_r\left(1 + \sqrt{1 + 12\frac{h}{W}}\right)} \tag{56}$$

The simpler version of temperature compensation condition eqn.(55) as well as condition eqn.(53) can be interpreted as follows: each substrate material regarding its dielectric constant and thermal coefficient of dielectric constant requires a particular patch geometry in terms of a patch width to substrate thickness ratio to accomplish a self-temperature resonant frequency compensation or to decrease a temperature effect on resonant frequency. If eqn. (53) or eqn. (55) can give the value of specified substrate's temperature coefficient of dielectric constant for a particular patch width to substrate thickness ratio then self-temperature resonant frequency compensation is achievable. The basis for this compensation technique lies in the possibility to control the patch width to substrate thickness ratio, $\frac{W}{h}$, to compensate for a change in the resonant frequency caused by changes in the resonant length of patch and substrate permittivity. The following Figure 3.17 shows a quasi-static resonant frequency compensation condition given by eqn.(54) in terms of patch width to substrate thickness ratio $u = \frac{W}{h}$ for the substrate dielectric constant as a parameter. Values of the lower and upper limit of the dielectric constant used in the antenna design are taken for parameters. For the

substrate temperature expansion coefficient in z-plane, a common value along substrates exhibiting a good temperature behaviour is used, $\delta_z = 60\ ppm/°C$.

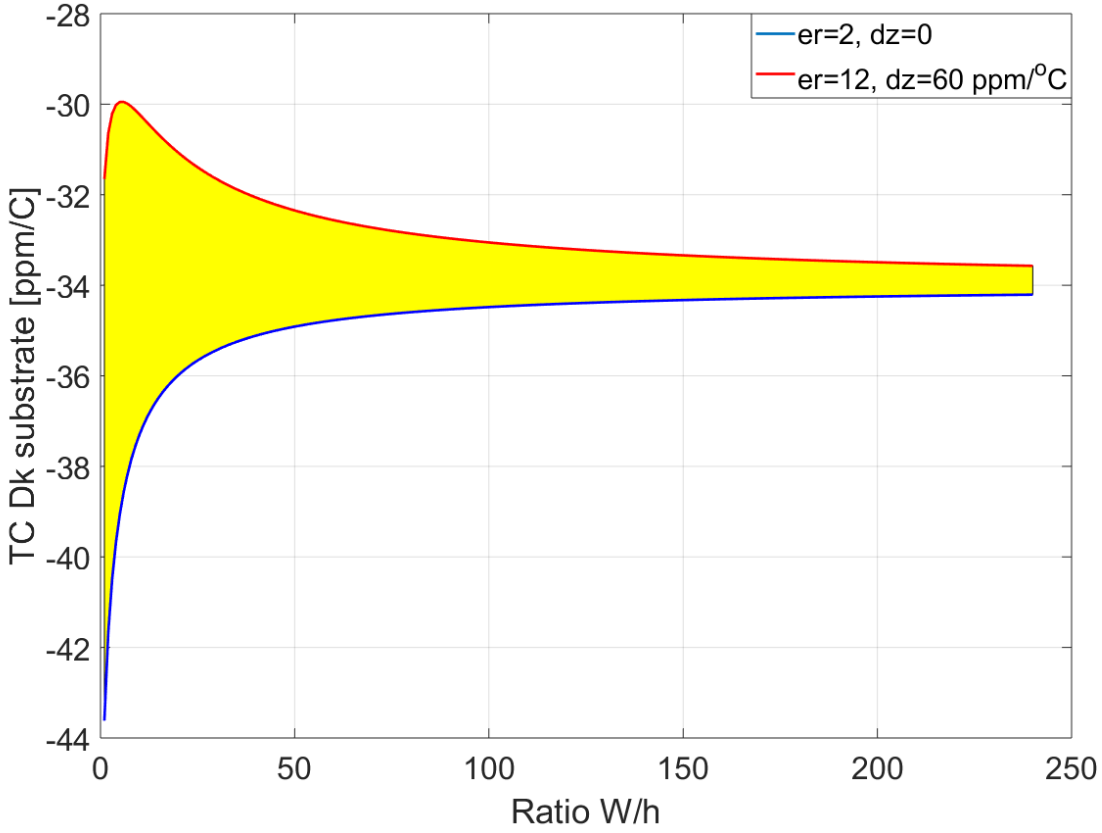


Figure 3.17 - Temperature Compensation Condition Given by eqn.(16)

Figure 3.17 shows that regardless of substrates dielectric constant the wider patches require substrates with temperature coefficient of dielectric constant close to value of $\delta_r = -34\ ppm/°C$. That value corresponds to the closed resonant cavity structure in which case temperature compensation condition is given by $\delta_r = -2\delta_c$. At a lower patch width to substrate thickness ratio, deviation from the cavity resonant condition is clearly understandable. Therefore, the patch designed with the patch width to substrate thickness ratio, $u = 1$, requires a substrate with $\delta_r \approx -44\ ppm/°C$ for $\varepsilon_r = 2$ or $\delta_r \approx -32\ ppm/°C$ for $\varepsilon_r = 12$ substrate.

The resonant frequency temperature compensation condition derived for a rectangular MPA can be applied on a circular and equilateral MPA through the structural transformation [53], Figure 3.18.

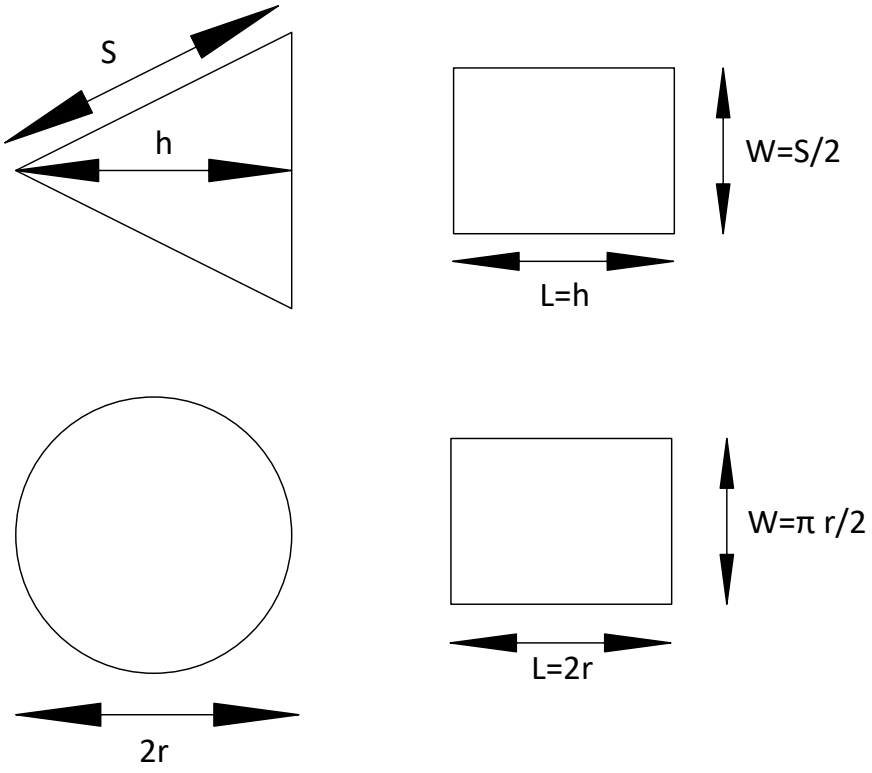


Figure 3.18 - Structural transformation between Triangular, Circular and Rectangular Patch Geometries

The structural transformation is based on an equivalence relation between the rectangular and the other patch geometries. Justification for equivalence lies in the invariance of electrostatic energy below the patch [54]. In Figure 3.18 a structural transformation between rectangular, circular, and rectangular patches is shown. Equivalence is based on equating circular and triangular patch area with the rectangular patch area, taking the resonant length of rectangular microstrip patch to be the same as diameter of the circular patch or the triangle height of the triangular patch. This is very important from the aspect of field variation under patch area. Then, the width of equivalent rectangular patch is obtained from equating these areas.

Figure 3.19 compares the compensation conditions for rectangular, circular and triangular MPAs in terms of $u = \frac{W}{h}$ , $\frac{r}{h}$ or $\frac{a}{h}$ ratios and substrate dielectric constant as a parameter. $r-$ and $a-$ parameters present circular patch diameter and the height of triangle of the triangular patch, respectively.

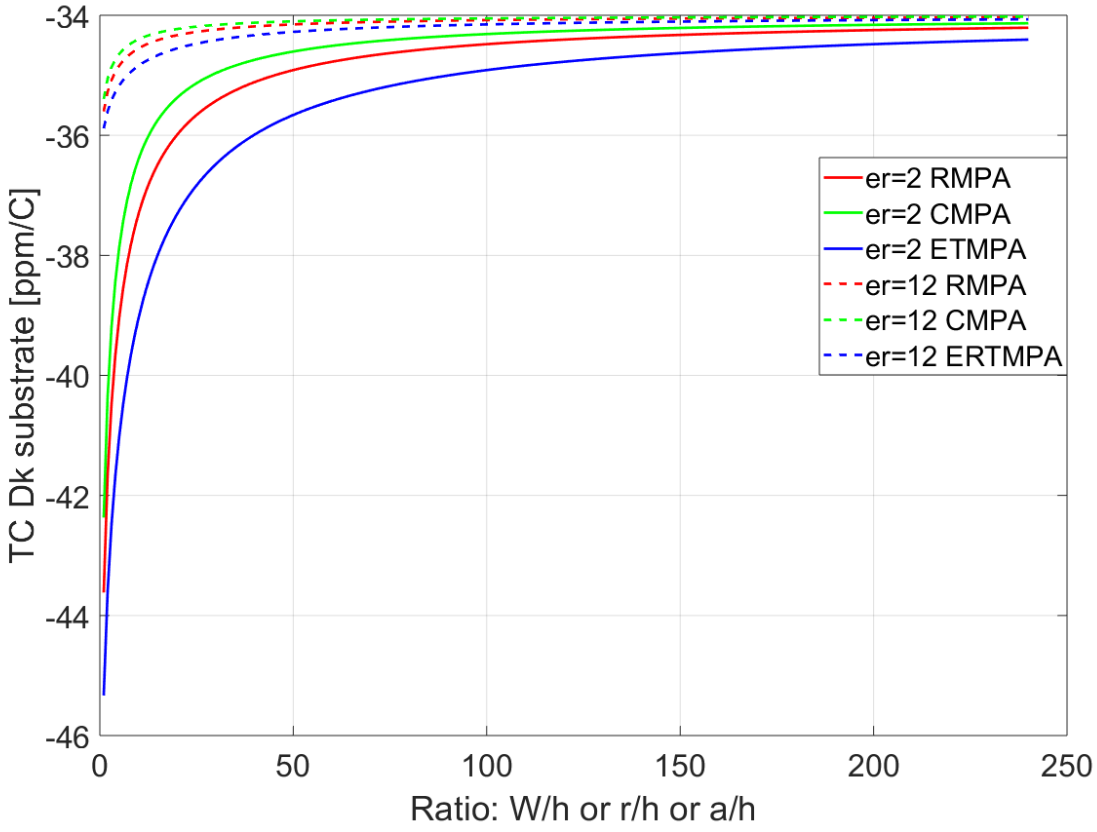


Figure 3.19 - Temperature Compensation Conditions for RMPA, CMPA and RMPA antennas

In Figure 3.19 it can be observed that for substrates with a high dielectric constant the temperature compensation conditions are almost the same regardless of the patch geometry, while for the low dielectric constant substrates, conditions for the rectangular and circular patches are almost the same.

Justification of the derived condition in eqn.(55) is verified through temperature impact analysis on rectangular MPAs using transmission line model and simulations in CST Microwave Studio electromagnetic simulator, giving almost zero frequency drift.

### 3.5.3 Experimental Verification

In order to validate the proposed temperature compensation technique, the rectangular and circular disk MPAs resonant at 2.4 GHz are fabricated. Rectangular microstrip antennas are fabricated on 15 mils thick RO6002 and TMM10 substrates. Circular disk microstrip antennas are fabricated on 20 mils RO6002, RO3035 and TMM10 substrates. Rectangular microstrip antennas are fabricated with following patch width to substrate thickness ratio: $u = 10,20,50,140$ for RO6002 substrate and $u = 10,20,50,80$ for TMM10 substrate. Circular disk microstrip antennas have ratio $u = 20,60,80$ for TMM10, RO3035, and RO6002 respectively. The obtained resonant frequency drifts are compared. Table 3.3 shows substrate specifications used for antenna fabrication.

Table 3.3 - Material properties

| Substrate | $\varepsilon_r$ | $tan\delta$ | Moisture absorption [%] | $\delta_r$ $[ppm/°C]$ | $\delta_x/\delta_y/\ \delta_z$ $[ppm/°C]$ | Thickness [mils] |
|---|---|---|---|---|---|---|
| TMM10 | $9.2 \mp 0.23$ | 0.0022 | 0.09 | -38 | 21/21/20 | 15 |
| RO3035 | $3.6 \mp 0.05$ | 0.0015 | 0.04 | -45 | 17/17/24 | 15 |
| RT/D6002 | $2.94 \mp 0.04$ | 0.0012 | 0.02 | 12 | 16/16/24 | 15 |

The values of permittivity temperature coefficient given in Table 3.3 are the averages at 10 GHz over $-55℃\ to\ 125℃$ temperature range. For all substrates, CTE is matched with that of copper. Substrate RT/Duroid 6002, due to its low temperature coefficient of permittivity is used as a referent to assess the temperature impact. Totally eleven MPAs are fabricated, thereof 8 rectangular MPAs and 3 circular disk MPAs. Figure 3.20 shows the set of fabricated antennas.

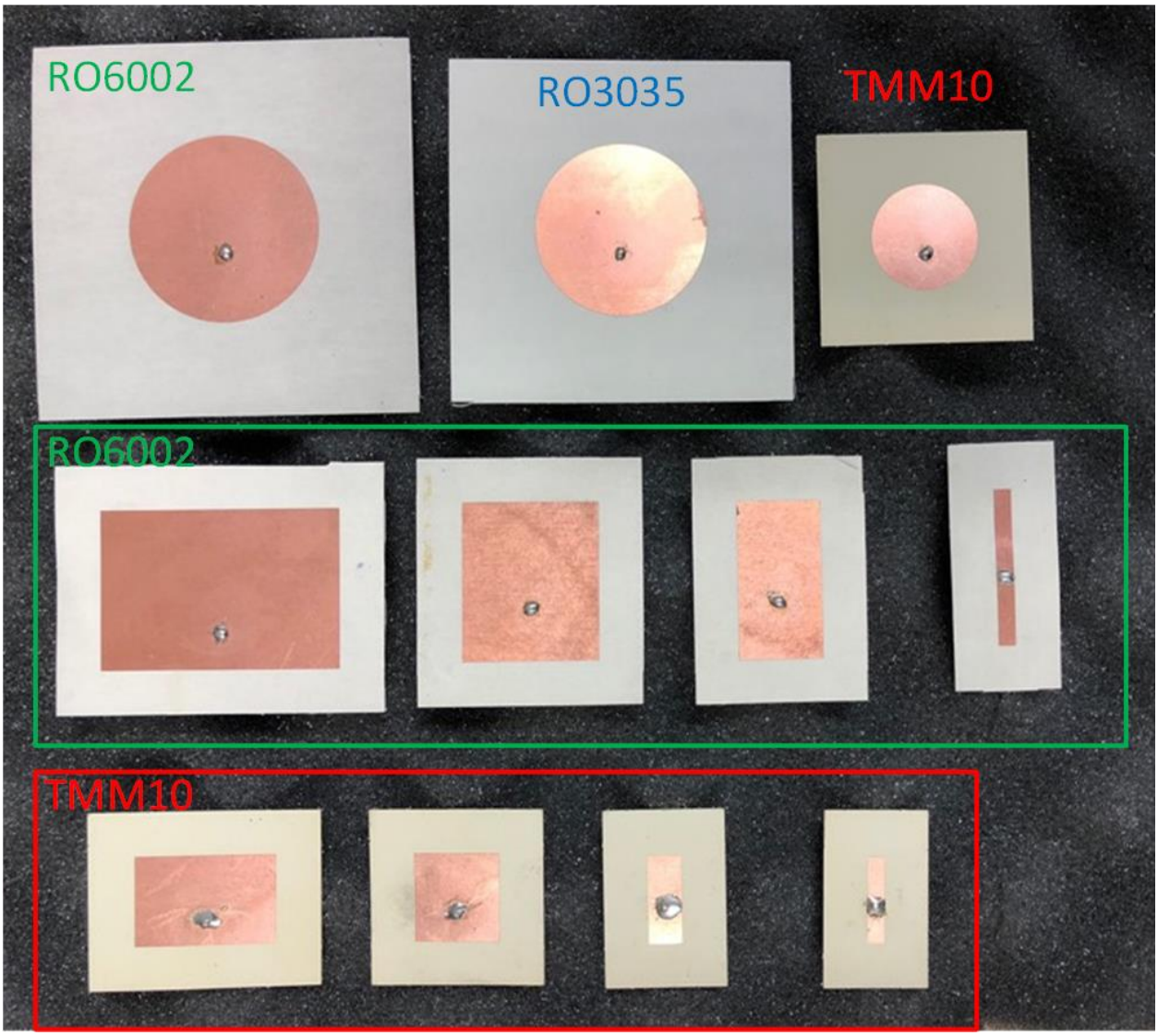


Figure 3.20 - Set of fabricated microstrip antennas

Antennas are measured using two port vector analyser (37397C) in conjunction with a standard temperature chamber Test Equity 105, operating between $-40℃$ to $+80℃$. Each antenna sample is measured at different temperature with sufficient stabilization time. Antennas are left 30 min at the given temperature before taking the measurement. All antennas are measured with positive and negative temperature variations. Measurement setup is shown in Figure 3.21.


Figure 3.21 - Measurement setup

Measuring the reflection coefficient of antennas inside the temperature chamber, which presents a cavity, requires measurement techniques other than those used when measuring antenna in free space. Creating free space environment inside the temperature chamber is impossible due to necessary thick absorbers and small chamber volume. The aim is to use high loss absorbers at the places of standing wave maxima. High dielectric permittivity or permeability of microwave absorbers trap most of the electromagnetic energy of excited cavity mode, leaving a small portion inside empty area of cavity, which reduces the effect on the antenna inside the cavity [55], [56]. See Figure 3.22.

Figure 3.22 - Temperature chamber coated with the absorbers

Figure 3.23, Figure 3.24, and Figure 3.25 show the measured resonant frequency drift results for fabricated rectangular and circular MPAs.

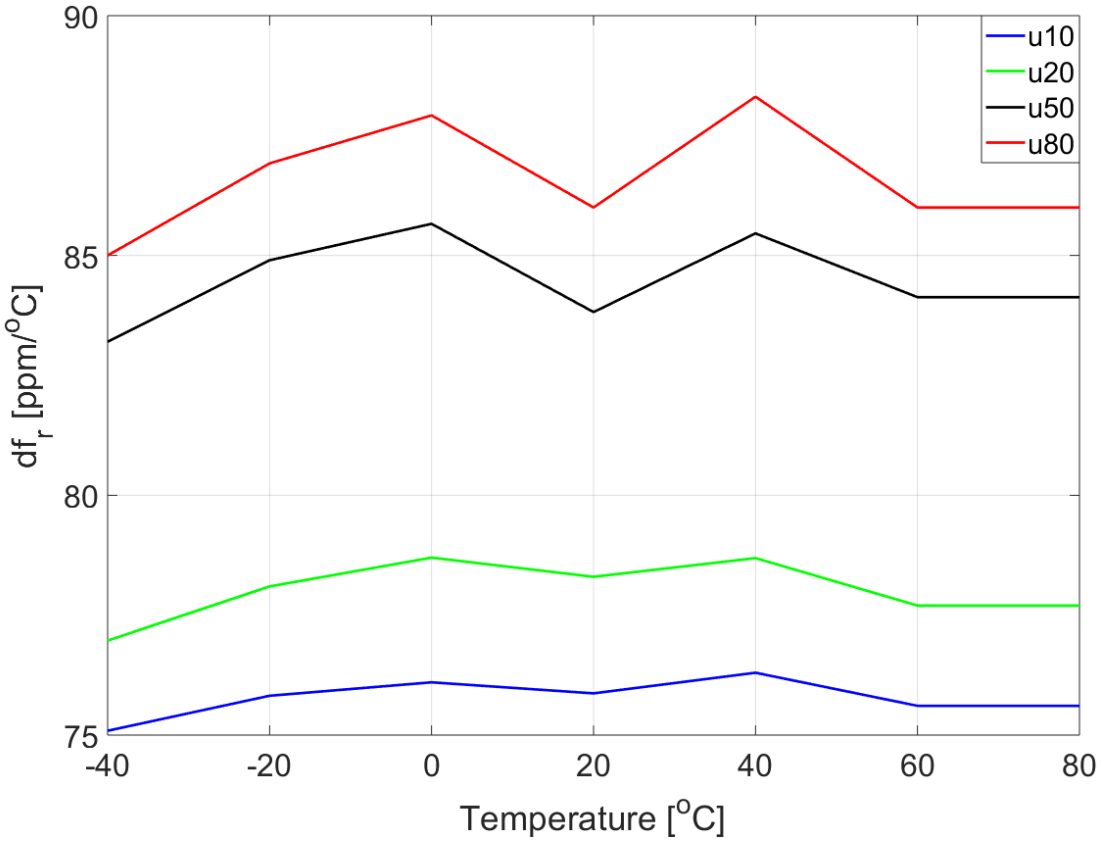


Figure 3.23 - Resonant frequency drift for RMPA fabricated on TMM10 substrate

Figure 3.23 shows experimentally determined the resonant frequency drifts for rectangular MPA fabricated on TMM10, 15 mils thick substrate. MPAs are fabricated for different patch width to substrate thickness ratio. The resonant frequency drift of totally four fabricated antennas with ratio $u = 10,20,50, \text{and } 50$ is measured in $-40℃$ to $+80℃$ temperature range. By observing the resonant frequency drift curves in Figure 3.23, variable nature of substrate permittivity TC over temperature range is observable. Experimental results obtained for the resonant frequency drift are in connection with the derived theory. MPAs fabricated with a larger patch width to substrate thickness ratio exhibit a larger frequency drift.

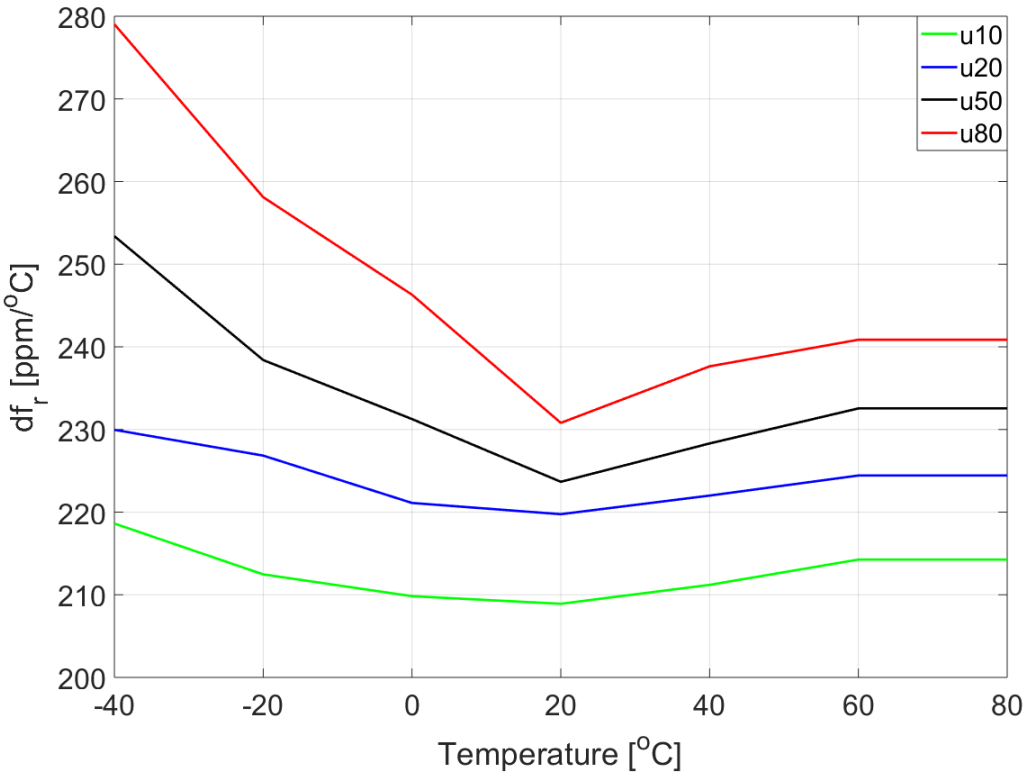


Figure 3.24 - Resonant frequency drift for RMPA fabricated on RO6002 substrate

Figure 3.24 shows experimentally determined the resonant frequency drifts for rectangular MPA fabricated on RO6002, 15 mils thick substrate. MPAs are fabricated for different patch width to substrate thickness ratio. The resonant frequency drift of totally four fabricated antennas with ratio $u = 10,20,50, \text{and } 50$ is measured in $-40℃$ to $+80℃$ temperature range. By observing the resonant frequency drift curves on Figure 3.24, variable nature of substrate permittivity TC over temperature range is observable. Experimental results obtained for the resonant frequency drift are in connection with the derived theory. MPAs fabricated with larger patch width to substrate thickness ratio exhibit larger frequency drift.

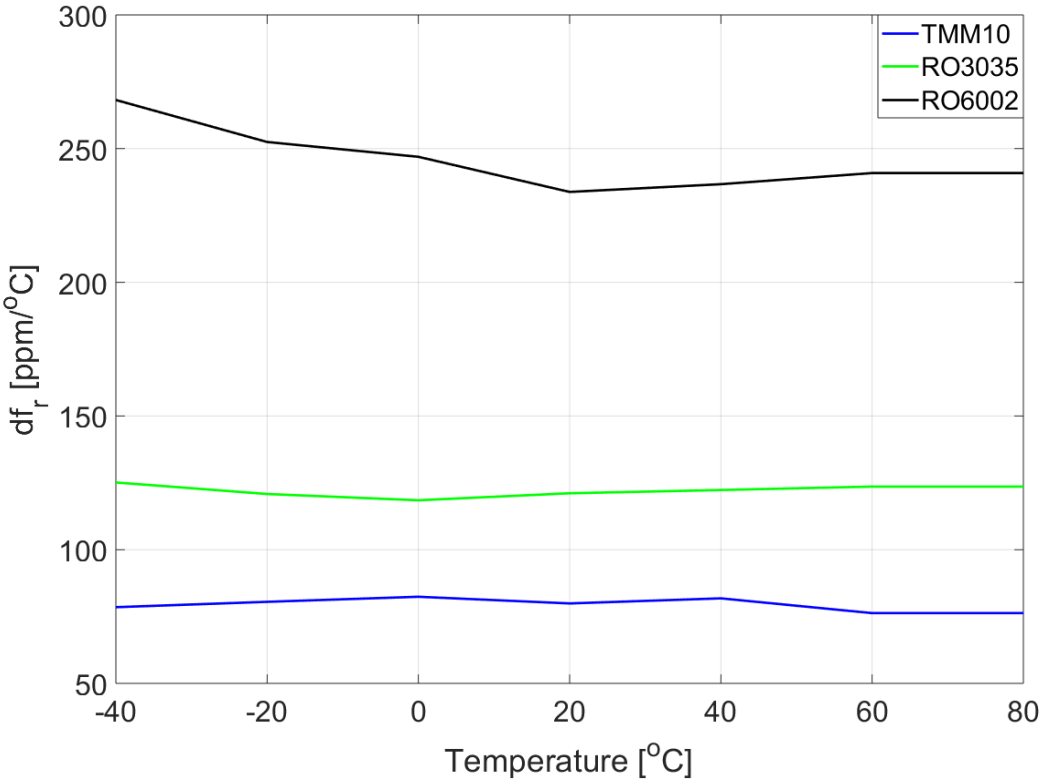


Figure 3.25 - Resonant frequency drift for CMPAs fabricated on the TMM10, RO3035, and RO6002 substrates

Figure 3.25 shows experimentally determined the resonant frequency drifts for circular disk MPA fabricated on TMM10, RO3035, and RO6002, 20 mils thick substrates. The CMPA fabricated on TMM10 substrate exhibits the best resonant frequency drift among its counterparts. The variable nature of substrate permittivity TC for all three substrate materials is noticeable from Figure 3.25.

Obtained experimental results are in connection with the theory. Due to measurement imperfections caused by the temperature chamber, the measured results are greater then theoretically predicted ones. The vibrations caused by mechanical switch in temperature chamber along air circulation inside chamber are disturbing factors with impact on measured results. The additional influencing factors leading to larger magnitude results are humidity and creation of a thin layer of ice over patch element.

The experimental as well as simulation results, along theoretically obtained results of a novel temperature compensation technique are superior over all other results obtained by other compensation techniques.

## 3.6 Conclusion

For the first time, the temperature impact on a resonant frequency of rectangular, circular, and triangular microstrip antenna is mathematically described and analyzed through a set of closed-form resonant frequency drift expressions. The closed-form expressions for a resonant frequency drift enable getting insight into parameters which affect a resonant frequency temperature behaviour. The resonant frequency drift of MPAs designed on different substrate materials is studied through theoretical analysis and comprehensive simulations. Performed analyses reveal the best appropriate substrates for reducing a resonant frequency drift of MPA. Regardless of the patch geometry the best substrates for temperature behaviour of resonant frequency of MPA are Rogers` substrates: TMM10, TMM10i, and RO3035. Among all analysed patch geometries the MPA with rectangular patch geometry exhibit the best performance in term of frequency drift temperature behaviour. The closed-form expression for frequency drift of RMPA reveal the crucial parameter affecting a frequency stability. Resonant frequency drift is dependent on the ratio of patch width to substrate thickness. RMPA designed with smaller patch width to substrate thickness exhibit smaller frequency drift. More stable resonant frequency behaviour with temperature is observed for RMPA designed on thicker substrates. In addition to simulations and theoretical analysis, the circuit model for analysing temperature impact on resonant frequency of MPA is adopted. The circuit model is based on a very accurate transmission line model with incorporated temperature parameters. The problem of parameter uncertainties is addressed through a tolerance analysis. The temperature coefficient of substrate permittivity has the serious effect on a resonant frequency temperature behaviour, making the resonant frequency drift sensitive on this parameter in large extent. Subsequently, the resonant frequency compensation condition is derived. Compensation condition derived for RMPA, through a structural transformation is applied on CMPA and TMPA. None of the commercially available substrates can perfectly satisfy the compensation condition. Among all the substrates of interest, two substrates closely satisfying a temperature compensation condition are chosen for experimental verification, which are Rogers substrates, namely RO3035 and TMM10. Eleven microstrip antennas were fabricated and went through extensive testing. Measurement results show a tendency in connection with the simulations and derived theory for both substrates.

# CHAPTER 4 ICE SENSOR MICROSTRIP PATCH ANTENNA

## 4.1 Introduction

Ice formed on the covered patch antenna will change electromagnetic field in its immediate vicinity, thus influencing the effective dielectric constant and consequently the resonant frequency. This ice loading effect is followed by temperature effect which has temperature on substrate permittivity and patch. The two effects are inseparable, but temperature-compensated microstrip antenna proposed in Chapter 3 can largely suppress effect due to temperature. Therefore, temperature-compensated microstrip patch antenna opens the possibility for exploiting the same one as ice thickness sensor. In this way, the effect of temperature on the resonant frequency of antenna will not be misinterpreted with the ice loading effect. Accurate ice electrical parameters are required for precise characterizing ice loading effect on microstrip antenna resonance. Due to versatility and disagreement in reported results on ice electrical properties, a new measurement has been proposed. Ice permittivity and loss tangent measurement, along ice loaded microstrip patch antenna simulations with measured ice parameters, are outlined in the following subsections.

## 4.2 Dielectric Properties of Ice

As a rule, ice is a hexagonal crystalline structure know as ice-phase-one $I_h$ [58]. It is present in the upper part of the atmosphere where the temperature can reach $-105℃$. This fact greatly facilitates the process of investigating electric properties of ice in terms of icing loading effect on MPA characteristics [59] [60]. Versatility in reported results emerges due to factors, such as ice density, homogeneity, impact of cracks, bubbles, stress, measurement conditions, and accuracy of measurement techniques. Despite large number of conducted measurements, literature reports contradictory results on the loss factor. [61]. The ice loss factor is mostly unknown and not accurately measured due to its small value and impurities. [59]. In [60] the results obtained by [59] are stressed as the most reliable and accurate. According to [59] the real part of the complex relative dielectric permittivity $\varepsilon = \varepsilon' - j\varepsilon''$ is approximately frequency independent in a wide frequency range $10MHz - 100GHz$ with the value $\varepsilon' \approx 3.17$. Real part of the complex relative dielectric permittivity also reveals the weak temperature dependence with increasing trend with the temperature. The same $\varepsilon'$ behaviour is confirmed at lower frequencies below $1GHz$ [62]. By the

linear regression of experimental data [59] the following $\varepsilon'$temperature dependence in $2GHz - 10GHz$ frequency range is obtained:

$$\varepsilon' = 3.1884 + 0.00091T \quad (57)$$

Equation eqn.(57) can be also applied for frequencies below $1\ GHz$, [57].

### 4.2.1 Measurement Method

Measuring electrical properties of ice is challenging, especially in terms of its loss. Measurement is particularly difficult for temperatures between $-5℃$ and $0℃$. To preserve the original properties of ice during measurement, the coaxial-open probe measurement technique is used. Open-ended coaxial probe technique is broadband measuring technique giving the opportunity to measure electrical parameters over large frequency ranges. This technique is characterized by [62]:

- "Simplicity
- Non-destructive feature
- Ability for broadband measurement, and
- Not demanding preparation sample processing of material under test", [62].

### 4.2.2 Measurement of Dielectric Properties of Ice

For measuring the dielectric properties of ice, a few samples of snow during February in winter 2016 were collected in Montreal area. According to [57] quite usual snow impurity level near cities was $10\ ppm$. Having this in mind and knowing that very small impurity content had large impact on loss factor the samples were carefully collected from different locations. Accent was put on a way of taking snow. Therefore, snow was collected from the middle layer of a snow pile in a woody area. Such area was selected for collecting samples due to environmental cleanliness. In that way pollution present in city air was avoided or decreased to a large extend.

Collected snow was then melted and subjected to process of freezing. To obtain the best ice samples possible (ice samples with as little as possible trapped air bubbles, cracks, contamination from air

and flat surface) the melted snow was cooled slowly in a hermetically closed plastic box. The used box had negligible impact on ice contamination, referring to [57]. In total, five ice samples were created. One of obtained ice samples is shown in Figure 4.1.

Figure 4.1 - Ice sample

Measurements were done within the PolyGrames research facilities of the Ecole Polytechnique, Montreal. Electrical properties of the ice were measured by means of open-ended coaxial probe method. The measurement set up was built up of the Agilent PNA-X N52478 vector network analyser, temperature chamber TestEquity Half Cube model 105 temperature chamber, and HP 85070B dielectric probe kits.

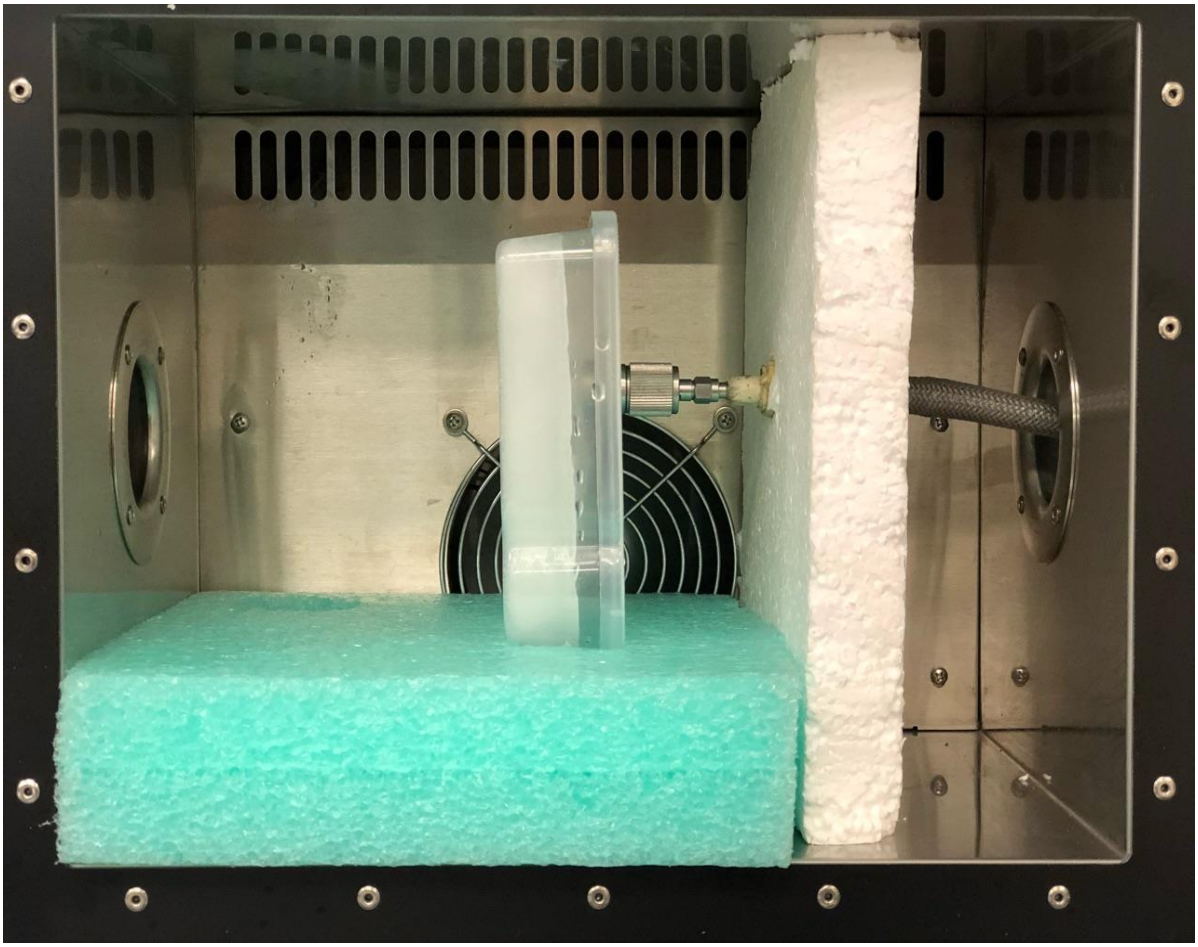

Figure 4.2 - Ice dielectric properties measurement setup

The used coaxial open-end probe was a high temperature probe from HP 85070B dielectric probe kit. Its large radii made it strongly sensitive to dielectric property variations. The probe withstood temperatures from $-40℃$ to $+100℃$ making it suitable for measuring ice dielectric properties over frequency and temperature. Probe calibration was done with well-known standards: air, distilled water, and short circuit. To avoid error due to sample thickness, we used approximate equation for thickness estimation [66]:

$$t \leq \frac{d}{\sqrt{\varepsilon_r}}\, mm$$

with sample diameter $d \geq 20\ mm$. This is known as the infinite sample criteria.

In order to provide satisfying sample's thickness, the aluminium foil was put behind the sample. Therefore, its effects on measurement results could be monitored.

The objective was to measure dielectric properties of ice over $400MHz - 12GHz$ frequency in $-40℃$ to $-5℃$ temperature range. The total five ice samples made of collected snow were measured in accordance with the following methodology: samples were first cooled down to temperature $-40℃$ in the temperature chamber. Open-ended coaxial probe was inserted through the opening of the side wall of the temperature chamber. The probe was fixed in position and cooled down to the same temperature as the samples. In this way, error caused by temperature difference during contact probe with the ice was avoided. The temperature difference would increase the temperature on the sample surface, thus creating a thin water layer. Each new measurement was performed after enough time for temperature stabilization had passed. Samples were left for a minimum of one hour at the new temperature before measurement. With gradually increasing by $20℃$ in temperature from $-40℃$ to $-5℃$ the measurements were done over the same frequency range $400MHz - 12GHz$. The upper temperature limit of $-5℃$ was chosen because reliable results were obtained with difficulty at temperatures closer to zero. For each sample, the measurements were performed several times under the same temperature conditions. Measurement results of ice permittivity and loss tangent are presented in Figure 4.3 and Figure 4.4.

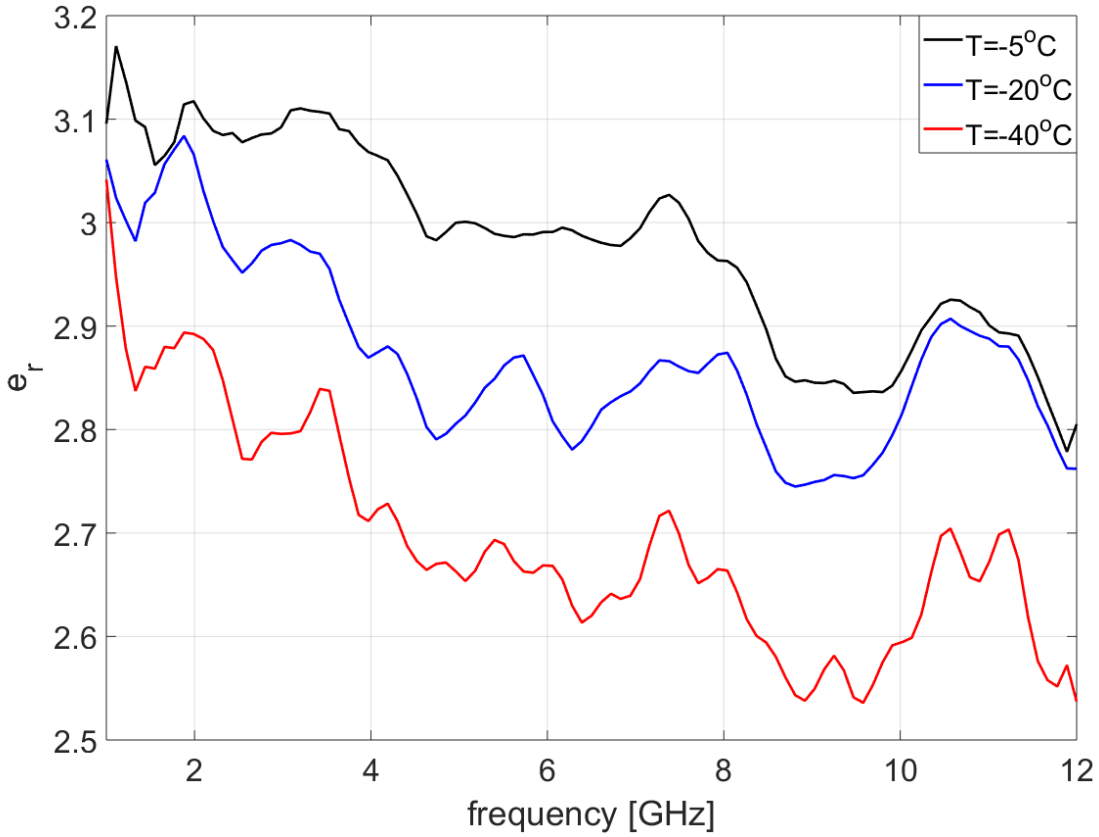


Figure 4.3 - Measured ice permittivity

In Figure 4.3 the averaged measured ice permittivity is shown at three different temperatures. The trend of decreasing ice permittivity with temperature decreasing is in agreement with the previously published results.

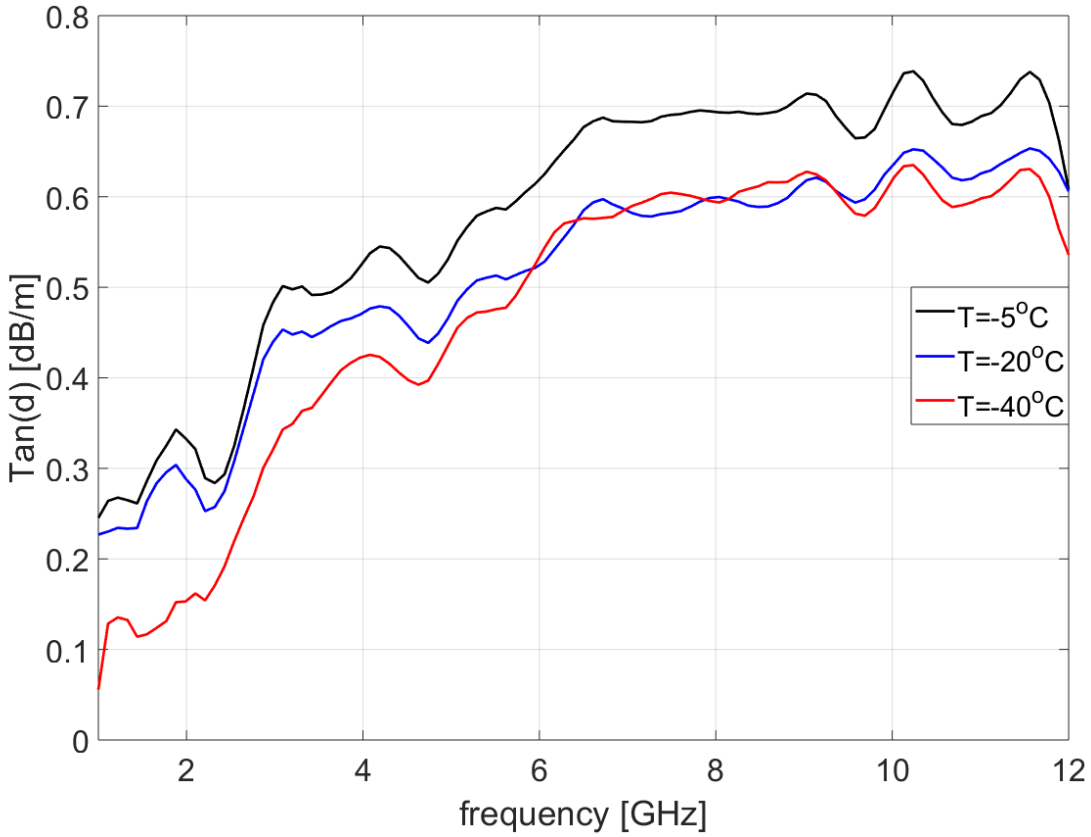


Figure 4.4 - Measured ice loss tangent

Figure 4.4 shows the average tangent loss of measured ice samples at three different temperatures. Tangent loss obtained by measurement is unexpectedly large compared to previously published results. Despite that, tangent loss following the same frequency dependence is reported in published results. As stated earlier by [57] the measurement tangent loss is susceptible to impurities. Another reason for high tangent loss can be very small ice loss which cannot be measured by coaxial-open ended probe. In that case, measurement uncertainties become dominant introducing error in measurements.

### 4.2.3 Conclusion

The measurement results for ice permittivity and loss tangent confirm observed behaviour as in previously published results [57]. The relative dielectric constant decreases with temperature and frequency, while tangent loss increases with frequency and decreases with temperature. The oscillating character of measured results is attributed to the measurement uncertainties.

## 4.3 Simulation Ice Loading Effect on MPA Resonant Frequency

Based on measurement results of ice permittivity, the ice loading effect on rectangular MPA, as the best performance antenna in terms of temperature behaviour among other patch geometries, is simulated. Two rectangular MPAs resonant at 2.4 GHz are designed on a TMM10 substrate. In the previous chapters it is shown that the antenna designed on TMM10 substrate exhibits the smallest frequency drift. Antennas are designed for the worst case of frequency temperature drift characteristic. This means that the antenna is designed on a thin substrate h=0.381 mm. Substrate thickness h=0.381 mm is thinnest TMM10 substrate thickness available on the market. Antennas are designed in terms of patch width to substrate thickness ratio. The obtained results by simulations are shown and commented.

### 4.3.1 Ice Loaded Rectangular MPA

Ice loading effect on resonant frequency of temperature-compensated rectangular MPA designed on TMM10 substrate material for patch width to substrate thickness ratio u=4 and u=80 for the same substrate thickness is shown in figures Figure 4.5 and Figure 4.6, respectively.

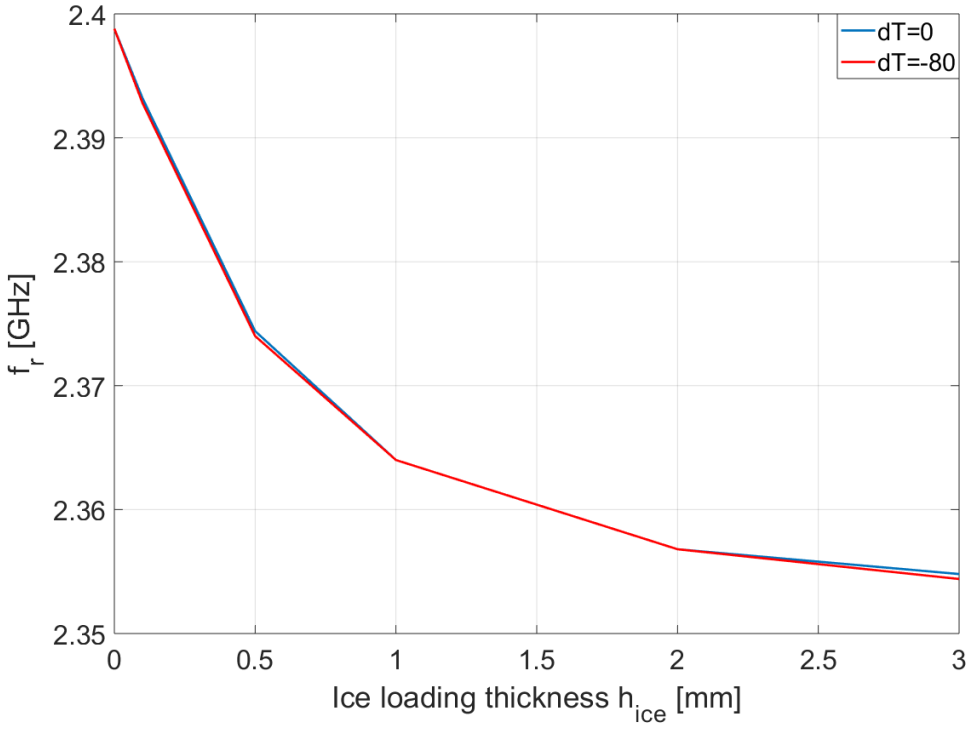


Figure 4.5 - Ice loading effect on resonant frequency of RMPA with parameter u=4

Simulation of ice loading effect is done for 0 to 3 mm ice thickness. Ice thickness larger than 3mm is not taken into account due to earnestness which has 3 mm ice thickness on helicopter performances. Two curves are shown in Figure 4.5. The blue curve represents the ice loading effect separated from the temperature effect. The red curve represents the total effect on resonant frequency. Comparing these two curves, the temperature impact effect has negligible impact on resonant frequency. The change in resonant frequency is mainly due to ice loading effect. In this way, it is shown that MPA can be exploited as an ice sensor for measuring ice thickness.

Figure 4.6 shows a resonant frequency change due to the ice loading for MPA designed with patch width t substrate thickness ratio u=80.

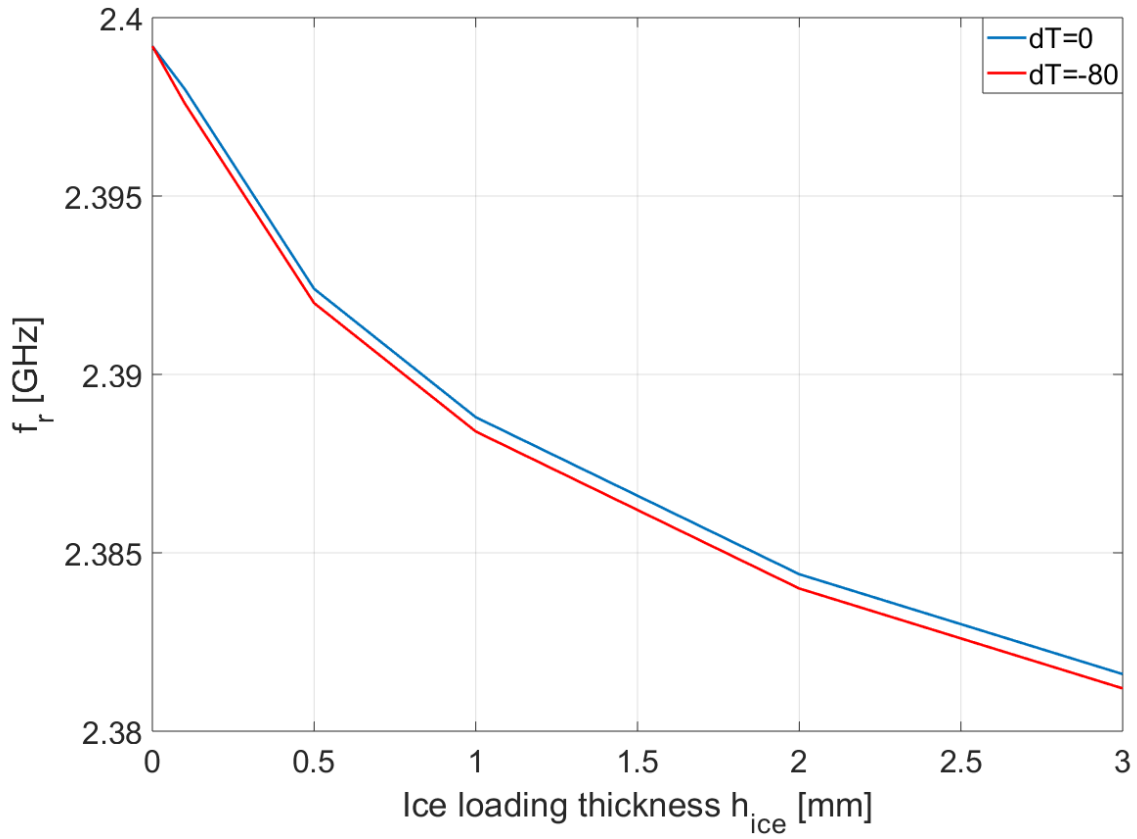


Figure 4.6 - Ice loading effect on resonant frequency of RMPA with parameter u=80

Analysis of curves in Figure 4.6 reveals a larger temperature impact effect on patch resonance. Consequently, it is expected that rectangular patch antennas with a larger patch width to substrate

thickness ratio exhibit larger frequency drift. Even in this case, the influence of temperature is negligible as compared to ice loading effect.

The following figure, Figure 4.7 gives interesting details.

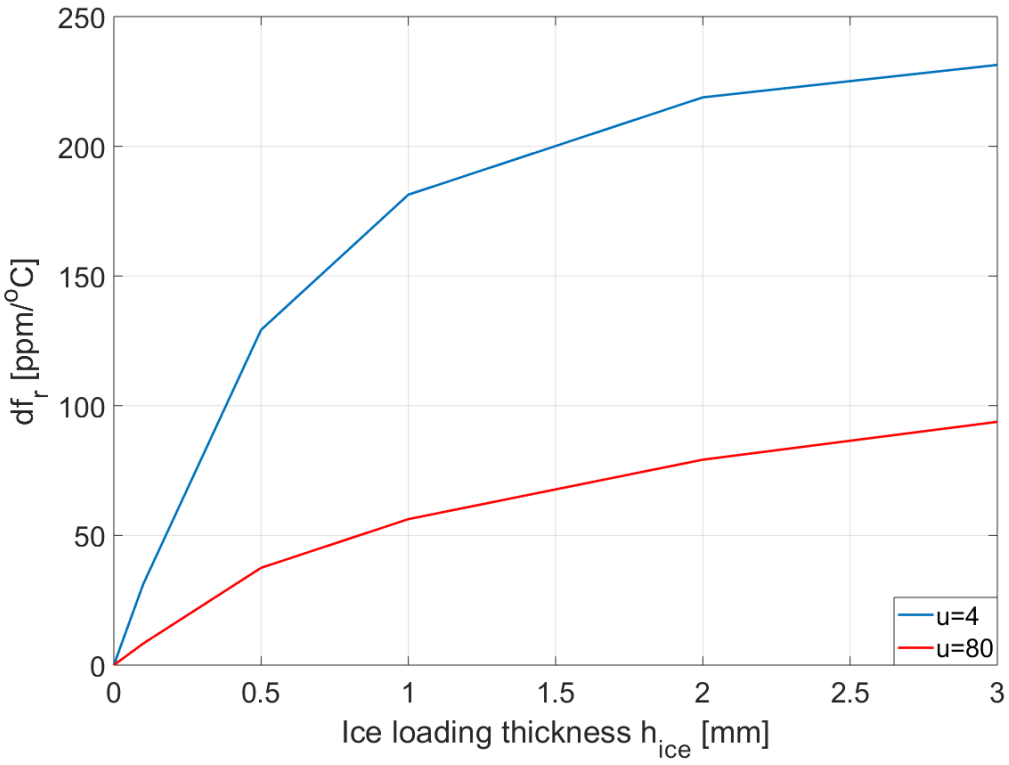


Figure 4.7 - Comparison frequency drifts

In Figure 4.7, frequency drifts caused by ice loading and temperature effects for u=4 and u=80 ratio antennas are compared. A rectangular MPA designed with u=4 ratio exhibit larger sensitivity on ice loading than rectangular MPA designed with ratio u=80. It makes temperature compensated RMPA with lower patch width to substrate thickness ratio candidates for measuring very thin ice layers.

### 4.3.2 Conclusion

Rectangular temperature-compensated MPAs on TMM10 substrates are designed and simulated to investigate the ice loading effect and examine their exploitation in ice thickness sensing. Antennas are designed to represent the worst case in terms of owned frequency drift. Simulations are performed for MPA designed on the same substrate thickness with different patch width to substrate thickness ratio. Obtained results show possibility of exploiting MPA designed on TMM10 substrate as an ice thickness sensor. Simulation analysis shows negligible temperature impact making these antennas very accurate in ice thickness sensing. Rectangular MPA designed with lower patch width to substrate thickness ratio exhibit larger sensitivity.

# CHAPTER 5 WIRELESS TEMPERATURE SENSOR NETWORK

## 5.1 Introduction

This chapter discusses a wireless temperature sensor network that is intended for use on helicopter blades employing the designed temperature-compensated microstrip antennas. Wireless temperature sensor system with its components to be placed on the helicopter is illustrated in Figure 5.1. Besides temperature sensing, this system offers an important function of switching ON and OFF de-icing heaters. The sensing system location on a helicopter dictates the use of wireless communication link between integral parts of a system, denoted with Master and Slave. Master is accommodated on a helicopter chassis, or helicopter stator, while Slave is accommodated on a helicopter rotor.

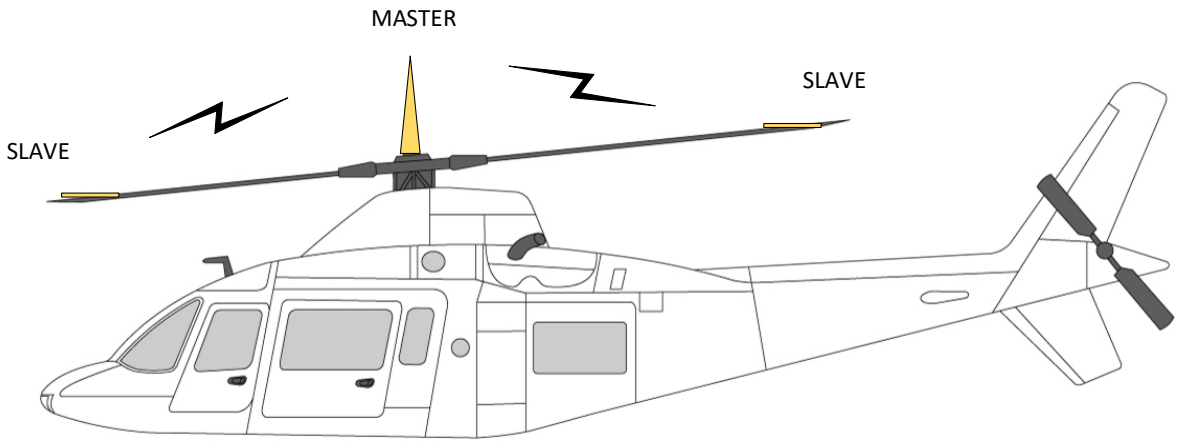


Figure 5.1 - Wireless temperature measuring system installation on a helicopter

## 5.2 System Block Diagram and System Description

Temperature wireless system intended for temperature sensing and activating/deactivating de-icing heaters on helicopter's blades is discussed in this section. Purpose of this system is an early signalling of icing phenomenon occurrence, which can harm helicopter. The specific algorithm which is not a part of this project, based on sensed temperature value and measured thickness of accumulated ice on the helicopter blades, will switch de-icing heaters. Due to the specificity of application, a temperature wireless sensor system needs to be operable in temperature range

of $-40℃\ to + 80℃$ with high reliability and accuracy. Therefore, all necessary system components have to be selected satisfying these temperature specifications. The block diagram of the temperature wireless sensor network intended for the development of a helicopter de-icing system is shown by the block diagram in Figure 5.2.

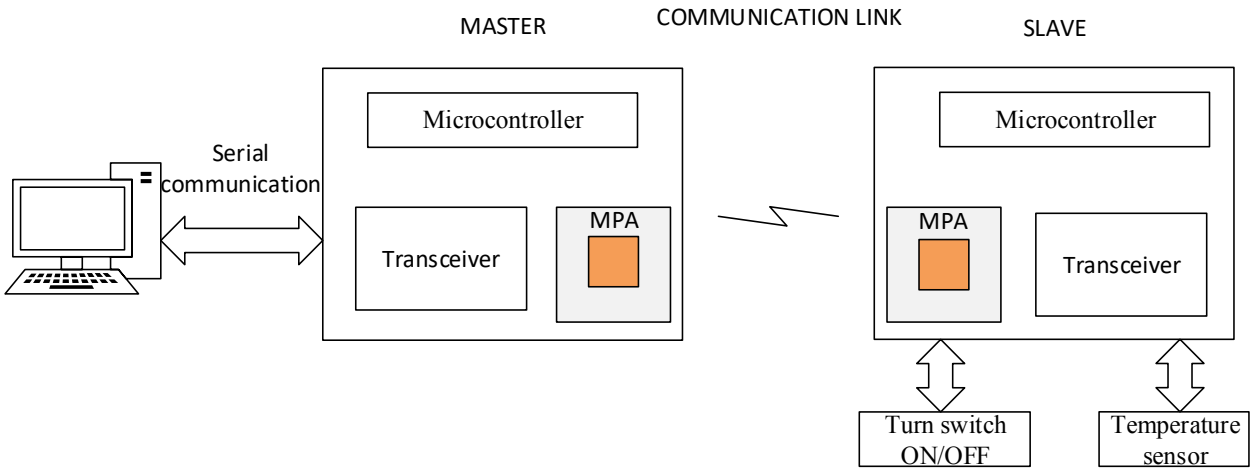


Figure 5.2 - Block diagram of a wireless temperature sensor system

The temperature measurement system given by the block diagram in Figure 5.2 consists of two main parts: Master and Slave units which are of a modular type. Master unit is the main part of system accommodated on helicopter stator or chassis and Slave is responsible for temperature sensing and switching ON/OFF de-icing heaters, accommodated on a helicopter rotor. Communication between Mater unit of the system and the helicopter cockpit is accomplished by serial wired communication interface. Communication between Master and Slave units is carried out through a wireless link.

The Master unit is composed of a microcontroller, transceiver circuit operating at 2.4 GHz and temperature-compensated microstrip antenna designed according to rules from Chapter 3. The microcontroller is responsible for communication initialization between Master and Slave, as well as Master communication with the helicopter cockpit. The command signal for de-icing heaters issued by the pilot in the cockpit is forwarded to system Slave unit, through a microcontroller.

Slave part of the system comprises of a microcontroller, transceiver circuit, temperature-compensated microstrip antenna, and an accurate and reliable digital temperature sensor. Slave

initiates its operation immediately after receiving the request signal from Master. The request signal is a command issued by Master for sensing the temperature and sending it back to the Master. The sensor continuously senses the temperature and forwards the data to the microcontroller, but microcontroller will not accept data from the sensor until the condition specified by a request signal is fulfilled. In our demonstration, the Master generates request signal every 0.5 s.

## 5.3 System Simulation and Power Budget Analysis

For the purpose of estimation, necessary characteristics of system components, such as the sensitivity of receiver circuit and transmitter output power level, the power budget analysis has been carried out using the Advance Design System (ADS) simulator. Wireless link reliability in harsh environmental conditions depends on the temperature characteristics of all the system components. We have studied the worst case scenario for assessment of power budget analysis and analyzed the minimum criteria which should be satisfied by each component for proper operation of the system. In the worst case scenario, the system operates at $-40℃$ for a maximum distance of $10\ m$ between Master and Slave units. The MPAs are taken with the minimum gain of $5\ dBi$ and critical ice loading thickness of 3 mm. Transmitter radiating power and system modulation techniques are the key characteristics taken into account for identifying the appropriate transceiver component.

### 5.3.1 ASK Transceiver

Schematic of the link power budget estimation utilizing the transceiver circuits for amplitude shift keying (ASK) signal modulation is presented in Figure 5.3. Due to the simplicity of the utilized system, regardless of the generality of obtained results, the only transmitting part of the system is considered for further analysis. Subsequently, in power budget analysis, the output power of the transmitter varies form $-20\ dBm$ to $6\ dBm$ , while the power level at receiving point is studied.

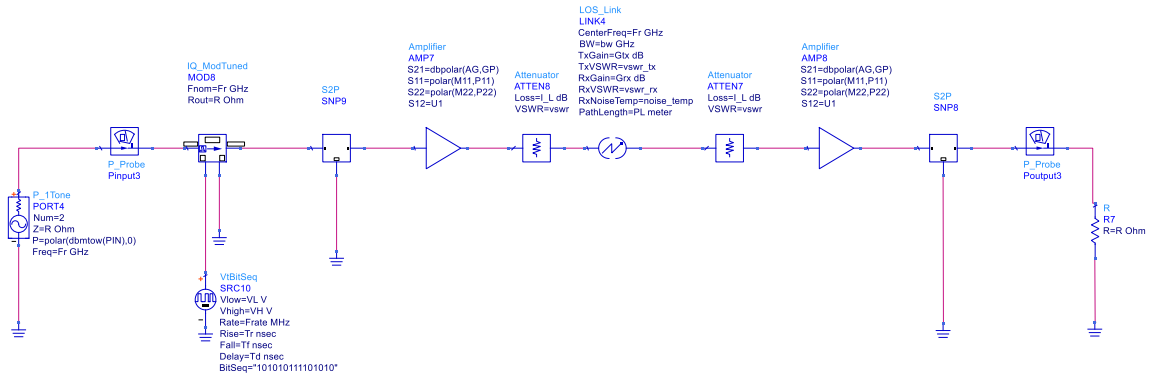


Figure 5.3 - Simulation of wireless system with ASK modulation

The ASK modulation is simulated with Quadrature modulator block (I/Q), fed with data at the in-phase signal port (I) and the quadrature-phase signal port (Q) connected to ground, in addition to input and output RF ports. Baseband binary signal is chosen to have a bit rate of 1 Mbps. The modulated signal is fed to the designed antenna modelled by its S-parameters extracted from CST simulator simulations. Power transmitted through antenna block is amplified by 5 $dB$ antenna gain of MPA. Attenuator component models signal loss due to ice loading, which is estimated to be 1.2 $dB$. All the components discussed so far model the Master part of the system. In a similar manner, system on the Slave part is modeled up to the receiver input for estimation of necessary receiver sensitivity, Figure 5.3.

Rectangular MPAs analyzed with the dielectric properties of RO6002, and TMM10 substrates are utilized in the simulation analysis for all different modulation schemes. MPAs are modelled on substrate thickness $h = 0.381\ mm$ with a patch to substrate thickness ratio $u = 100$ and $u = 80$ as the worst case of frequency drift temperature dependence, respectively. Characteristics of received input power by Slave over transmitted power are shown in Figure 5.4.

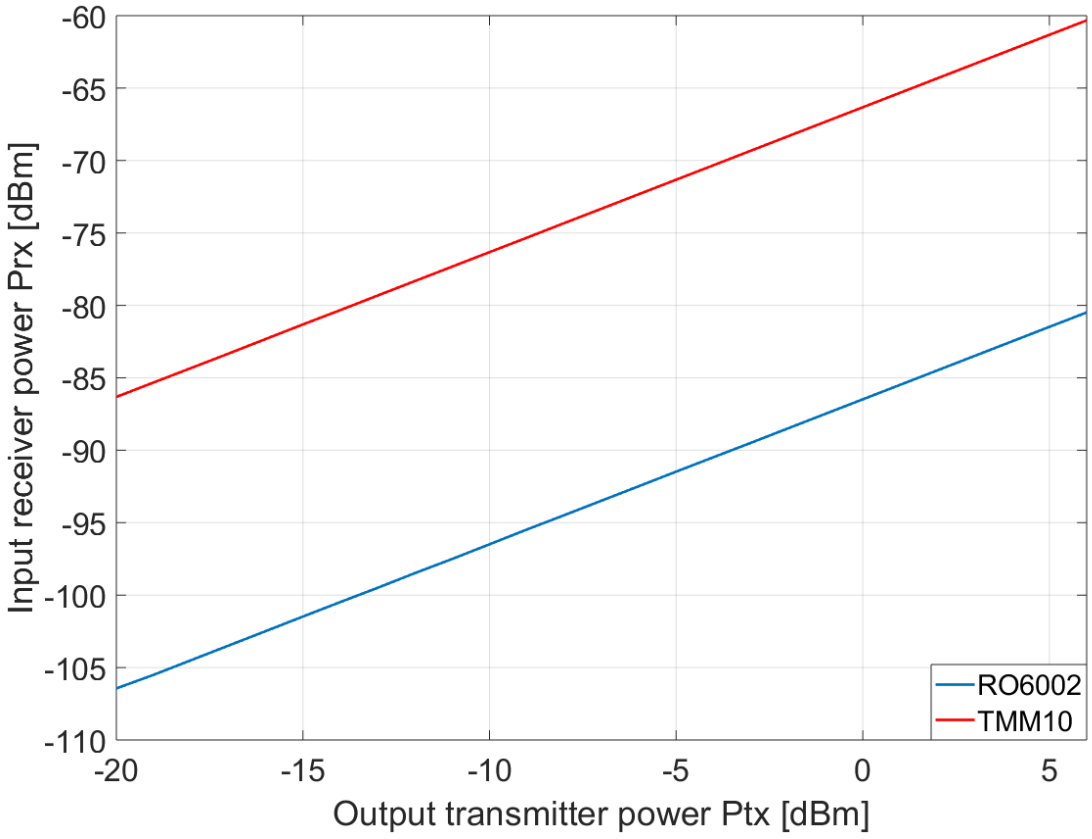


Figure 5.4 - Simulation results of received power for ASK modulated data

Figure 5.4 shows noticeable superiority of wireless link employing temperature-compensated MPA designed on TMM10 substrate over referent antenna designed on RO6002 substrate. Difference between received powers for both the cases is around 20 $dBm$.

### 5.3.2 FSK Transceiver

Frequency shift keying (FSK) signal modulation analysis is also carried out in a similar manner, and the schematic model is shown in Figure 5.5. Frequency modulator block is utilized here for the modulation of the carrier.

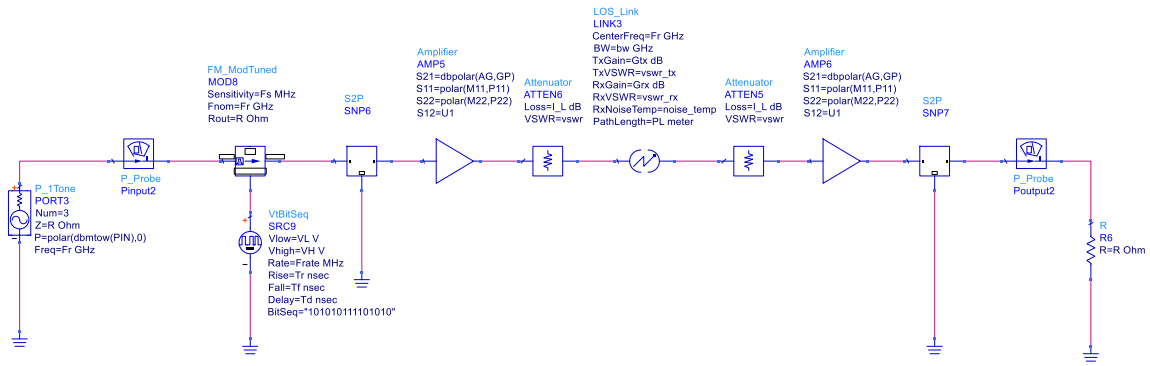


Figure 5.5 - Simulation of wireless system with FSK modulation

Simulation results which compare received power over transmitted power for wireless link modelled with MPA designed on RO6002 and TMM10 substrates are shown in Figure 5.6.

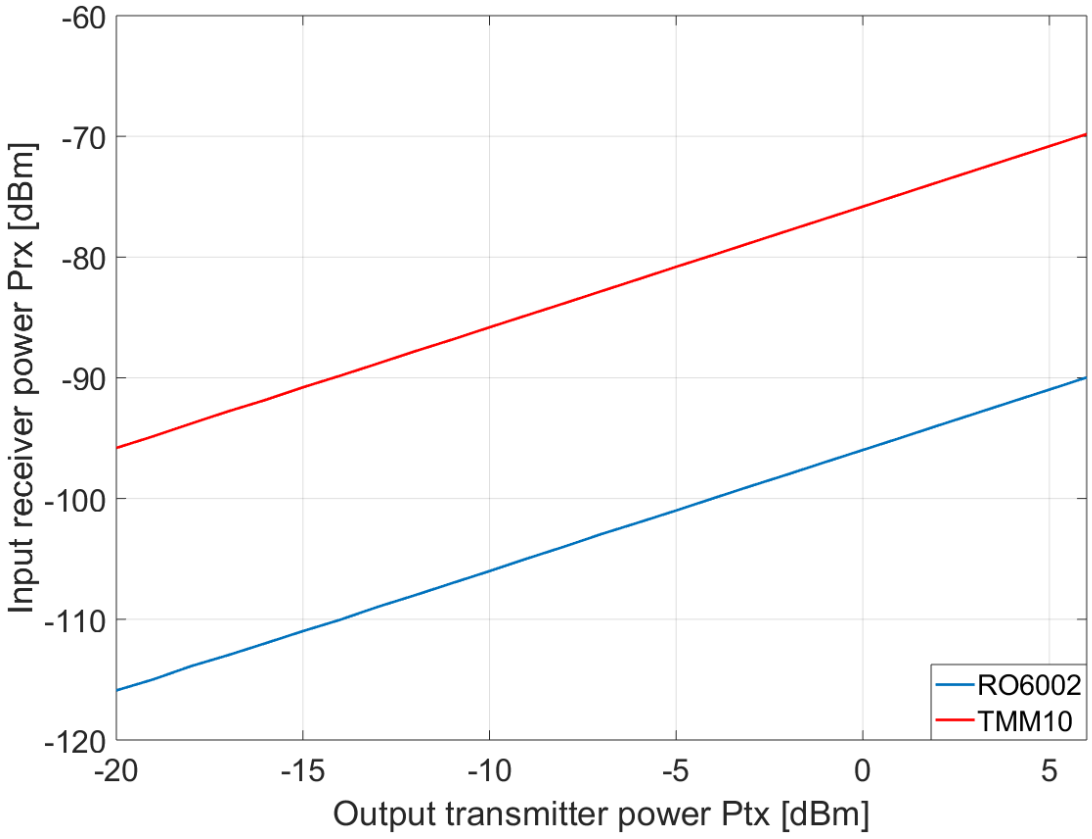


Figure 5.6 - Simulation results of received power for FSK modulated data

Figure 5.7 illustrates evident superiority of the wireless link modelled with temperature-compensated MPA designed on TMM10 substrate over referent antenna designed on RO6002 substrate with the smallest permittivity temperature coefficient. Difference between received power for both the cases considered is around 25 $dBm$.

### 5.3.3 QPSK Transceiver

Power budget analysis for the quadrature phase shift keying (QPSK) modulation scheme is analyzed by circuit model, as shown in Figure 5.7.

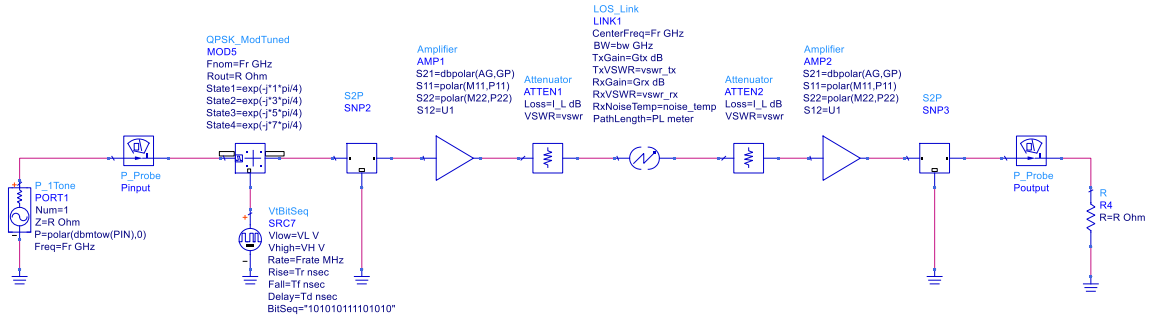


Figure 5.7 - Simulation of wireless system with QPSK modulation

Simulation results comparing the received power over transmitted power for a wireless link with MPA designed on RO6002 and TMM10 substrates are shown in Figure 5.8.

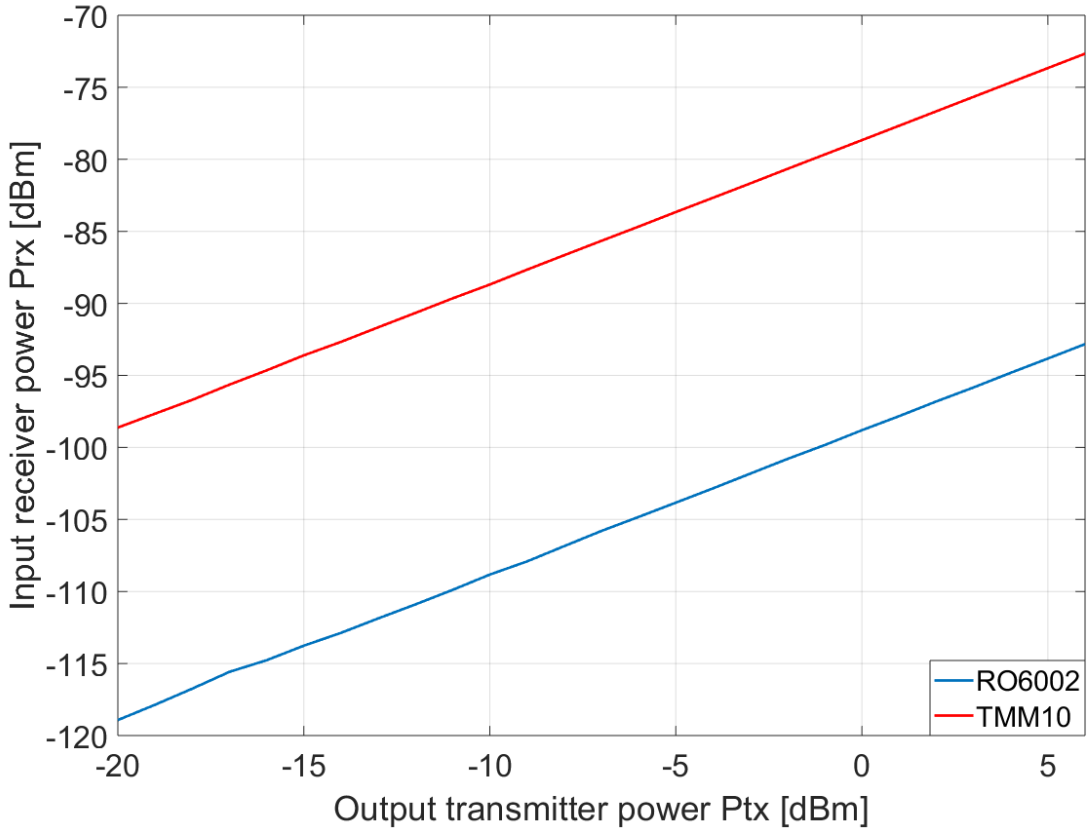


Figure 5.8 - Simulation results of received power for QPSK modulated data

QPSK modulation scheme has a trend similar to FSK, as shown in Figure 5.8, with temperature-compensated MPA designed on TMM10 substrate performing better than the referent antenna designed on RO6002 substrate with the lowest permittivity temperature coefficient. Difference between received powers for this modulation scheme is around $20\,dBm$ in lower limit of transmitting power range and around $30\ dBm$ in higher limit of transmitting power range.

### 5.3.4 Comparison of Simulated Modulation Schemes

Comparison results obtained from the simulation of different modulation schemes are shown in Figure 5.9.

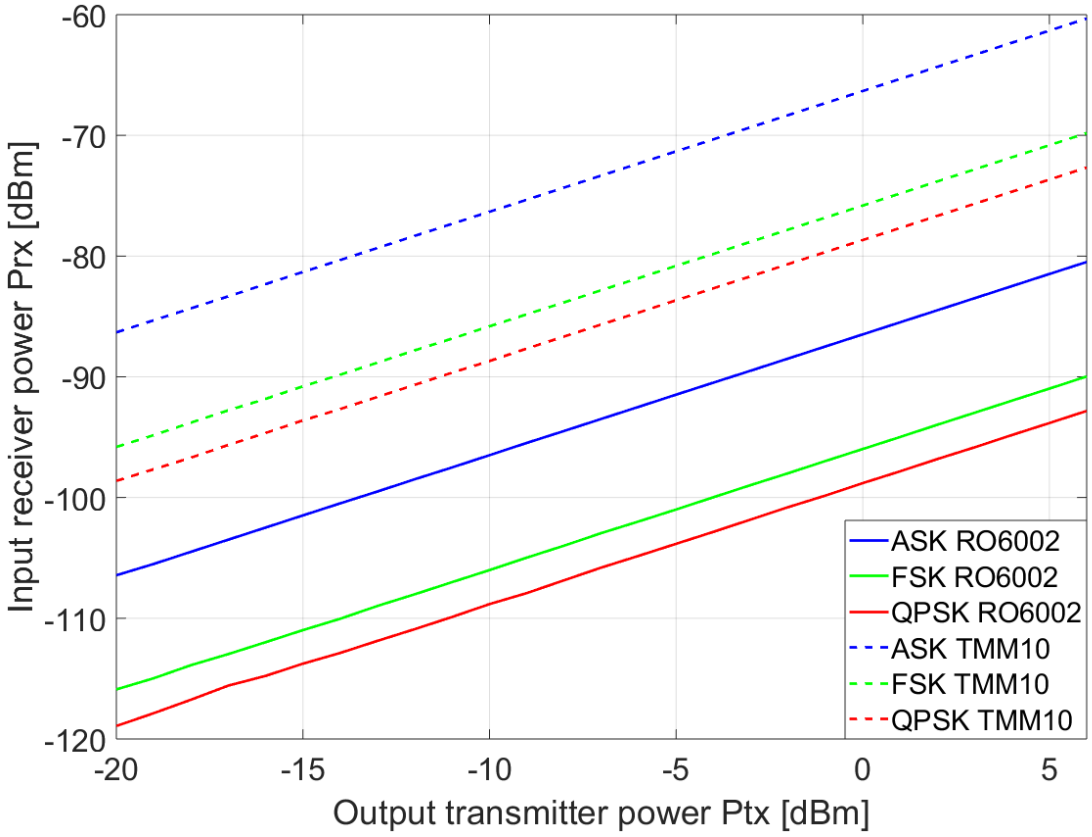


Figure 5.9 - Comparison of budget power simulation results

It can be verified from Figure 5.9 that amplitude modulation has the best characteristics from the received power point of view. Therefore, the wireless communication link for ASK modulated signal exhibits the best performance, requiring a receiver with smaller sensitivity or transmitter with lower radiating output power for the reliable wireless link.

## 5.4 System Implementation

This section describes the technical details of components utilized for implementation of Master and Slave parts of the wireless temperature sensor network.

The microcontroller used in this application has to consume low power, operate over a large temperature range and be preferably easier to program. Given the specifications, the 8-bit ATmega328P microcontroller is ideal for our project with its characteristics of powerful architecture, easiness in programming, and operating in range of $-40℃\ to + 105℃$.

Based on the power budget analysis, transceiver circuit module NRF24L01 is chosen. Transceiver module NRF24L01 is GFSK module for ultra-low power operations. It offers the freedom to adjust output power level, data rate and frequency channel (totally 127 RF channels). Table 5.1 lists the NRF24L01 specifications for reference.

Table 5.1 - NRF24L01 Transceiver specifications

| Parameter | Value |
|---|---|
| Maximum output power | $-18\ to\ 0$ [dBm] |
| Maximum data rate | 2000 [kbps] |
| Temperature range | $-40℃\ to\ 85℃$ |
| Sensitivity | $-85$ [dBm] |

In addition, one wire digital temperature sensor DS18B20, operating in $-55℃\ to + 125℃$ temperature range is utilized. In addition to numerous advantages, the critical advantage of a digital sensor over the analog one is noise for our intended application. Additionally, this temperature sensor does not require any external circuits or additional calibration. DS18B20 is characterized by 9- to 12-bit adjustable resolution and $\mp 0.5℃$ temperature error.

Block diagram of the wireless temperature sensor system with selected components is shown in Figure 5.10.

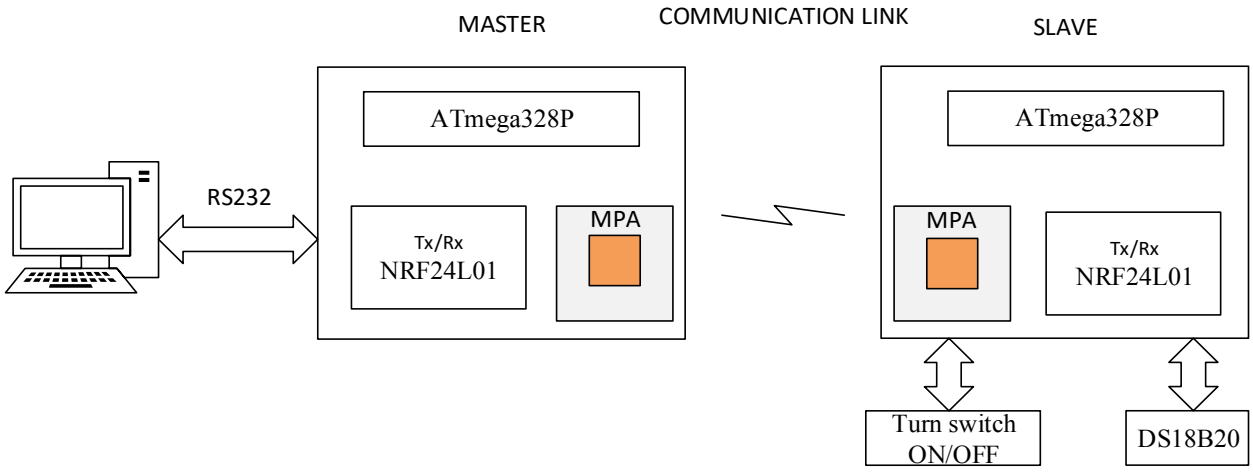


Figure 5.10 - Block diagram of an implemented system

## 5.5 Experimental Validation

The built wireless temperature measurement system is shown in Figure 5.11. The platform used for connecting Master and Slave module elements is Arduino Uno Rev 3 board. The other components utilized for experimental system validation are temperature chamber Test Equity 105, a personal computer (PC) substituting the main computer of helicopter cockpit, temperature-compensated antennas designed on TMM10 substrate and one LED diode as an indication of activating de-icing heaters. System test is performed by placing the antennas of Master and Slave along temperature sensor in a temperature chamber, operating in $-40℃$ to $+80℃$ temperature range. Antennas are oriented for a line of sight communication, and high loss absorber is placed at the point of standing wave maxima to suppress cavity effect on antennas, as shown in Figure 5.12.

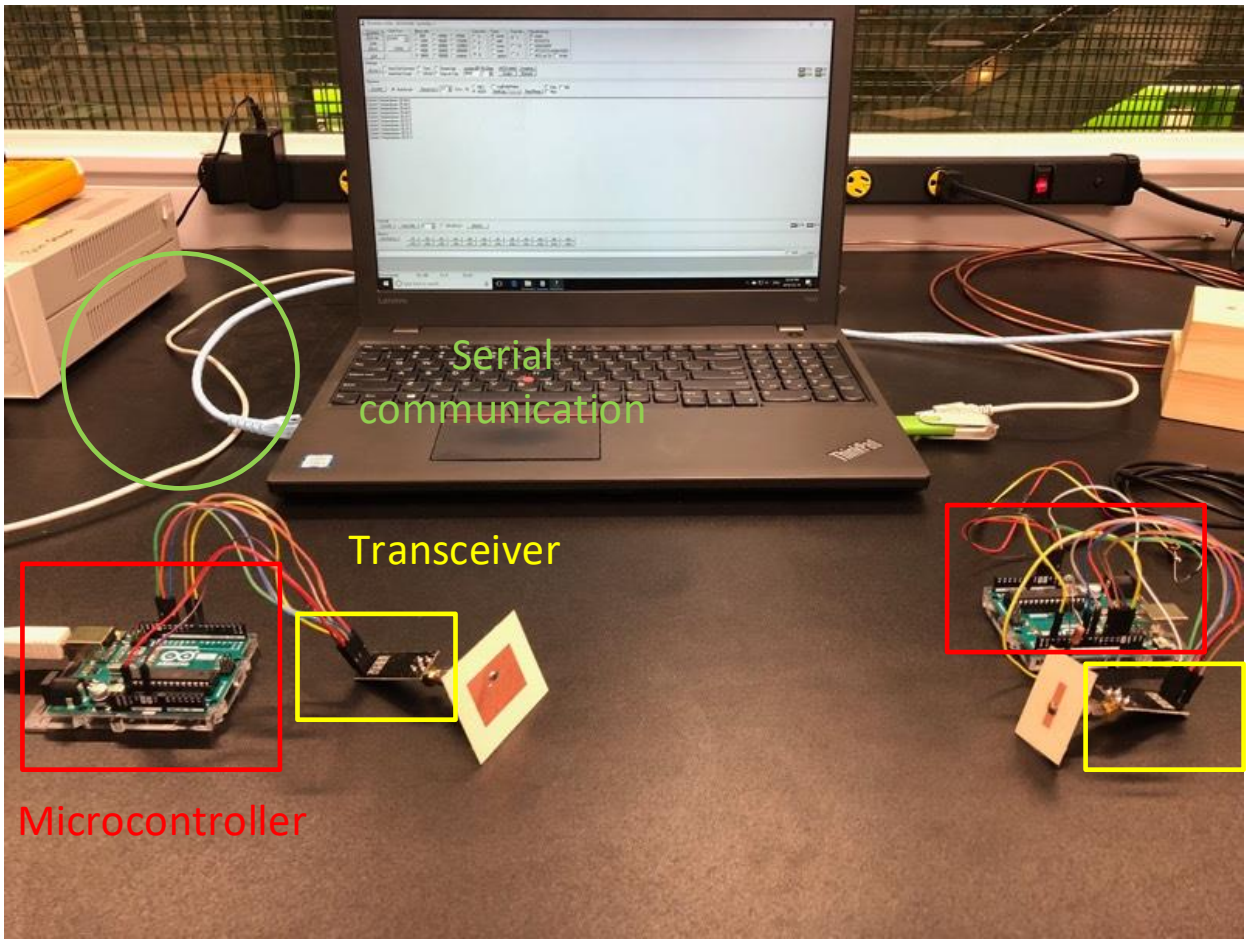


Figure 5.11 – Built wireless temperature sensor system

The temperature in the chamber is varied from $-40℃$ to $+80℃$ in steps of $20℃$. Antennas installed in this chamber are ensured to be stabilized at each temperature change by observing the reading of chamber with the antenna in it. It is observed that each temperature change requires an approximate average time of 30 min for stabilization. Even at such wide range of temperature changes, measurements have showed that the signal is not lost and the sensed temperature value is correctly interpreted on personal computer (PC) terminal, verified from the reading on the chamber. By specifying command ‘ON’ or ‘OFF’ on PC terminal the command signal for turning ON/OFF LED diode is sent to the Slave.


Figure 5.12 – Testing signal transmission of wireless temperature sensor network system

## 5.6 Conclusion

In this chapter, we have presented the comprehensive analysis, simulation, design and experimental validation of the prototyped wireless temperature sensor network intended for use on the helicopter as a part of helicopter de-icing system. A brief description of system purpose, its requirements and working principle are discussed. In order to estimate the system requirements accurately, the link power budget analysis is performed. System simulation is carried out for the worst case scenario by ADS software. The main parameters evaluated are the transmitter output power, receiver sensitivity and signal modulation scheme. Then, an appropriate transceiver circuit is selected with the system components to meet the simulation criteria. As the final stage, the selected system components are interconnected, and the system performance is experimentally analyzed in $-40℃$ to $+80℃$ temperature range. Temperature-compensated MPAs fabricated on TMM10 substrate case has demonstrated a better performance in all the cases considered with the loss in the signal being low. However, this is not the case for MPAs fabricated on RO6002 substrate characterized by the lowest permittivity temperature coefficient.

# CHAPTER 6 CONCLUSION AND FUTURE WORK

This M.Sc. thesis, as a part of de-icing helicopter system project, is mainly focused on temperature compensation technique for the resonant frequency of a MPA. For the first time, the temperature impact on a resonant frequency of microstrip antenna is mathematically described and analyzed through the closed-form resonant frequency drift expressions. The closed-form expressions for a resonant frequency drift enable getting insight into parameters which affect a resonant frequency. The thesis presents comprehensive mathematical models for analyzing temperature impact on resonant frequency of rectangular, circular and triangular MPA. The circuit model for analyzing temperature impact on antenna's resonant frequency is also adopted. The electromagnetic software simulations, along with the results of the circuit model simulation, support the derived theory. Based on the derived theory, the resonant frequency compensation condition is devised for rectangular, circular and triangular MPA. The new compensation technique is characterized in terms of antenna geometry, i.e. the patch width to substrate thickness ratio for a particular substrate material and a temperature coefficient of substrate permittivity in order to achieve the maximum available temperature performance. Based on a comprehensive literature review, the developed compensation technique is superior to the existing counterparts. The compensation technique is characterized by its simplicity and a high level of frequency stability through temperature variations. Nothing similar has ever been done before for microstrip patch antennas. The devised compensation technique is accompanied by design methodology in order to decrease the resonant frequency sensitivity to temperature variation. By analyzing the antennas on different substrates, it has been found that none of the commercially available substrates can completely satisfy the compensation condition. Two substrates that closely satisfy the best possible temperature compensation condition are chosen for experimental verifications. Both substrates are Rogers substrates, namely RO3035 and TMM10. In total, eleven microstrip patch antennas were fabricated for experimental verification. The measurements conducted in our lab have confirmed that the best behaviour is observed in the rectangular microstrip patch antenna manufactured on TMM10 substrate, as expected based on the simulations and theoretical predictions. Such temperature-compensated microstrip antenna proved to be a good candidate for a new concept of using microstrip antennas - ice thickness sensing.

A new concept of using microstrip patch antennas as ice thickness sensor is proposed. For a better characterization of ice loading effect on patch resonance, ice dielectric properties are measured.

Measurement has been conducted in our lab. As expected, based on the derived theory and the electromagnetic simulator simulations, rectangular patch antenna with smaller patch width to substrate thickness ratio has exhibited the best performance at measuring very thin ice layers.

In the end, a wireless temperature sensor network intended for development of a helicopter de-icing system has been designed and built. The working ability of the wireless sensor network using temperature compensated antennas is tested in a wide temperature range. Experimental testing has been done in our lab. The signal transmission of the wireless sensor network during testing within the broad temperature range has been undisturbed showing a good withstanding of the antennas designed by the proposed temperature compensation method.

In order to improve the compensation technique and make it applicable for wide range of substrates, the multilayer structures have to be thoroughly investigated in the future. Experimental validation of microstrip patch antenna ice sensor concept should also be conducted. Finally, the overall implementation of the wireless sensor network at one board with temperature-compensated and ice-senor microstrip patch antennas should be done and deployed on a helicopter for overall testing purposes.

# BIBLIOGRAPHY

[1] W. C. F. A. Meteorology, "WMO Commission for Aeronautical Meteorology," [Online]. Available: http://www.caem.wmo.int/_pdf/icing/icing_02_effects.pdf. [Accessed 2 2017].

[2] C. D. J. F. Kevin R. Petty, "A Statistical Review of Aviation Airframe Icing Accidents in the U.S."

[3] R. R. T.P. Ratvasky, "Icing Effects on Aircraft Stability and Control Determined From Flight Data," Lewis Research Center, Cleveland, Ohio, 1993.

[4] W. C. F. A. Meteorology, "WMO Commission for Aeronautical Meteorology," [Online]. Available: http://www.caem.wmo.int/_pdf/icing/icing_01_teacher_notes.pdf. [Accessed 2 2017].

[5] W. C. F. A. Meteorology, "WMO Commission for Aeronautical Meteorology," [Online]. Available: http://www.caem.wmo.int/_pdf/icing/icing_01_introduction.pdf.

[6] F. A. Administration, "Federal Aviation Administration," [Online]. Available: https://www.faa.gov/documentLibrary/media/Advisory_Circular/AC%2000-6A%20Chap%2010-12.pdf.

[7] F. A. Administration, "Federal Aviation Administration," [Online]. Available: https://www.faa.gov/.

[8] N. A. D. A. Synopses, "NTSB Accident Database and Synopses," [Online]. Available: https://www.ntsb.gov/_layouts/ntsb.aviation/index.aspx.

[9] N. A. S. R. System, "NASA Aviation Safety Reporting System," [Online]. Available: https://asrs.arc.nasa.gov/.

[10] P. Appiah-Kubi, "U.S Inflight Icing Accidents and Incidents, 2006 to 2010," Masters Theses, Tennessee, Knoxville, 2011.

[11] F. M. S. N. Agathe Aventin, "Statistical Study of Aircraft Accidents and Incidents Related to De-icing/Anti-Icing Procedures in Canada between 2009 and 2014".

[12] T. C. C. A. D. O. R. System, "Transport Canada Civil Aviation Daily Occurrence Reporting System," [Online]. Available: http://wwwapps.tc.gc.ca/saf-sec-sur/2/cadors-screaq/m.aspx?lang=eng.

[13] R. Bancroft, Microstrip and Printed Antenna Design, Raleigh, NC: SciTech, 2009.

[14] P. B. I. B. A. I. Ramesh Garg, Microstrip Antenna Design Handbook, London: Artech House, 2001.

[15] C. A. Balanis, Antenna Theory Analysis and Design, Hoboken, New Jersey: John Wiley & Sons, 2005.

[16] C. Wood, R. James, Microstrip Antenna Theory and Design, London: Peter Peregrinus, 1986.

[17] M. A. Weiss, "Temperature Compensation of Microstrip Antennas," *IEEE,* pp. 347-350, 1981.

[18] M. E. B. Pawel Kabacik, "The Temperture Dependence of Substrate Parameters and Their Effect on Microstrip Antenna Performance," *IEEE Antennas and Propagation,* vol. 47, no. 6, pp. 1042-1049, 1999.

[19] G. K. Sarath Babu, "Parametric Study and Temperature Sensitivity of Microstrip Antennas Using an Improved Linear Transmission Line Model," *IEEE Antennas and Propagation,* vol. 47, no. 2, pp. 221-226, 1999.

[20] Ashutosh Kedar, "Parametric and Temperature Sensitivity Study of Resonance Frequency of Microstrip Antennas Using Spectral Domain Method," *Microwave and Optical Technology,* vol. 30, no. 4, pp. 276-280, 2001.

[21] M. Walpita, "Temperature-Compensated Thermoplastic High Dielectric-Constant Microwave Laminates," *IEEE Microwave Theory and Techniques,* vol. 47, no. 8, pp. 1577-1584, 1999.

[22] J. Masiulis, "Passive Temperature Compensation Scheme for Microstrip Antennas". US Patent US5021795 A, 4 June 1991.

[23] Ke Wu, Dominic Deslandes, Tarek Djerafi, "A Temperature-Compensation Technique for Substrate Integrated Waveguide Cavities and Filters," *IEEE Microwave Theory and Techniques,* vol. 60, no. 8, pp. 2448-2454, 2012.

[24] Q. S. Yidong Wang, "A New Temperature Compensation Method of Rectangular Waveguide Resonant Cavities," in *APMC2005*, Suzhou, 2005.

[25] J. Ju, "A Novel Configuration of Temperature Compensation in the Resonant Cavities," *IEEE Microwave Theory and Techniques,* vol. 52, no. 1, pp. 139-143, 2004.

[26] C. Wang, "Temperature Compensations for Microwave Resonators and Filters," in *WMB4*, 2005.

[27] K. A. Z. Chi Wang, "Temperature Compensation of Combline Resonators and Filters".

[28] D. M. Dobkin, RF Engineering for Wireless Networks, San Diego, California: Elseiver, 2005.

[29] ITU, "ITU," [Online]. Available: http://www.itu.int/en/about/Pages/default.aspx.

[30] ITU, "ITU Radio Regulations," ITU, 2016.

[31] "European Telecommunication Standards Institut," [Online]. Available: http://www.etsi.org/.

[32] E. R. 70-03, "ERC Recommendation 70-03," ERC Recommendation 70-03, 2007.

[33] ICAO, "International Civil Aviation Organization," [Online]. Available: https://www.icao.int/Pages/default.aspx.

[34] H. Mazar, "International, Regional and National Regulation of Short Range Devices (SRDs)," Singapure, 2016.

[35] N. Kinayman, Modern Microwave Circuits, Boston: Artech House, 2005.

[36] D. M. Pozar, "Considarations for Milimeter Wave Printed Antennas," *IEEE Antennas and Propagation,* vol. 31, no. 5, pp. 740-747, 1983.

[37] R. G. A.K. Bhattacharyya, "Generalised Transmission Line Model for Microstrip Patches," *IEEE Antennas and Propagation,* vol. 132, no. 2, pp. 93-98, 1985.

[38] G. Dubost, "Linear Transmission Line Model Analysis of Arbitrary Shape Patch Antenna," *Electronic Letters,* vol. 22, no. 12, pp. 798-799, 1986.

[39] G. B. G. Dubost, "Linear Transmission Line Model Analysis of a Circular Patch Antenna," *Electronic Letters,* vol. 22, no. 22, pp. 1174-1176, 1986.

[40] Sarath Babu, "Improved Linear Transmission Line Model for Rectangular, Circular and Triangular Microstrip Antennas," in *IEEE Antennas and Propagation Society International Symposium*, 1997.

[41] Russell W. Darnley, "A Broad Band Transmission Line Model for a Rectangular Microstrip Antenna," *IEEE Antennas and Propagation,* vol. 37, no. 1, pp. 6-15, 1989.

[42] Shunshi Zhong, "Improved Transmission Line Model for Input Impedance of Rectangular Microstrip Antennas with Multy Dielectric Layers," in *IEEE Antennas and Propagation Society International Symposium and URSI National Radio Science Meeting*, 1994.

[43] R. Shavit, "Dielectric Cover Effect on Rectangular Microstrip Antenna Array," *IEEE Transactins on Antenna and Propagation,* vol. 42, no. 8, pp. 1180-1184, 1994.

[44] R. H. J. M. Kirsching, "Accurate Model for Effective Dielectric Constant of Microstrip with Validity up to Milimetre Wave Frequencies," *Electronic Letters,* vol. 18, no. 6, pp. 272-273, 1982.

[45] N. K. Ingo Wolff, "Rectangular and Circular Microstrip Disk Capacitors and Resonators," *IEEE Microwave Theory and Techniques,* vol. 22, no. 10, pp. 857-863, 1974.

[46] W. K. Nirun Kumprasert, "Simple and Accurate Formula for the Resonant Frequency of the Circular Microstrip Disk Antenna," *IEEE Antennas and Propagation,* vol. 43, no. 11, pp. 1331-1333, 1995.

[47] W. C. C. m. J. A. Kong, "Effects of Fringing Fields on the Capacitance of Circular Microstrip Disk," *IEEE Microwave Theory and Techniques,* vol. 28, no. 2, pp. 98-103, 1980.

[48] X. Gang, "On the Resonant Frequencies of Microstrip Antennas," *IEEE Antennas and Propagation,* vol. 37, no. 2, pp. 245-247, 1989.

[49] Van de Cappel, H. Pues, "Accurate Transmission Line Model for the Rectangular Microstrip Antenna," *Microwaves, Optics and Antennas,* vol. 131, no. 6, pp. 334-340, 1984.

[50] R. K. Hoffmann, Handbook of Microwave Integrated Circuits, Norwood, MA: Artech House, 1987.

[51] E. Lier, "Improved Formulas for Input Impedance of Coax-Feed Microstrip Patch Antennas," *Microwaves, Optics and Antennas,* vol. 129, no. 4, pp. 161-164, 1982.

[52] Russell W. Dearnley, "A Comparison of Models to Determine the Resonant Frequencies of Rectangular Microstrip Antenna," *IEEE Antennas and Propagation,* vol. 37, no. 1, pp. 114-118, 1989.

[53] P. Ray, "Determination of the Resonant Frequency of Microstrip Antennas," *Microwave and Optical Technology Letters,* vol. 23, no. 2, pp. 114-117, 1999.

[54] A. K. Verma, "Modified Wolff Model for Determination of Resonance Frequency of Dielectric Covered Circular Microstrip Patch Antenna," *Electronics Letter,* vol. 27, no. 24, pp. 2234-2236, 1991.

[55] Emerson, Cuming, "Theory and Applications of RF/MW Absorbers," Emerson & Cuming, Randolph, MA.

[56] P. Dixon, "Cavity-Resonance Dampening," Emerson & Cuming, 2005.

[57] C. M. A. U. Wegmuller, "Dielectric Properties of Fresh-Water Ice at Microwave Frequencies," *Journal of Applied Physics,* vol. 20, pp. 1623-1630, 1987.

[58] D. S. Kreidenweis, "Atmospheric Thermodynamics and Cloud Physics," [Online]. Available: http://chem.atmos.colostate.edu/AT620/Sonia_uploads/ATS620_F11_Lecture19/Lecture19_AT620_101011.pdf.

[59] Shuji Fujits, "The Measurement on the Dielectric Properties of Ice at HF, VHF and Microwave Frequencies," pp. 1258-1260.

[60] S. Warren, "Optical Constants of Ice from the Ultraviolet to the Microwave," *Applied Optics,* vol. 23, no. 8, pp. 1206-1225, 1984.

[61] S. R. Gough, "A Low Temperature Dielectric Cell and the Permittivity of Hexagonial Ice to 2K," pp. 3046-3051, 1972.

[62] A. Technologies, "Basics of Measuring the Dielectric Properties of Material," Agilent Technologies, USA, 2006.

[63] H. Packard, "HP 85070B Dielectric Probe Kit," Hewlett Packard, USA, 1997.

[64] Jonathan Geisheimer, "Microstrip Patch Antenna for High Temperature Environments". US Patent US20070024505 A1, 1 Februar 2007.

[65] A. G. Derneryd, "Linearly Polarized Microstrip Antennas," *IEEE Antennas and Propagation,* vol. 24, no. 6, pp. 846-851, 1976.

[66] E. Hammerstad, "Accurate Models for Microstrip Computer Aided Design," *IEEE MTT-S International Microwave symposium,* pp. 407-409, 1980.

[67] R. Waterhouse, Microstrip Patch Antennas A designer's Guide, New York: Springer Science+Business Media,, 2003.

[68] N. W. Service, "Nathional Weather Service," [Online]. Available: http://www.weather.gov/source/zhu/ZHU_Training_Page/icing_stuff/icing/icing.htm.

[69] S. Evans, "Dielectric Properties of Ice and Snow - Review," pp. 773-792.

[70] S. F. S. M. Takeshi Matsuoka, "Effect of Temperature on Dielectric Properties of Ice in the Range 5–39 GHz," *Applied Physics,* vol. 80, no. 10, p. 1996, 5884-5890.

[71] V. V. G. V. M. Petrov, "Microwave Absorbing Materials," *MAIK Nauka,* vol. 37, no. 2, pp. 93-98, 2001.

[72] N. K. Ingo Wolff, "Rectangular and Circular Microstrip Disk Capacitors and Resonators," *IEEE Microwave Theory and Techniques,* vol. 22, no. 10, pp. 857-864, 1974.

[73] J. Y. S. Debatosh Guha, "Resonant Frequency of Circular Microstrip Antenna Covered With Dielectric Superstrate," *IEEE Antennas and Propagation,* vol. 51, no. 7, pp. 1649-1652, 2003.